The Uptake and Toxicity of Silver Nanoparticles in Choanoflagellates

By

Adam Davis

A dissertation submitted to the University of Birmingham for the degree of

Masters of Research in Human and Environmental Impacts of Nanoscience and Nanotechnology

Division of Environmental Health and Risk Management

School of Geography, Earth and Environmental Sciences

University of Birmingham

2012

Abstract

Silver nanoparticles are currently being widely used for a variety of applications, primarily for their novel biocidal properties. Upon release into the environment silver nanoparticles have the potential to be highly toxic towards a range of microorganisms. Choanoflagellates are a filter feeding bacteriovore protozoa which occupy a niche in the microbial loop. Choanoflagellates have previously been shown capable to ingesting sub-micron particles, however little information is known about whether the cells are capable of assimilating manufactured nanoparticles released into the environment. In this study citrate capped silver nanoparticles with a core size of 20 nm were synthesised using a chemical reduction method. The particles were characterised using a multi-method approach both as synthesised and in the presence of the Choanoflagellate's culture medium (Pratt's medium). At 5.5 mg/L in Pratt's medium the nanoparticles were found to be stable over 24 hrs, whilst at 11 μg/L the z average diameter increased to 442 nm as measured by DLS. The Choanoflagellates cells were exposed to various concentrations of silver nanoparticles in medium. Reflectance confocal microscopy was then used to image the uptake of these particles into the Choanoflagellate cells. Silver nanoparticles were found ingested by the Choanoflagellate cells at concentrations as low as 11 μg/L when incubated in nanoparticle suspension for 24 hrs. Using phase contrast microscopy the toxicity of particles washed via ultrafiltration and unwashed particles was then examined. Non washed particles were found to be significantly more toxic than those which had been ultrafiltrated.

Acknowledgements

Firstly, I would like to thank my supervisor Professor Jamie Lead, for his support, direction and encouragement over the course of this degree.

Many thanks go to Dr. Mohammed Baalousha for his advice, support and time during the course of my project, along with his training on the AFM. I would like to thank Dr. Ruth Merrifield for her guidance on various topics and training with DLS and nanoparticle synthesis. Dr. Bjorn Stolpe for the training he provided in the operation of the NTA. Thank-you to the entire research group with particular mention to; Isabella Romer, Mila Tejamaya, Yusuf Nur, Laura-Jayne Ellis and Marie-France Belinga for all their helpful comments and advice.

I especially would like to express my gratitude to Dr. Michala Pettitt whose knowledge and assistance made the biological world a lot less daunting. Special mention should also go to Dr. Robert Shaw and Dr. Julie Mazzolini, without whom the reflectance imaging would not have been possible.

Last but not least, I would like to thank my fellow MRes student Dr. Christine Elgy, whose experience and inspiration made the completing the project a much easier task.

Contents

List of Figures

List of Tables

Abbreviations

AFM – Atomic Force Microscopy

Ag – Silver

Ag^{+} - Ionic silver

AgNPs – Silver Nanoparticles

DLS – Dynamic Light Scattering

EDX/EDS – Energy dispersive x-rays

EEM – Excitation Emission Matrix

EM – Electron Microscopy

MNP – Manufactured/Engineered Nanoparticle

NM – Nanomaterial

NP – Nanoparticle

ROS – Reactive Oxygen Species

STP – Sewage Treatment Plant

TEM – Transmission Electron Microscopy

1. Introduction

1.1 Definition of Nanoparticle

There are many variations upon the definition of nanoparticle (NP), however most are based upon a size range between 1-100 nm. Recently, the European Commission (2011) upon the scientific advice from Scientific Committee on Emerging and Newly Identified Health Risks (SCENIHR, 2010) and the Joint Research Centre (Lovestam et al., 2010), has established the following definition of a nanomaterial (NM): "A natural, incidental or manufactured material containing particles, in an unbound state or as an aggregate or as an agglomerate and where, for 50 % or more of the particles in the number size distribution, one or more external dimensions is in the size range 1 nm - 100 nm." These NMs often exhibit novel size dependent effects not seen in their bulk material counterpart. It has been argued that these size-dependent effects, not particle dimensions should be the primary consideration for a NM or NP definition (Auffan et al., 2009).

1.2 Production of Nanoparticles

Natural NPs can be generated from a range of geological and biological processes and are already present in the environment as a sub-fraction of fresh water colloids (1 nm to 1 μm), volcanic ash, soil erosion and many others (Lead and Wilkinson, 2006; Ammann et al., 1990; Hasegawa et al., 2007). Incidental NPs are produced through a range of human activity, in particular the production of ultrafine air-borne particles from vehicle exhaust (Handy and Shaw, 2007). Carbon Black, is an industrial form of soot which is incidentally produced with a particle size distribution between 20 and 300 nm which is partially in the nanoscale range. Carbon black is commonly used filler in rubber compounds such as those used for automobile

tyres (Nowack and Bucheli, 2007). More recently NPs are being deliberately manufactured for a wide range of technological applications for their novel properties and these are considered within this project.

Manufactured nanoparticles (MNPs) may be carbon-based such as fullerenes and carbon nanotubes or based upon inorganic materials such as metals (gold, silver and iron), metal oxides (ceria, titania, zinc oxide and iron oxide) and quantum dots (cadmium sulfide and cadmium selenide) (Ju-Nam and Lead, 2008). These MNPs may be amorphous or crystalline in structure, have various shapes and morphologies and exist individually or be incorporated into a matrix (Ashby et al., 2009). NPs may be manufactured using a variety of techniques which may be broadly categorised as either top-down or bottom-up approaches. The top-down approach to NP synthesis consists of taking a bulk material and reducing it in size via a physical or chemical process. Top-down nanofabrication methods such as high energy ball milling otherwise known as mechanical attrition or mechanical alloying, have been of major industrial importance in the development of wide spread use of NMs (Kelsall et al., 2005). During the process of ball milling coarse grained materials such as metals in the form of powders are crushed mechanically in rotating drums with hard balls consisting of steel or tungsten carbide. This milling process may be operated at a large scale, leading to the strong industrial interest and application (Kelsall et al., 2005). This use of top-down approaches has led to the currently available MNPs to be polydisperse, heterogeneous and difficult to disperse into suspension (Cumberland and Lead, 2009). For both top-down and bottom up approaches any imperfections as a result of the synthesis method has the potential to have a significant impact upon the physical properties and surface chemistry of the NMs, (Cao, 2004). Bottom-up approaches to nanofabrication involve building up the NPs atom by atom or molecule by molecule, usually utilising a chemical or biological mechanism. The advantage in using a

bottom-up approach is that the NPs are often more homogeneous and have fewer defects than those produced via top-down methods. (Thakkar et al., 2010). The driving force behind bottom-up approaches is the resultant reduction in Gibbs free energy, bringing the NPs produced from the reaction closer towards thermodynamic equilibrium, resulting increased stability (Cao, 2004).

1.3 Nanoparticle Applications

As a result of their novel chemical and physical properties MNPs are being incorporated into a wide range of consumer products, with 1317 products currently listed in the Woodrow Wilson Nanotechnology project (2011). Of these 1317 products, only a small fraction specifically reference the NM used, however the most common material listed in this subset of products is silver (Ag). The use of Ag for the production of silver nanoparticles (AgNPs) in the European market has been predicted to reach 110-230t per annum by 2015 (HeiQ as cited Blaser et al., 2008).

These AgNPs are being utilised for a wide range of applications, the majority of which use the materials intrinsic biocidal properties. Such applications for AgNPs include medicinal fabrics and surgical appliances, food contact applications, cosmetics and clothing (Landsdown, 2006; Blaser et al., 2008; Benn and Westerhoff, 2008).

1.4 Environmental Exposure to Nanoparticles

With the wide spread use of NPs in consumer products such as AgNPs present in clothing as an anti-microbial agent it is likely that the environment will receive an increasing input of NPs. It has been estimated that in 2010 biocidal fabrics and plastics accounted for 15% of the total Ag released into the aquatic environment in the European Union (Blaser et al., 2008). Benn and Westerhoff (2008) demonstrated that in the case of sock fabrics that AgNPs are released through washing, with commercially available socks capable of releasing up to 650 μg in a single wash with distilled water.

1.5 Nanoparticle Fate in the Environment

The majority of AgNPs released from commercially available products would be expected to enter a Sewage Treatment Plant (STP). Although, in 2010 only 80% of the Northern and Southern European population were connected to STPs, with Eastern European countries at 67% and South-Eastern European countries having a mere 40% (European Environment Agency, 2012). Evidence collected from a model STP suggests that most AgNPs are retained in the sewage sludge in the form of silver sulfide (Kaegi et al., 2011). The percentage of AgNPs remaining in the effluent and subsequently able to enter the freshwater environment, relies on the fraction of wastewater effectively treated (Blaser et al., 2008). Once processed the sewage sludge now potentially containing AgNPs, may then be spread onto agricultural land. Upon deposition onto agricultural land Ag concentrations are likely to remain highest in the uppermost layers of soil, with concentrations decreasing rapidly below in subsequent layers (Hou et al., 2005). A notable exception to this method of handling sewage sludge is

Switzerland, in which sewage sludge is incinerated potentially leading to environmental exposure to air-borne AgNPs (Mueller and Nowack, 2008).

Remaining AgNPs in the STP's effluent or those which bypass the treatment process entirely may then enter natural freshwaters. AgNPs have been shown to aggregate in synthetic seawater and other water in which the concentration of sodium chloride is greater than 20 mmol L^{-1}. In simulated freshwaters with lower salt content the 20 nm citrate-capped AgNPs maintained varying degrees of colloidal stability over 48 hrs, indicating some AgNPs may remain dispersed as single particles long enough in freshwaters to enter estuarine or marine waters (Chinnapongse et al., 2011).

The potential fate of the AgNPs upon entering into a natural water environment include; agglomeration or aggregation, dissolution or reaction with natural dissolved materials such as natural organic macromolecules (Luoma, 2008, Fabrega et al., 2011). Due to their high surface area to volume ratio and reactivity MNPs are likely to be highly dynamic in the environment, resulting in transformations to the MNPs which will affect their fate, transport and potential toxicity (Lowry et al., 2012a). Among other chemical transformations (see figure 1.1) a large proportion of AgNPs entering terrestrial soils or subaquatic sediment are likely to be transformed into silver sulfide (Lowry et al., 2012b), this sulfidation process strongly affects the surface properties of the AgNPs. Particularly in terms of the AgNP surface charge and rate of dissolution, with silver dissolution decreasing as function of sulfide exposure (Levard et al., 2011). Such an effect on AgNP dissolution and surface properties could have a dramatic effect upon NP aggregation state, persistence and toxicity. It has also been demonstrated that NP interactions with natural organic macromolecules such as humic substances, along with changes in solution conditions such as pH can have an effect upon the surface properties of the NPs (Cumberland and Lead, 2009). In order to study the transport,

exposure, biological uptake and effects of NPs in a manner which is accurate and reproducible, consistent and accurate measurements of their physical structure and chemical structure are required (Baalousha and Lead, 2012). Therefore, it has been established that particles with well controlled size and shape, which are fully characterised using a multi-method approach are needed in order to fully quantify their properties and potential interactions in the environment (Domingos et al., 2009).

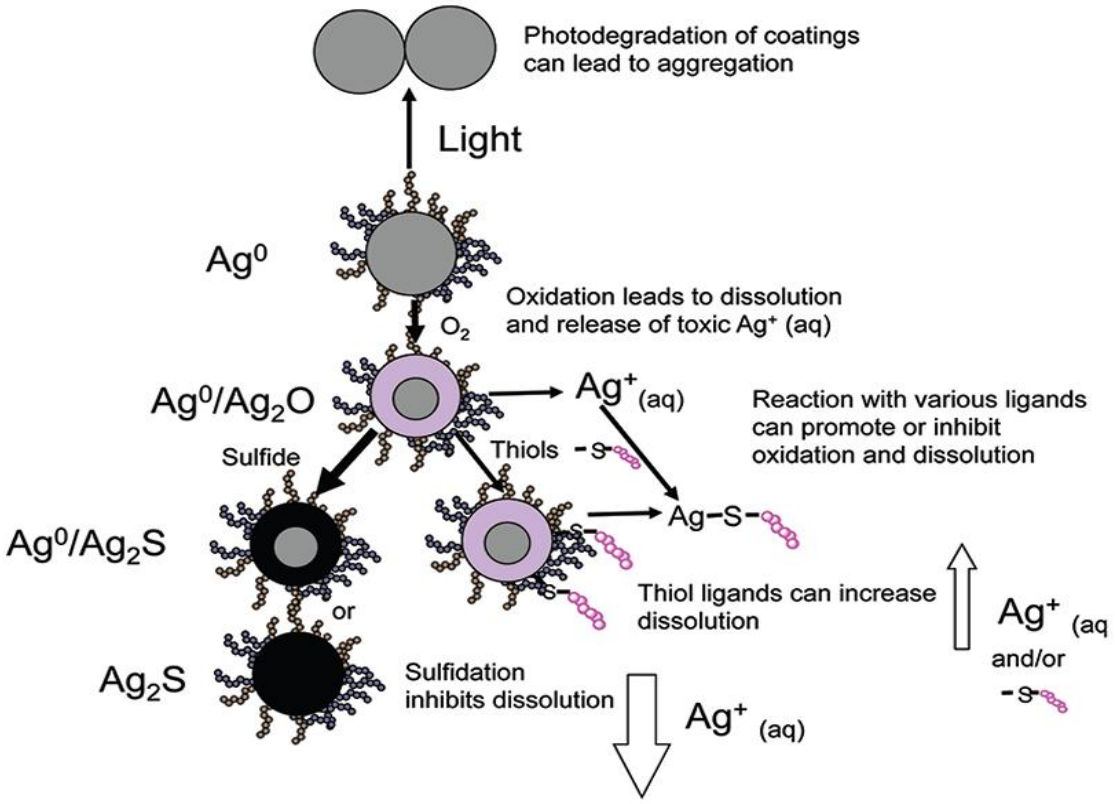

Figure 1.1. An overview of the types of chemical interactions and transformations silver nanoparticles may experience in the environment (Lowry et al., 2012a).

1.6 Environmental Hazard of Nanoparticles

The environmental risk associated with the use of MNPs can be calculated from the product of the likelihood of exposure to the environment and the hazard they present. The release of AgNPs into the environment as a result of the use and washing of NP containing products and their fate in the environment are therefore critical considerations when calculating the risk of AgNP use. The hazard that AgNPs present to the environment whilst better understood than exposure, is still largely unknown, although it is well established that silver ions (Ag^+) are highly toxic towards aquatic organisms (Wood et al., 1999). AgNPs which have novel chemical and physical properties may prove to have enhanced toxicity compared to Ag^+ (Luoma, 2008).

In order for AgNPs to be considered hazardous towards aquatic organisms they must first be available to and retained by the organism (Luoma and Rainbow, 2005). This bioavailability can be defined as the ability of the AgNPs to associate with a cell membrane and to be internalised by that cell (Croteau et al., 2011). For a variety of organisms some trace elements such as copper, zinc, and iron are important nutrients and their uptake from the environment is therefore essential for survival, (Bury et al., 2003), however in the case of Ag there is no such biological function (Shaw and Handy, 2011). It was found by Lowry et al. (2012b) that even at concentrations as low as, 2 μg/L, and after partial sulfidation of the AgNPs, they were still bioavailable to organisms in both terrestrial and aquatic environments, with 0.5-3.3 μg Ag/g wet weight found in mosquito, fish and chironomids.

For many aquatic organisms assimilation of AgNPs will likely occur through dietary exposure. In the case of filter feeders such as the freshwater cladoceran *Daphnia magna* it has been demonstrated that at concentrations of 2 μg/L, 20 nm AgNPs had an uptake rate constant

of 0.060 l/g/h (Zhao and Wang, 2010). When AgNPs were associated with the Dapnids algal food source, it was found that the efficiency of the dietary assimilation was between 22-45%. When the results were interpreted using a biokinetic model it was shown that 70% of the AgNPs that accumulated in the Daphnids was through their ingestion of algae. Similarly, in the freshwater snail species *Lymnaea stagnalis* it has been found that dietary exposure gave an assimilation efficiency of between 49-58% when the snails were exposed to 17-187 nmoles/g for the humic acid capped AgNPs and 7-250 nmoles/g for citrate capped AgNPs. The AgNPs were mixed into the snails diatom (*N. palea)* food source (Croteau et al., 2011). When this dietary exposure was compared with water born exposure to AgNPs, dietary exposure was considered to have the greatest importance and once taken up from the diet Ag was lost at a comparatively low rate from the snails. It was also found that the Ag NPs damaged the snails' digestion, leading to a reduction in feeding and caused impairment in the snails' ability to process the digested food, subsequently this adversely effected the growth of the snails.

The uptake of AgNPs in higher eukaryotic organisms has also been demonstrated, AgNPs are capable of penetrating through semi-permeable membranes including the chorion which surrounds zebra fish embryos (Lee et al., 2007; Asharani et al., 2008; Asharani et al., 2011; Bar-llan et al., 2009). AgNPs are also able to penetrate across other biological barriers including both intact and damaged human skin, with a concentration of up to 0.46 ng/cm^{-2} present in the uppermost two layers of skin after 24 hrs (Larese et al., 2009).

In prokaryotes it has been demonstrated that AgNPs are highly effective against a wide range of both gram negative and gram positive bacteria (Feng et al., 2000). Upon interaction with AgNPs bacteria have been shown to undergo morphological changes resulting in the rupture of the bacteria cells, along with a reduction in bacterial growth (Wang et al., 2012).

It has been suggested that AgNPs may present a greater hazard when compared to ionic forms of silver alone (Ag^+), through a novel Trojan horse mechanism of toxicity (Luoma, 2008). This hypothesis suggests that AgNPs are more readily bioavailable to organisms, and upon uptake dissolution of the NPs may occur, releasing highly toxic Ag^+. Park et al. (2010) found mouse peritoneal macrophages (RAW 264.7) exposed to 69 nm diameter AgNPs at a concentration of 1.6 ppm over 24 hrs, decreased in viability by 80% when compared to the control macrophages. Upon further investigation it was observed that AgNPs were present in the activated mouse macrophages, whilst in those macrophages that were damaged no AgNPs were present. This led the authors to speculate that AgNPs after entering the cells though phagocytosis, had undergone complete dissolution, resulting in cell death via a Trojan horse type mechanism.

In addition to inducing cell death through the release of Ag^+, it has also been proposed that AgNPs may be potentially toxic through the production of reactive oxygen species (ROS) (Foldjberg et al., 2009). AgNPs may be capable of producing ROS through a variety of ways (see figure 1.2) such as; through surface chemistry promoting the Fenton reaction, ingestion by natural killer cells leading to production of NADPH oxidase ROS release, and disruption of the normal function of the cells mitochondria (Li et al., 2008).

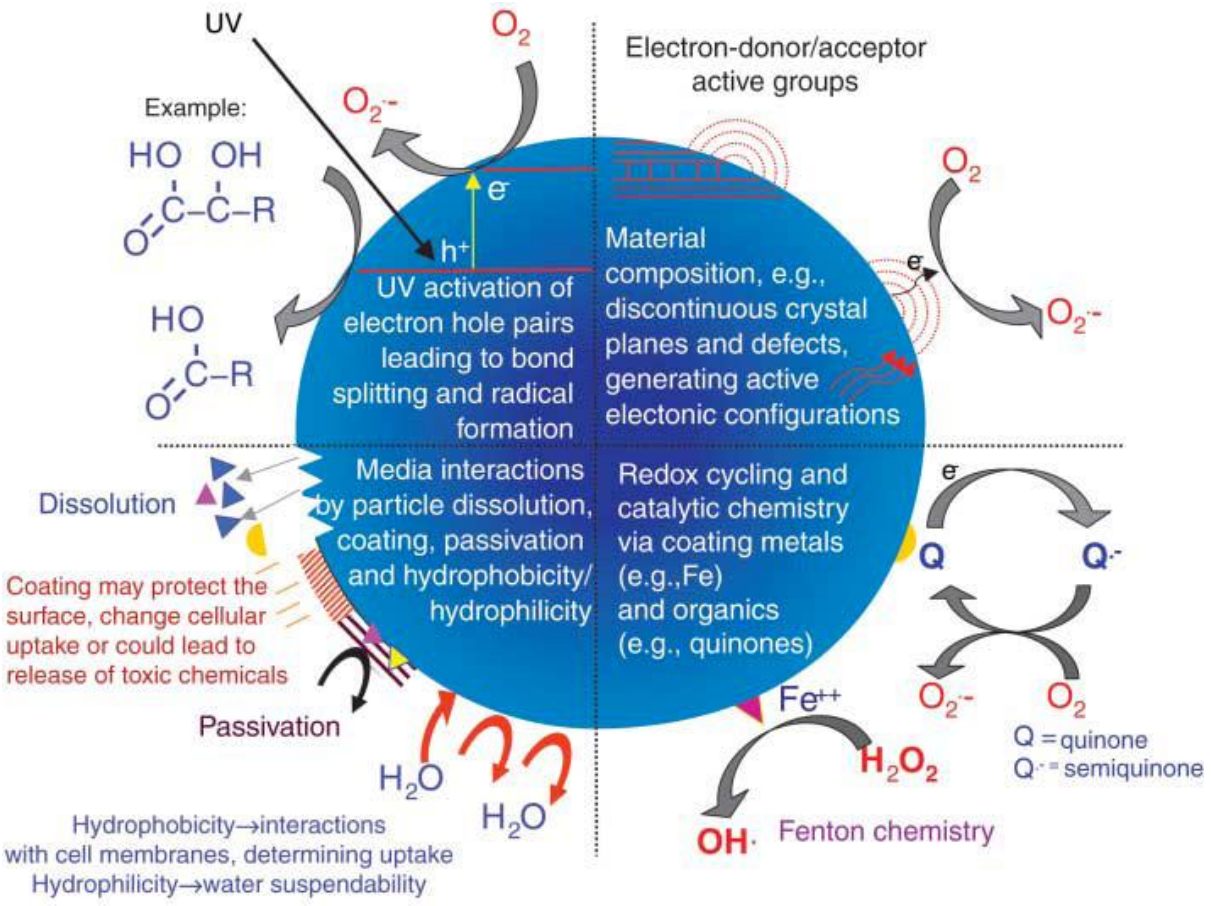

Figure 1.2. Possible mechanisms by which nanoparticles may interact with biological tissue in order to promote toxicity (Nel et al., 2006).

1.7 Choanoflagellates

Choanoflagellates are single celled eukaryotic organisms of the phylum Choanozoa (Cavalier-Smith, 1993), which are geographically widely distributed being found in the majority of aquatic environments. There are approximately 250 species of Choanoflagellates which have been currently described (http://choanoflagellates.lifedesks.org/), with the majority of these Choanoflagellate species from a marine environment however there are over 50 freshwater species (Carr et al., 2008).

Choanoflagellates are traditionally categorised into three separate families, distinguishable by distinctive extracellular structures, notably the possession or absence of a firm polysaccharide theca or a lorica comprised of siliceous strips (Adl et al., 2005). Members of the Choanoflagellate family Codosigidae are characterised by the absence of any significant extracellular structures, with only a thin fibrillar coat, termed the glycocalyx as an outer covering (Leadbeater and Morton, 1974). Many species in the family Codosigidae attach themselves to solid surfaces using a flexible stalk termed a pedicel, the length of which is highly dependent upon species and individual (Pettitt et al., 2002). The family Acathoecidae is exclusively marine, and indentified via the presence of a lorica comprised of silica strips termed costae. These costae are accumulated in bundles on the cell surface and assembled in a series of rapid movements into rib-like arrays (Carr et al., 2008). The morphology of the lorica is highly variable between species, and may be formed using 150 – 185 costal strips in total (Pettitt et al., 2002). The lorica of the Acathoecidae provides a rigid framework around the cell, resisting the locomotory forces generated by flagellar movement, it also directs and enhances water flow over the collar and for planktonic species the lorica contributes towards maintaining the cells in suspension (Leadbeater et al., 2009). The Salpingoecidae are distinguished by the possession of a firm polysaccharide theca which surrounds the protoplast, this theca is used to attach the Choanoflagellate directly to solid surfaces, the theca maybe flask, cup or tube-shaped (Carr et al., 2008). A relatively large example of freshwater Salpingoecidae are *Salpingoeca amphorium* shown in figure 1.3.

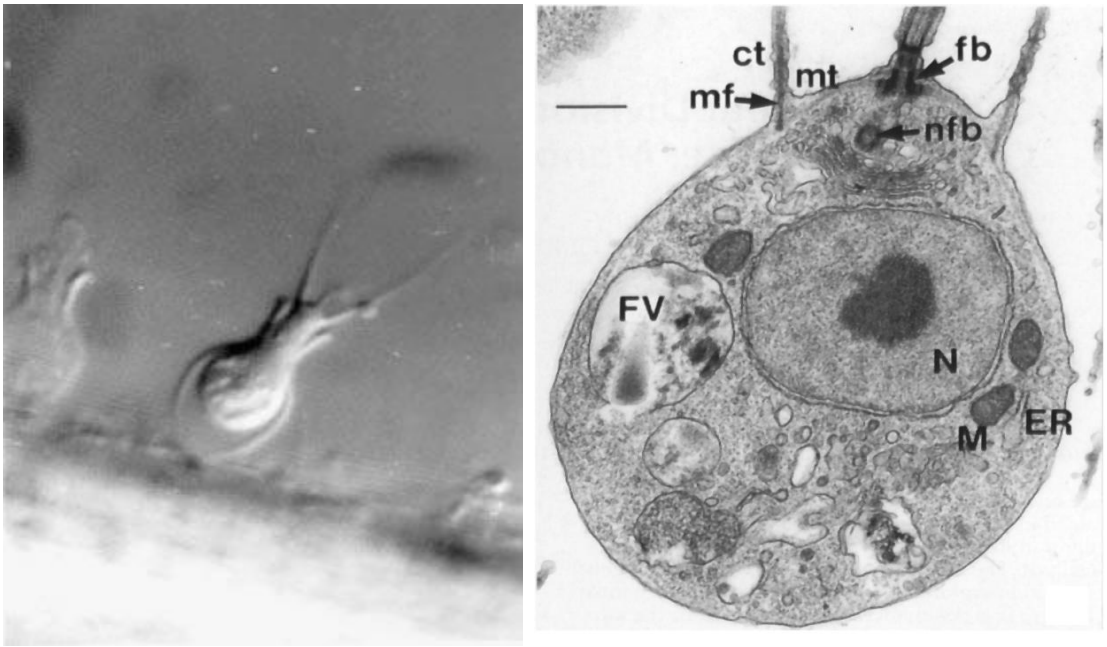

Figure 1.3 Left hand side image: A light micrograph of *Salpingoeca amphoridium* (Orme et al. 2003).

Right hand side image: Electron micrograph of *Monosiga ovata* where ct - collar tentacle; ER - endoplasmic reticulum; fb - flagellar basal body; FV - food vacuole; M - mitochondrial profile; mf - microfilament; mt - microtubule; N - nucleus; nfb - non-flagellar basal body; (Karpov and Leadbeater, 1997).

Choanoflagellates are primarily filter feeding bacteriovores, occupying a niche in the microbial loop (Pettitt et al., 2002). These and other heterotropic nanoflagellates are recognised as important grazers of bacteria in many aquatic environments (Boenigk and Arndt, 2002) and under some circumstances choanoflagellates may be responsible for the majority of the grazing pressure on bacterial populations (Fenchel, 1982).

1.8 Choanoflagellate Feeding Mechanism

The Choanoflagellates have a unique morphology which consists of a cell with a single flagellum surrounded by a symmetrical collar of microvilli (Carr et al., 2008). This collar acts as a filter trapping bacteria on the outward facing surface, prior to being transported towards the main body of the cell in order to be phagocytosed. Bacteria are drawn towards the microvilli as a result of entrainment in the fluid motion generated by the motion of the Choanoflagellates flagellum (Pettitt et al., 2002). Attachment to a substrate via the use of a pedical, theca or lorica is considered an important mechanism for increasing the likelihood that an individual will contact prey particles due to hydrodynamic forces, subsequently increasing the rate of particle ingestion (Fenchel, 1986).

Feeding strategies other than filter feeding employed by heterotrophic nanoflagellates (see figure 1.4) may be generalised as; direct interaction also known as raptorial feeding in which prey particles are captured after being carried along flow lines caused by flagellate motility, and diffusion feeding in which mobile prey particles contact a motionless consumer (Boenigk and Arndk, 2002).

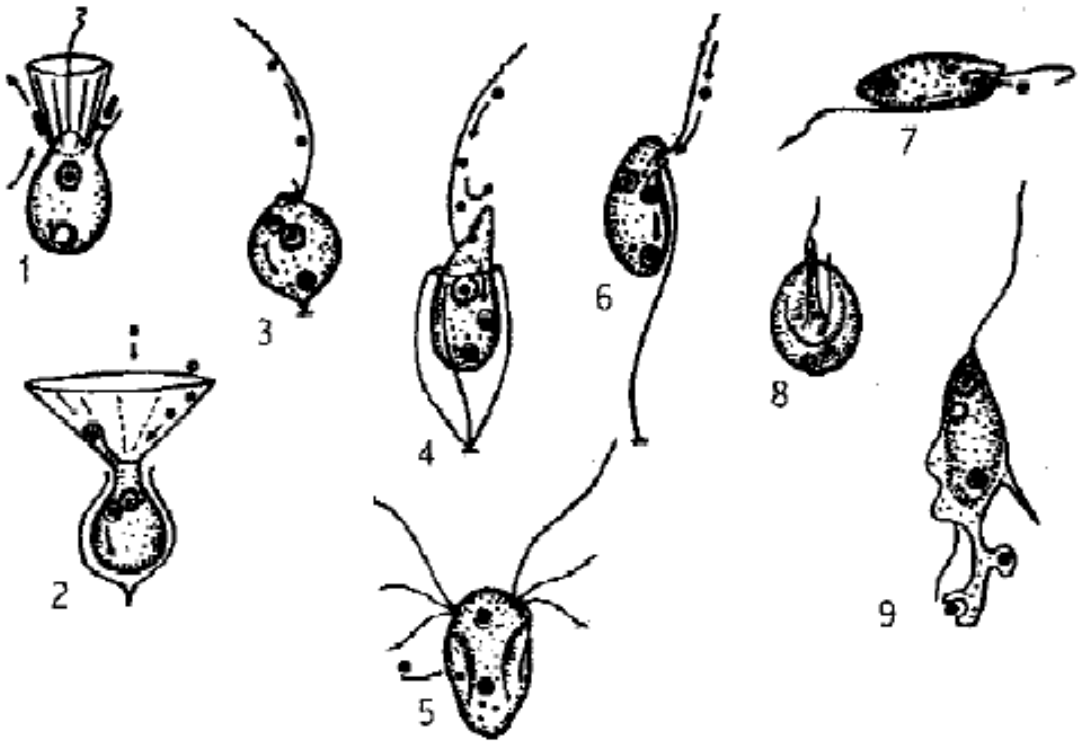

Figure. 1.4 Feeding strategies of different bacterivorous heterotrophic nanoflagellates: filter-feeding (1, choanoflagellate *Monosiga*), sedimentation (2, choanoflagellate *Choanoeca perplexa*), interception feeding (3, chrysomonad *Spumella*; 4, bicosoecid *Bicosoeca*; 5, diplomonad; 6 bodonid *Bodo saltans*), raptorial feeding by a pharynx (7, bodonid) or by pseudopod like structures (8, apusomonad *Apusomonas*; 9, cercomonad *Cercomonas*) (Boenigk and Arndk, 2002).

Filter-feeder Choanoflagellates such as *Monosiga ovata* are capable of handling several prey particles simultaneously, with each particle taking over 300 seconds to ingest once captured. Whilst the average speed of prey particles within the feeding current of the flagellates is only 9.3 μm s^{-1} the large surface area of the collar allows for 6.4 nl h^{-1} of water to be filtered (Boenigk and Arndk, 2000). It was observed by Boenigk and Arndk (2000) that the size of bacteria (biovolume) in contact with the flagellate (0.16 ± 0.08 μm^3) did not differ from the

size spectrum of the bacteria in the medium, however the bacteria which were eventually ingested by the Choanoflagellates were significantly smaller (0.03 ±0.05 μm^3) demonstrating size selection during the handling of prey particles.

It has been demonstrated in a variety of Antarctic species that Choanoflagellates are capable of ingesting submicron particles in the range of 0.063 – 1 μm. During incubation with fluorescent polystyrene particles for 30 minutes 80% of the Antarctic Choanoflagellates species Acanthocorbis unguiculata had ingested 0.25 μm particles, with 100% up take for the 0.5 μm particles (Marchant and Scott, 1993). The ability of most flagellates to take up particles of different sizes, facilitated in the case of Choanoflagellates by pseudopod formation is suspected to be an important feature for the survival in environments with low food concentrations (Boenigk and Arndk, 2002). With the flagellates feeding upon large particles upon their occasional contact with the cell, along with the uptake of smaller particles brought towards the cells via the filter current generated by the flagellum.

Non-living sub-micron organic particles in the size range 0.38-1 μm have been found to be abundance in the upper layers of the ocean environment, with concentrations on the order of 10 million particles per millilitre (Koike et al., 1990). In addition to these organic colloidal particles, trace metals such as iron, aluminium and cobalt may also be present (Wells and Goldberg, 1991). A high abundance of viruses have also been shown to be in the aquatic environment, with up to 2.5 x 10^8 particles per millilitre found in natural waters (Bergh et al., 1989). The rate at which suspension feeders such as flagellates encounter colloidal particles and viruses in an aquatic environment through diffusion and direct interception has been suggested to be between 1-21 times greater than the encounter rates for bacteria (Shimeta, 1993). Heterotrophic flagellates including the Choanoflagellate *Codosiga* have been shown capable of directly ingesting high molecular weight dissolved organic matter independent of

the presence of bacteria. When exposed to the polysaccharide dextran labelled with fluorescein isothiocyanate, 6 -20% of the individual flagellates ingested dextran with a M_r of 2000K, whilst 2-17% of flagellates ingested 500K dextran (Sherr, 1988). This gives rise to the possibility that heterotropic nanoflagellates such as Choanoflagellates could be capable of intercepting and ingesting AgNPs.

The grazing of heterotrophic protozoa upon bacteria, algae and high molecular weight molecules has been suggested as a mechanism for the conversion of small particles into larger particles in aquatic systems via a repacking effect (Sherr and Sherr, 1988). Similarly it has been observed that nanoflagellates such as *Paraphysomonas imperforata* which are attached to sinking or suspended particles in a marine environment are capable of enhancing the agglomeration and enlargement of sub-micron sized particles. It was found that the agglomeration of model 0.5 μm fluorescent latex particles to larger particles (5 -20 μm) was enhanced upon entrainment in the feeding current of the flagellates (Fukuda and Koike, 2000).

1.9 Use of Choanoflagellates in Nanoparticle Biomonitoring

Biomonitoring is a technique capable of indicating the potential environmental effects of unknown contaminants and substances which are difficult to assess chemically (Pronk et al., 2009). It has been suggested that microorganisms particularly protozoa such as choanoflagellates could serve as a useful tool for the biomonitoring of NMs (Zoloterev, 2010). Due to their ubiquity nanoflagellates facilitate the comparison of test results over different geographical areas. They are often the most abundant microorganism in artificial and natural periphyton communities, fulfilling every tropic role from primary producers to

carnivores. This together with their high reproductive rate and close contact with the environment potentially make them more useful biomonitors of the environment than higher eukaryotic organisms such macroinvertebrates and fish (Zoloterev, 2010).

Whilst the uptake of sub micron fluorescent particles has been examined with Choanoflagellates previously (Pettitt, 2001) the experiments were conducted in order to determine the feeding mechanism of the protozoa. High particle concentrations were used to optimise visualisation of the particles and were not designed to be environmentally realistic. Therefore it is not known whether MNPs at low concentrations will be intercepted by Choanoflagellates. During a review of the literature, no reference to the uptake of MNPs comprised of other materials such as metals or metal oxides has been found for Choanoflagellates. It is therefore unknown whether these environmentally relevant protozoa are capable of ingesting these types of MNPs and if so whether the particles prove to be toxic. Due to the relativity high abundance of AgNPs currently in use in commercial applications, along with Ag's long history as an aquatic pollutant, it is important to determine whether they are bioavailable to organisms such as the Choanoflagellates.

1.10 Aim

To investigate whether silver nanoparticles at near environmentally realistic concentrations are bioavailable and toxic to the environmentally relevant species of protozoa, the Choanoflagellate *Salpingoeca amphorium.*

1.11 Objectives

To synthesise monodispersed silver nanoparticles using a chemical reduction method.

To fully characterise the silver nanoparticles and effect of the Choanoflagellates culture medium upon the agglomeration state of the silver nanoparticles using a multi-method approach.

Use reflectance confocal microscopy in combination with transmitted light to simultaneously image the Choanoflagellates and nanoparticle reflected light, to ascertain whether nanoparticles are assimilated by the protozoa.

To quantitatively assess the toxic effects of the silver nanoparticles upon the Choanoflagellates during the time course of uptake studies.

1.13 Hypotheses

H_0 - In dilutions of Pratt's medium with greater ionic strength nanoparticle stability will not decrease and therefore agglomeration will not increase.

H_A - In dilutions of Pratt's medium with greater ionic strength nanoparticle stability will decrease and therefore agglomeration will increase.

H_1 - Silver nanoparticles will not be assimilated by the Choanoflagellate Salpingoeca amphoridium.

H_B - Silver nanoparticles will be assimilated by the Choanoflagellate Salpingoeca amphoridium.

H_2 - Silver nanoparticles will be not toxic towards Choanoflagellates.

H_C - Silver nanoparticle will be toxic towards Choanoflagellates.

H_3 - The toxicity of silver nanoparticles towards Choanoflagellates will not be greater for particles which are unwashed compared to those washed by ultrafiltration.

H_D - The toxicity of silver nanoparticles towards Choanoflagellates will be greater for particles which are unwashed compared to those washed by ultrafiltration.

2. Methodology

2.1 Synthesis of Silver Nanoparticles

2.1.1 Sodium Citrate Capped

Citrate stabilised AgNPs were synthesised in four sizes and labelled NPa, NPb, NPc and NPd. The NPs were synthesised using a chemical reduction method previously developed by Römer et al. (2011) from the methods used by Henglein and Giersig (1999) Doty et al (2005) and Cumberland and Lead (2009). For NPa, solutions of 100 ml sodium citrate (0.31 mM), 100 ml silver nitrate (0.25 mM) and sodium borohydride (10 mM) (see figure 2.1) were prepared by weighing appropriate amounts of solid and using ultrapure water (18.2 MΩ cm). These solutions were then equilibrated in the dark at 4^{o}C for 30 minutes. Under vigorous stirring 100 ml of sodium citrate and 100 ml of silver nitrate were then mixed together in a conical flask. After which 6 ml of sodium borohydride was added in one aliquot. After 10 minutes stirring at room temperature the solution was then slowly heated to boiling for 3 hrs. The change in appearance can be seen over the course of the nanoparticles synthesis as shown in figure 2.2.

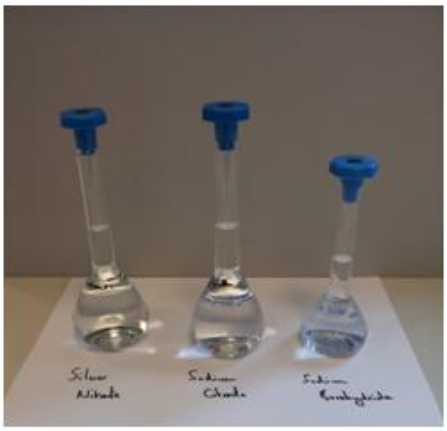

Figure 2.1 Solutions as prepared, left to right: 0.25 mM silver nitrate, 0.31 mM sodium citrate and 10 mM sodium borohydride.

Figure 2.2 Change in suspension during the synthesis of NPa. From left to right: Mixing of silver nitrate and sodium citrate, addition of sodium borohydride, after 10 mins of cold stirring and after 3 hrs of heating at boiling temperature.

Similarly, NPb and NPc were produced using the reduction method of preparation, however the concentrations of sodium borohydride were 0.25 mM and 1 mM respectively. Also prepared were NPd, using the same solutions as detailed in the NPa synthesis. In this case the heating process was carried out prior to the addition of the sodium borohydride solution, the mixture of sodium citrate and silver nitrate was heated for 3 hrs, 6 ml of sodium borohyride was then added and the solution was then stirred under heating for an additional 10 minutes.

2.1.2 Filtration

Filtration was used in order to remove Ag aggregates and agglomerates which may have formed during synthesis, in addition to any contamination in the form of dust which may have entered the sample. This was achieved using a Millipore Inc. filtration flask and funnel, the NP preparations were filtered through a 0.1 μm cellulose nitrate membrane (Millipore Inc.). In order to ensure the filter membranes were free of metal ion contaminants they were rinsed using 3 aliquots of 50 ml 10% nitric acid solution, prior to rinsing using 3 aliquots of 100 ml

ultrapure water in order to remove any remaining nitric acid. The NP suspensions were then filtered through the membrane 3 times before being stored in acid washed containers.

2.1.3 Ultracentrifugation

Ultracentrifugation was investigated as a method for reducing the amount of polydispersity within a NP suspension as synthesised via the sedimentation of large primary particles and agglomerates/aggregates within the sample. Samples were centrifuged at 15,000 rpm for 1hr, 10,000 rpm for 1hr, 10,000 rpm for 40 mins and 10,000 rpm for 30 mins (see figure 2.3)

Using the Beckman L7-65 ultracentrifuge in combination with the swing bucket SWTi40 rotor a pair of tubes containing 13 ml each of AgNP were used for each run. After which the top 5 ml (T5) and middle 5 ml (M5) of the centrifuge tube were transferred into separate acid washed containers for analysis. The pellet (P) formed at the bottom of the centrifuge tube was resuspended in the remaining 3 ml of fluid. These three fractions were then analysed using a combination of Dynamic Light Scattering, UV-Vis spectroscopy and Flame Atomic Absorption Spectroscopy.

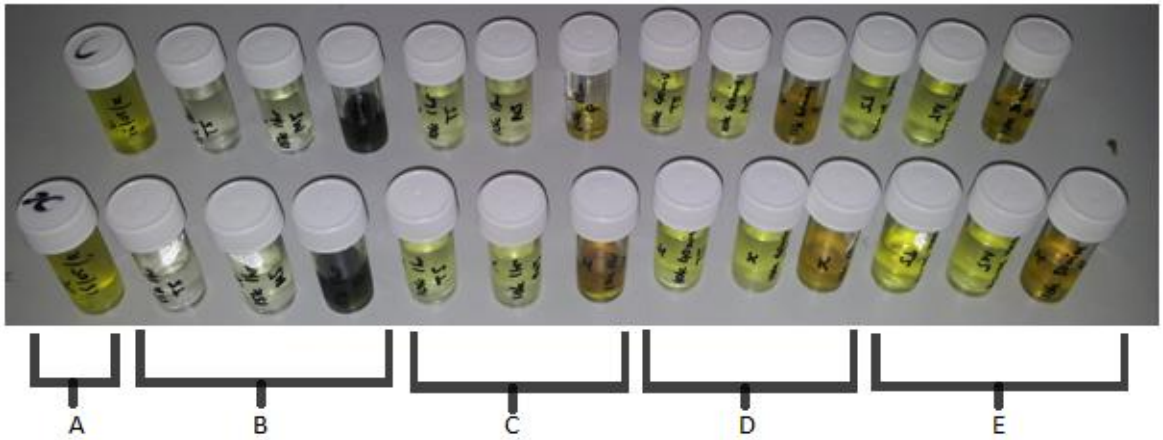

Figure 2.3 From left to right: A: original nanoparticle suspensions, B: fraction generated at 15,000 rpm 1hr, C: 10,000 rpm for 1hr, D: 10,000 rpm for 40 mins and E: 10,000 rpm for 30 mins.

2.2 Characterisation

2.2.1 Dynamic Light Scattering

Also known as Photon Correlation Spectroscopy or Quasi-electric Light Scattering, Dynamic Light Scattering (DLS) is used to measure the hydrodynamic diameter of NPs in suspension. NPs in suspension undergo Brownian motion, as a result of collisions with solvent molecules which are moving due to thermal energy, upon illumination with a laser (figure 2.4) the intensity of light scattered from these particles fluctuates depending on the particles size. (Malvern Instruments Ltd, 2012). In solution the NPs are dynamic and are hydrated, the diameter derived from the diffusion of these NPs is therefore the size of the dynamic/hydrated particles, hence the term hydrodynamic diameter (Malvern Instruments Ltd, 2011) as shown by figure 2.4a.

A.

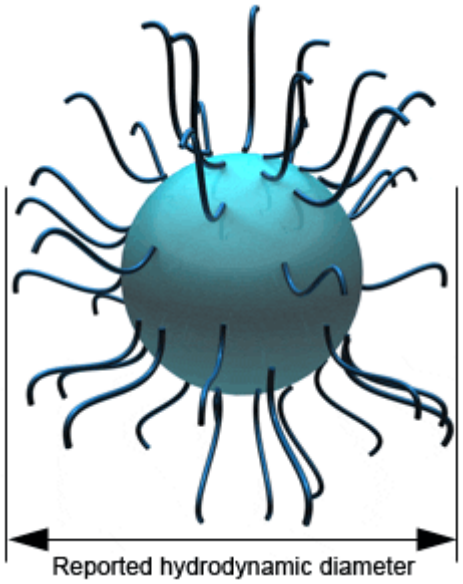

B.

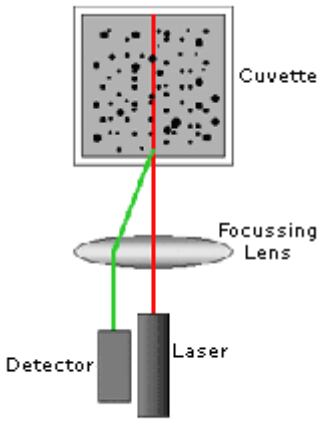

Figure 2.4 Diagram A: shows a hydrated nanoparticle and its hydrodynamic diameter. Diagram B: shows the set-up of dynamic light scattering operating in backscatter mode (173^{o}). (Mavern Instruments Ltd, 2012).

As the NPs diffuse though a solvent due to thermal motion, the scattered light from their surface undergoes interference effects. The intensity of this scattered light fluctuates randomly with time. The rate at which these fluctuations in light intensity decay reveals information about the particle size, with small particles having a relatively fast decay of fluctuations compared to their larger counterparts (Borkovec, 2002). An autocorrelation function based upon measurements of scattered light intensity over time can therefore be constructed (Baalousha and Lead, 2012).

This intensity correlation function may be written as followed:

Equation 2.1

$$g_2(t) = \frac{\langle I(t)I(0)\rangle}{\langle I^2\rangle}$$

This function can then be related to the normalized correlation function of the electric field of the scattered light g_1 (t) by the Siegert relationship (Borkovec, 2002).

Equation 2.2

$$g_2(t) = 1 + \ g_1(t)^2$$

As previously mentioned the autocorrelation function decays exponentially as a function of the correlator time decay is a function of the particle diffusion coefficient. By utilising the Stokes-Einstein equation it is then possible to calculate the hydrodynamic diameter of the NPs from the measured particle diffusion coefficient (Baalousha and Lead, 2012).

The Stokes-Einstein equation is as followed:

Equation 2.3

$$D = \frac{K_B T}{6\pi\eta R_h}$$

Where K_B, is the Boltzmann constant, T, the absolute temperature, η, is the viscosity of the solvent, and R_h, the hydrodynamic radius of the particles. Since the decay rate of the time correlation function can be measured very accurately, the particle size can then be reliably determined. The DLS technique works best with particles which are monodisperse and can be used to make measurements with accuracy of a few percent, although moderately polydispersed samples may also be analysed (Borkovec, 2002). With light scattering the

polydispersity of a sample can be derived from the polydispersity index, a parameter which can be calculated from a cumulant analysis of the measured intensity autocorrelation function (Malvern Instruments Ltd, 2011). Cumulant analysis is a relatively popular technique in which the correlation function is expanded as follows:

Equation 2.4

$$\ln g_1(t) = -\mu t + \frac{\mu_2}{2} t^2 + \ldots$$

This analysis is able to give a measure of particle polydispersity (Borkovec, 2002). Also obtained from the cumulant analysis is the z average diameter of the particles, which is defined by ISO 22412 as the harmonic intensity average particle diameter.

All DLS measurements were performed using a Malvern Zetasizer nano with the NP samples placed in plastic low volume disposable sizing cuvettes (ZEN0112). A standard operating procedure (SOP) was kept constant and used for all measurements. The Zetasizer instrument was operated in backscatter mode at an angle of 173^{o} (Hackley and Clogsten, 2007). The values for the refractive index and absorption of the material (Ag) were obtained from the Malvern instrument manual, and the refractive index was set to 0.540 and absorption set to 3.00 according. The dispersant in this instance was water with a refractive index of 1.330 and a viscosity of 1.0031 cρ both selected from the preset instrument options. The temperature used during the measurements was set to 20^{o}C with an equilibration time of 120 seconds allowed for each sample. In order to ensure reliability of the measurements, a minimum of 5 runs replicates were performed for each sample.

2.2.2 Nanoparticle Tracking Analysis

Nanoparticle Tracking Analysis (NTA) uses a 635 nm laser beam passed through a prism-edged optical flat, with a refractive index which allows the beam to refract at the interface between the flat and a layer of liquid above. Due to this refraction the laser beam compresses to a low profile, intense illumination region in which NPs present in the liquid can be visualised (Nanosight Ltd, 2009a).

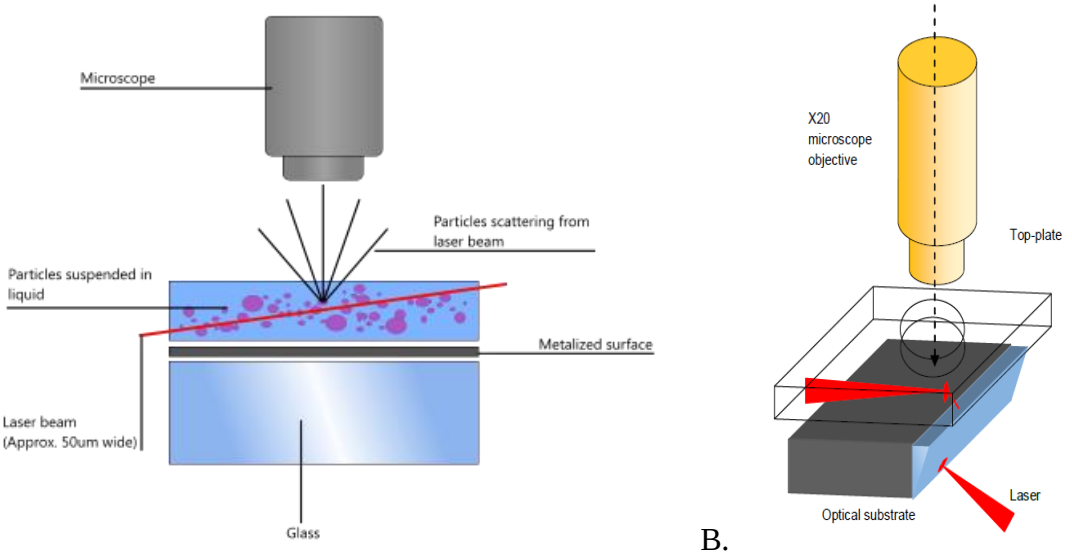

A. B.

Figure 2.5 Diagrams to showing the setup used during Nanoparticle tracking analysis (Nanosight Ltd, 2009a).

A x20 magnification objective lens on a conventional microscope is used in conjunction with a CCD camera operating at 30 frames per second is used to capture video images of the NPs. Using the camera it is possible to visualise NPs in the scattering volume moving under Brownian motion, the NTA software is then able to simultaneously indentify and track the centre of each NP (see figure 2.5)

A.  B. 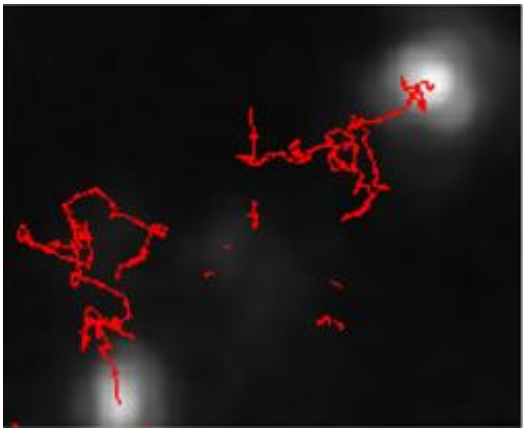

Figure 2.6 A: Frame of a video micrograph of sample NPa. B. An images demonstrating the output from the analysis software whilst tracking particles. (Nanosight Ltd, 2009).

The distance each individual NP travels in the X-Y plane is then calculated by the NTA analysis software (figure 2.6). From this distance, the particle diffusion coefficient may be obtained, once this information is combined with the sample temperature and the solvent viscosity, the particle hydrodynamic diameter can then be calculated. The following variation on the Stokes-Einstein equation is then used in order to accommodate the 2D tracking of 3D brownian motion:

Equation 2.5

$$\frac{(x,y)^2}{4} = D_t = \frac{TK_B}{3\pi\eta d}$$

Where Dt, is the particle diffusion coefficient, T, is the temperature, η, the solvent viscosity, $K_{B,}$ is the Boltzman constant and d, the particle hydrodynamic diameter.

NTA analysis was used to characterise the AgNPs as synthesised and provide a comparison between the alternative technique DLS. The sample cell containing the optical flat was dismantled prior to use and thoroughly washed using a 70% ethanol solution. The sample cell

was then reassembled and washed 70% ethanol solution injected into the cell using a 5 ml syringe followed by 3 aliquots of ultrapure water.

2.2.3 UV- Vis Spectroscopy

In metal NPs such as Ag, their conduction band and valence band are in very close proximity, which gives rise to a collective oscillation of electrons known as surface plasmon resonance. The electric field of an incoming wave of light induces a polarization of the electrons with respect to much heavier ionic core of the AgNP (Cao, 2004). This results in a net charge difference which in turn acts as a restoring force creating a dipolar oscillation of all the electrons with the same phase, the observed colour of the suspension is as a result of the frequency of the electromagnetic field which when resonant with the coherent electron motion gives rise to a strong absorption of the light (Das et al., 2009). This strong absorption of light can be measured using a UV-Vis spectrophotometer.

The double-beam UV-Vis spectrophotometer is able to switch between a Tungsten halogen lamp in order to generate wavelengths of light in the visible region and a deuterium lamp for wavelengths in the UV region (Jenway, 2009). In order to restrict and isolate wavelengths of light from the lamps the light beam must be passed through a light filter. Refractive and absorption filters are the types commonly used. Refractive filters rely on the refraction of light as it passes through different materials creating constructive and destructed interference. Whilst the absorption filters simply absorb wavelength of light that are not of interest, although these types of filters tend to be less precise than the refractive filters, still allowing some unwanted wavelengths through (U.C. Davis, 2012).

The double beam design as opposed to the simpler single spectrophotometer (figure 2.7), allows for inconsistencies such as fluctuations in the source beam intensity to be corrected for. This is achieved by splitting the light beam at the monochrometer, as shown in figure 2.7 part of the light beam travels through the sample cell, whilst part travels through a reference cell containing a blank, both are received at independent detectors. The signal from the reference cell can then be subtracted from the sample cell to remove background noise.

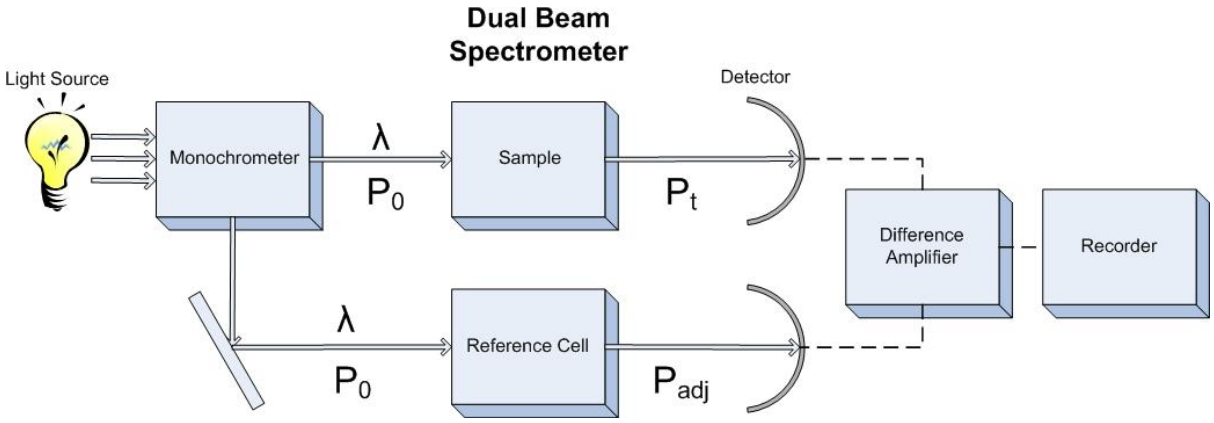

Figure 2.7 A diagram showing the components and setup of a typical double UV-Vis spectrophotometer (U.C. Davis, 2012).

All UV-Vis spectroscopy measurements were performed using a 6800 Jenway UV-Vis spectrophotometer, with samples contained in Plastibrand disposable cuvettes with a 1 cm path length. For measurements on NP suspensions the instrument was blanked using ultrapure water prior to each session and each sample was run a minimum of 3 times to ensure reliability. UV-Vis spectroscopy was also used to investigate the stability of AgNPs in Pratt's medium used during the preparation of experimental cultures of Choanoflagellates and during the uptake and toxicity studies. To examine the initial effect upon stability of the AgNPs in

the media the spectrophotometer was blanked using Pratt's medium and a minimum of 10 measurements were recorded.

2.2.4 Fluorescence Spectroscopy

It has been demonstrated that silver nanoclusters may act as bright photostable fluorophores, these nanoclusters may be synthesised using a variety of scaffolds including NPs. These silver nanoclusters below 1 nm in diameter process discrete energy levels comparable to the energy levels present in molecules allowing silver nanoclusters to interact strongly with light to produce intense light absorption and emission (Diez and Ras, 2011). At room temperature electrons in discrete energy levels generally occupy the lowest electronic state available. Upon excitation via absorption of light electrons may be promoted to occupy higher energy levels, this excess energy maybe rapidly lost with the resultant emission of a quanta of energy in the form of a photon (PerkinElmer, 2006). This absorption of light at one wavelength and emission of light at a longer wavelength is termed fluorescence.

Excitation-emission matrix fluorescence spectroscopy was used to examine the fluorescent properties of AgNPs. All fluorescence measurements were performed using a Cary Varian Eclipse 3D fluorescence spectrophotometer, with samples contained in a quartz cuvette with a path length of 1 cm. In order to obtain the excitation-emission matrices a slit width of 5nm and an excitation voltage of 725V were used. With a range of excitation between 300-800 nm and a minimum excitation scan step size of 10 nm intervals. A Raman background was performed using a sealed water cell at an excitation wavelength of 370 nm (Baker, 2002) at the beginning of each session, in order to compensate for variation in lamp intensity.

The data could then be corrected to 20 Raman units using the following equation:

Equation 2.6

$$Corrected\ intensity = \frac{Raman\ Units}{20}\ x\ Uncorrected\ Units$$

2.2.5 Atomic Force Microscopy

Atomic Force Microscopy (AFM) can be used to give qualitative and quantitative information on the physical properties including size, morphology, surface and texture of NP samples along with statistical information such as; surface area, and volume distributions. Using AFM it is possible to attain data on NPs in three dimensions, however accuracy in the vertical, or Z axis is greater than in the horizontal, or X-Y plane. The accuracy on the Z axis (typically 0.1 nm) is limited by the amount of vibration present during the measurement, whereas the accuracy in the X-Y plane (typically 1 nm) is limited by the interaction between the AFM tip and sample surface (Scalf and West, 2006).

Typically an AFM setup includes (see figure 2.8) a microcantilever probe with a sharp tip which is mounted to a piezoelectric actuator with a position sensitive photo-detector, used to receive a reflected laser beam off the back of the cantilever and allows for deflection feedback (Pishkenari et al., 2006).

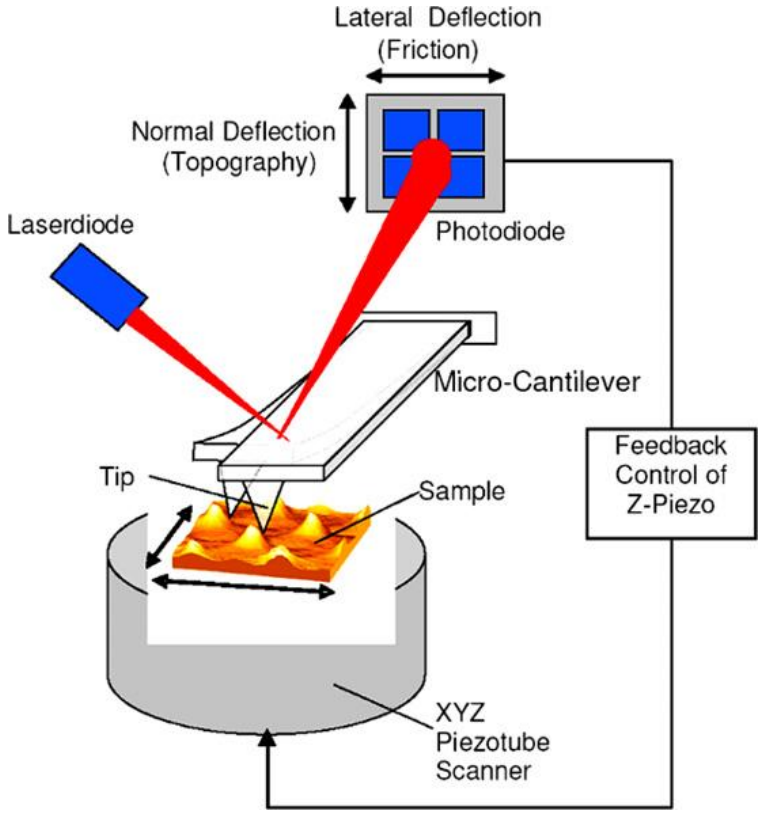

Figure 2.8 A diagram showing the components of a typical AFM setup and operation (Pishkenari et al., 2006).

Potential energy between the sample and the cantilever tip (V_{ts}) as the tip moves over the sample results in a tip-sample force (F_{ts}) with a component in the Z direction. This relationship between the potential energy and force of the tip-sample interactions is given by the following equation:

Equation 2.7

$$F_{ts} = \frac{-\partial V_{ts}}{\partial z}$$

Forces included in these interactions are; van der Waals, electrostatic and chemical interactions, particularly Morse potential and Lennard-Jones potential (Bhushan, 2004). The

van der Waals forces are caused by the fluctuations in the electric dipole moments of atoms and their mutual polarisation. For a spherical tip next to a flat sample surface the van der Waals forces (V_{vdW}) are given by:

Equation 2.8

$$V_{vdW} = -\frac{A_H}{6z}$$

Where Z is the distance between the centres of the surface atoms and the centre of the closest atom of the AFM tip. The Hamaker contant (A_H) used is dependent upon the atomic polarisablity and density of the tip and the sample, but for most solids is often on the order of 1 eV (Bushan, 2004). Electrostatic forces may also play a role in the tip-sample interactions if both the AFM tip and the sample are conductive materials, with an electrostatic potential difference with does not equal zero. For a spherical tip this relationship can be described by:

Equation 2.9

$$F_{electrostatic} = -\frac{\pi\varepsilon_0 R U^2}{z}$$

The Morse and Lennard-Jones potentials are the empirical model potentials for chemical bonds.

Equation 2.10

$$V_{Morse} = E_{bond}(2e^{-\kappa(z-\sigma)} - e^{-2\kappa(z-\sigma)})$$

Equation 2.11

$$V_{Lennard-Jones} = E_{bond}\left(2\frac{\sigma^6}{z^6} - \frac{\sigma^{12}}{z^{12}}\right)$$

These potentials describe a chemical bond with a bonding energy, E_{bond}, where σ, is the equilibrium distance and in the case of the Morse potential κ, is the decay length.

Prior to analysis using AFM the NP samples were prepared using ultracentrifugation (Wilkinson et al., 1999). Freshly cleaved mica sheets (Agar Scientific) were placed in Ultra-Clear™ 14 ml centrifuge tubes (Beckman Coulter). 200 µl of AgNP suspension were diluted by addition of 12 ml of ultrapure water. The tubes were then sealed using parafilm and were centrifuged at 30,000 rpm for 1 hour using a Beckman L7-65 ultracentrifuge with SW40Ti swing bucket rotor.

The length of time needed to sediment the AgNPs onto the mica sheet was calculated from the following equation:

Equation 2.12

$$D = \left(\frac{18\eta \ln(R_f/R_0)}{(\rho_p - \rho_f)\omega^2 t}\right)^{0.5}$$

Equation 2.12 may then be rearranged to give:

Equation 2.13

$$t = \left(\frac{18\eta \ln(R_f/R_0)}{d^2(\rho_p - \rho_f)\omega^2}\right)$$

Where t, is time for sedimentation (s), η, is the viscosity of the solution (Poise), $R_{p,}$ is the final radius of rotation (cm), $R_{0,}$ is the initial radius of rotation, d, is the diameter of the nanoparticles (cm), $\rho_{p,}$ is the density of the particle (gcm^{-2}), $\rho_{f,}$ is the density of the fluid and ω, is the angular rotation speed ($rads^{-1}$) (CPS Instruments, 2007). Once the samples were

removed from the ultracentrifuge they were suspended in ultrapure water for 2 minutes, with the water replaced after an interval of 1 minute. This procedure was used in order to remove excess salts which may have accumulated on the mica surface.

All AFM measurements were performed using a XE-100 AFM (Park systems Corp., Suwon, Korea) in true non contact mode. The pre-mounted silicon non contact cantilevers (NSC36) used, were purchased from Park systems Corp., Suwon, Korea. The topographical AFM images were analysed and the NP heights were obtained using the analysis software package XEI (Park systems Corp., Suwon, Korea). For each sample at least 100 height measurements were performed, excluding those of agglomerates to avoid including data from sample artefacts. These measurements were taken from images obtained from a random selection of areas on the mica surface.

2.2.6 Transmission Electron Microscopy

The optics employed in the use of an electron microscope may be regarded as analogous to those used in conventional light optics. Although, due to their strong interaction with matter compared to that of photons, electrons must be accelerated in a high vacuum of at least 10^{-4} Pa (Kelsall et al., 2005). The wavelength of accelerated electrons however is considerably smaller than the wavelength of light, significantly increasing resolution by up to 1000 times (Aguilera and Stanley, 1996).

The wavelength, λ, of the electrons used in the microscope is given by the de Broglie relationship:

Equation 2.14

$$\lambda = \frac{h}{\sqrt{2mqV}}$$

Where m and q, are the electron mass and charge, h, is Planck's constant, and V, is the potential difference through which the electrons are accelerated. The greater the operating voltage of a TEM instrument, the smaller the electron wavelength which therefore increases lateral spatial resolution (Cao, 2004). An electron beam may be produced using two methods, thermionic emission in which thermal energy is utilised to overcome the surface potential barrier of a solid source to allow release of electrons from the materials conduction band. A typical thermionic electron gun consists of a tungsten filament heated resistivity to 2800K. Alternatively an electron beam may be produced by field emission in which an extremely high electric current is used to reduce the surface potential barrier of the emitter (Kelsall et al., 2005). Due to the negative charge of the electrons it is then possible to focus the electron beam using magnetic or electric fields. Typically the highly focused electron beam is then capable of penetrating samples between 100-200 nm in thickness (Ebnesajjad and Khaladkar, 2005), prior to project on to a fluorescent screen or video camera. Figure 2.9 shows a typical TEM setup.

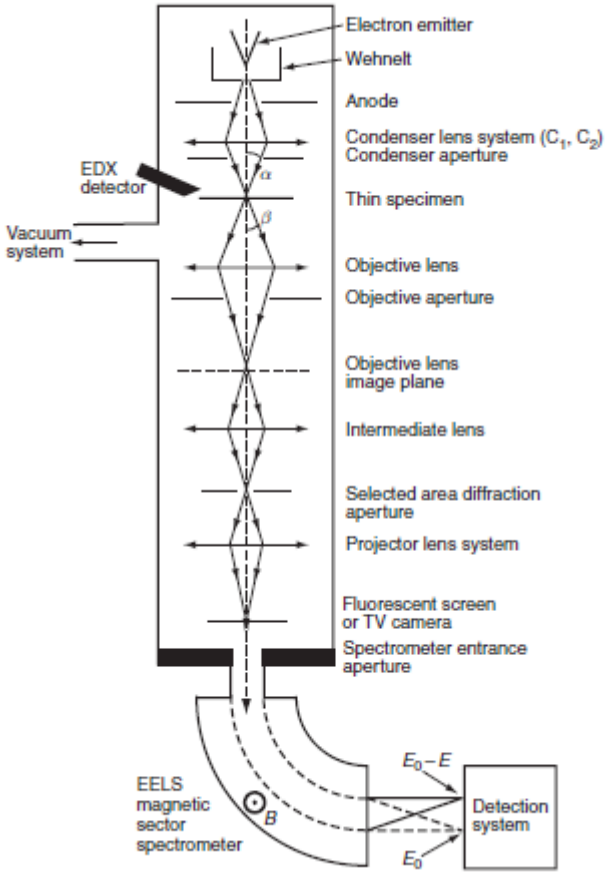

Figure 2.9 A diagram showing the typical setup and operation of a Transmission Electron Microscope (Kelsall et al., 2005).

Samples were prepared for TEM analysis using copper mesh TEM grids coated in a holey carbon film, purchased from Agar Scientific. Holey grids were used as the edges in the carbon film serve as a focusing guide, greatly aided the process of image focusing. A drop deposition method of TEM preparation was utilised with 20 µl of neat stock suspension of NPs as synthesised placed upon the grid surface for 1 hr. During this time the grids were covered to prevent contamination and any sample lost through evaporation was replaced to ensure the grid surfaces were exposed to NP suspension throughout the hour. In order to remove any excess salt upon the surface of the sample the TEM grids were suspended in ultrapure water

for 1 minute, with the water replaced after an interval of 30 seconds. The grids then were analysed using a JEOL JEM-2010 TEM, with a maximum resolution of 0.19 nm.

2.2.7 Energy Dispersive X-ray Spectroscopy

Energy Dispersive X-ray Spectroscopy (EDX or EDS) is a powerful technique used to identify the elemental composition of a sample, the spectrometer is attached to an electron microscope and is capable of giving information on the sample under investigation with a sensitivity of >0.1% for elements heavier than carbon (Cranfield, 2010). Atoms at the surface of the sample in the path of the electron beam become excited by the electrons, releasing x-rays which are characteristic of the atomic structure of the element they originated from (Ebnesajjad and Khaladkar, 2005).

EDX was used to give the elemental compositions of the sample sent for TEM analysis, in order to ensure that the AgNPs were free from any contamination which may affect their toxicity. The measurements were performed with a Oxford Instruments LZ5 windowless energy dispersive X-ray spectrometer controlled by INCA, which was fitted to a JEOL JEM-2010 TEM.

2.2.8 Flame Atomic Absorption Spectroscopy

Flame Atomic Absorption spectroscopy (FAAS) (figure 2.10) is an analytical chemistry technique which can be used to determine the concentrations of approximately 70 elements, the majority of which are metals. During analysis the sample is atomised at a temperature between 2500-3000^{o}C, these free atoms may only absorb specific wavelengths of line depending on their electronic configuration in the excited state (Luca, 2004). These excitation energies are determined by the difference between the energy level of the ground state and one of the excitation states of the electrons. In order to generate the source radiation of light a hollow cathode lamp is required, the lamp consists of a tungsten anode along with a cup-shaped cathode made from the element being analysed and a carrier gas such as neon (Higson, 2004). When a voltage is applied to the lamp radiation is emitted primarily from the atom to be observed in absorption.

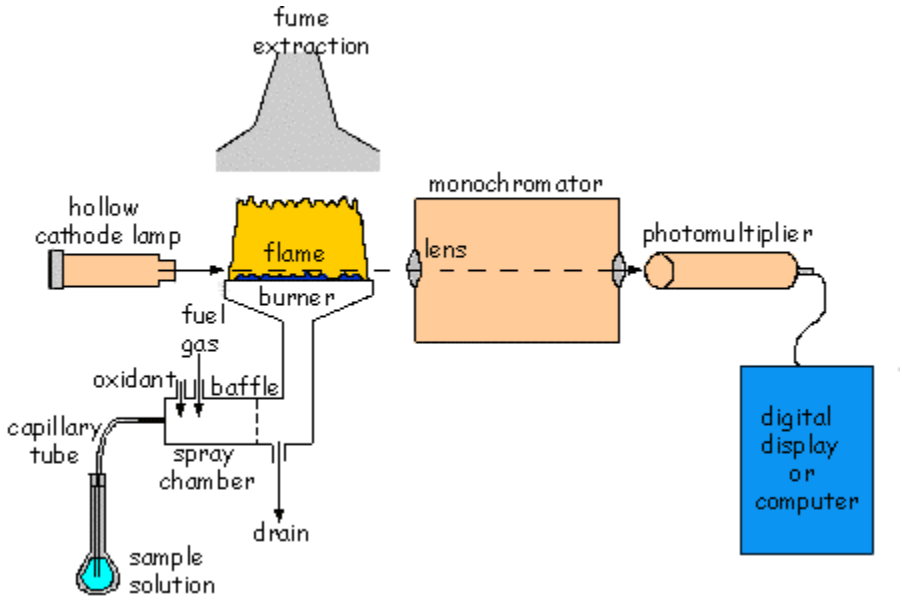

Figure 2.10 A schematic diagram of a typical Flame Atomic Absorption Spectrophotometer (British Museum as cited in Luca 2004).

All FAAS measurements were performed using a Perkin Elmer Instruments AAnalyst 300 atomic absorption spectrophotometer, equipped with a Ag specific hollow cathode lamp with a maximum current of 10 mA. During analysis the Ag samples were atomised using an acetylene-air flame. Standard solutions at 0.1, 0.2, 0.5, 1 and 2 ppm were prepared by dilution of a 1000 ppm stock solution containing Ag dissolved in 2% nitric acid and were then used to generate a calibration curve. To ensure the Ag concentration of the samples fell within the range of the calibration curve dilute solutions i.e. those that were colourless were diluted 2 times and concentrated samples i.e. those dark in appearance were diluted by at least 10 times using ultrapure water. This also had the effect of reducing the quantity of sodium from the capping atomised in the spectrophotometer, which otherwise may have influenced the analysis for Ag. Each sample measurement was repeated three times with water aspirated in the spectrophotometer between samples, to prevent cross contamination.

2.3 Culturing of Choanoflagellates

A stock of *Salpingoeca amphoridium* was maintained in a non specified broth, cereal grass infusion at 20^{o}C. The Cereal Grass medium for the maintenance of the *Salpingoeca amphoridium* stock culture was prepared as followed:

Powdered cereal grass leaves	2.5g
Na_2HPO_4	0.5g
Ultrapure Water	1.0L

Water was heated to boiling point, followed by the addition of the cereal leaves. The mixture was heated for 5 minutes before being filtered through Whatman No. 1 filter paper (removing leaves and dust). Na_2HPO_4 was then added prior to placing 60 ml of the infusion into a 100 ml acid washed conical flask, which was then sealed and autoclaved. This infusion allowed for their prey bacteria *Klebsiella pneumoniae* to be co-cultured along with the Choanoflagellates, in order to provide them with a source of nutrition. Two duplicate stocks were subcultured every two weeks by transferring 5 ml of stock solution into 40 ml to new sterile media.

To gain the best quality images using confocal microscopy high numbers of choanoflagellates that were fixed to a substrate was required, along with low levels of bacteria which could otherwise interfere with imaging. To achieve this, fifteen lengths of human hair were washed in absolute ethanol, air dried and placed into 25 ml of sterile Pratt's medium (Karpov and Leadbeater, 1997). The Pratt's medium for the experimental cultures of *Salpingoeca amphoridium* was prepared as follows:

Stock Solutions

KNO_3	10g
$MgSO_4 \bullet 7H_2O$	1g
$K_2HPO_4 \bullet 3H_2O$	1g
$FeCl_3 \bullet 6H_2O$	0.1g
Ultrapure Water	400 ml

Each compound was dissolved in 100 ml of ultrapure water in acid washed 200 ml Duran flasks, then autoclaved before storing at 4^{o}C. To prepare the media 1 ml of each stock solution was placed into a autoclaved Duran flask (1L) and 996 ml of ultrapure water were added to make the solution up to 1L. The solution was then mixed and the pH adjusted to 7.2. To the Pratt's medium *Klebsiella pneumonae* which had been grown on nutrient agar for 48 hrs at 25^{o}C was added. The nutrient agar was prepared by the following method:

Yeast Extract	4g
Powdered D-Glucose	0.16g
Oxoid No. 3 Agar	20g
Ultrapure Water	800 ml

Each ingredient was into the ultrapure water in a 1L Duran flask and autoclaved. Whilst the solution was still warm 22 ml of the liquid was dispensed under aseptic conditions into disposable Petri dishes. For the experimental cultures of Choanflagellates 1.5 ml Nitrate / Phosphate additive was added to the Pratt's medium in order to promote the growth of *Klebsiella pneumoniae* which would otherwise not be sustained by the medium. The additive was produced as follows:

$NaNO_3$	5g
Na_2HPO_4	0.75g
Ultrapure Water	100 ml

Each compound was dissolved in the ultrapure water, 3 ml aliquots were then taken and dispensed into 5ml, acid washed screw top vital and autoclaved. 3 ml of the additive was then added to 1L of Pratt's medium as required. The medium was then inoculated with 1 ml of the choanoflagellates stock culture and maintained at 20^{o}C, this allowed for the growth of high numbers of choanoflagellates.

In order to reduce the number of residual bacteria sixteen hours prior to imaging with the confocal microscope the strands of human hair were removed from the culture medium, and transferred to 15 ml of fresh Pratt's medium. This also had the effect of starving the choanoflagellates, which was beneficial in increasing the number of cells that exhibited a feeding response when presented with prey particles, along with increasing the length of time individual cells exhibited the feeding response. Human hair was used for the substrate due the superior degree of Choanoflagellate attachment when compared to other materials. It also refracts less light than other substances (important for use with the confocal microscope) and is easily autoclaved (Pettitt, 2001).

For initial uptake studies, immediately prior to imaging the cells were removed from the starvation media and placed into a AgNP suspension within an imaging dish. In order to investigate the uptake of AgNPs at the lowest concentrations it was necessary to incubate the Choanoflagellates with AgNPs for 24 hrs. Choanoflagellates incubated with AgNPs for 24 hrs were taken directly from the experimental cultures and not placed in starvation media prior due to the additional cell stress and cell loss caused by the starvation process over extended periods of time.

2.4 Imaging of Nanoparticle Uptake

2.4.1 Reflectance Confocal Microscopy

In wide field microscopy as an image is formed using a lens in which multiple points may be viewed simultaneously, for example in figure 2.11 (frame 1) cells are present one at the focal point and another away from that point. In frame 2 a pinhole conjugate has been introduced to pass all the light from the focal point, whilst receiving very little of the light from the other point which is out of focus. Frame 3, uses a light source confocal to the focal point, in order to intensify the light on the point of interest, without significantly increasing the amount of light on the other out of focus point (Webb, 1996). This is allows for a very high increase in contrast even in very thick specimens with lots of bright objects, and is the basis for confocal microscopy. When compared to the more conventional widefield optical microscopy, confocal microscopy holds several advantages. Using confocal microscopy it is possible to control the depth of field, eliminate or reduce background light away from the focal plane which could otherwise cause degradation, and it is possible to collect several optical sections from a single specimen (Claxton et al., 2008).

Confocal microscopy is more commonly associated with the use of fluorescence imaging. Confocal reflectance microscopy uses light reflected back from the sample as opposed to the transmitted light. This can give additional information about a sample including information from unstained tissues, tissues labelled with probes that reflect light, and in combination with fluorescence (Paddock, 2002).

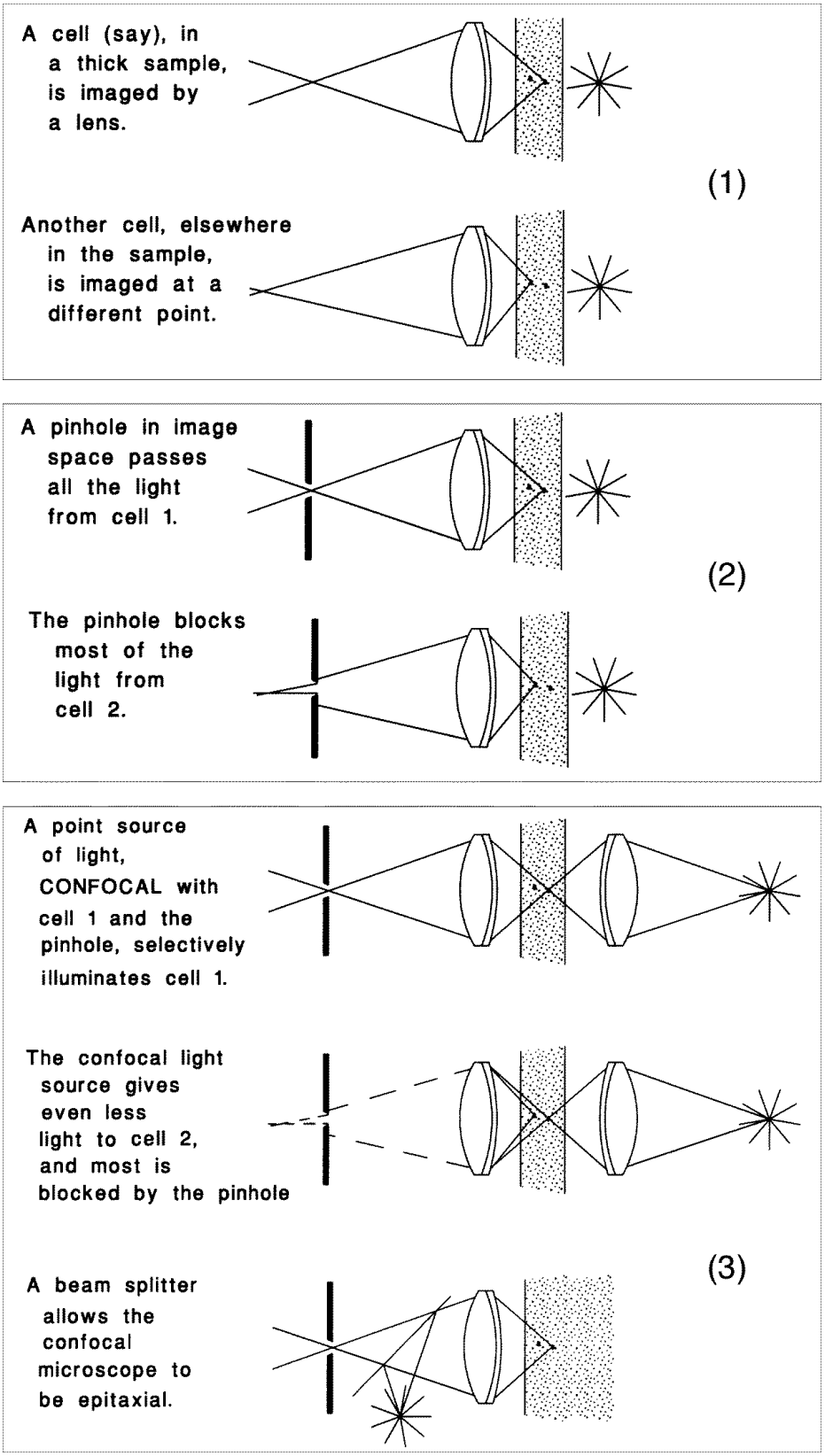

Figure 2.11. Diagram showing the progression from wide field microscopy to confocal microscopy (Webb, 1996).

Metal NPs such as gold and silver have been shown to scatter coloured light when illuminated with white light (Yguerabide and Yguerabide, 1998). In contrast, the light reflected from living tissue has been demonstrated to be minimal in comparison with the light reflected from metal NPs (Davies et al., 2011). This allows metal NPs to act effectively as probes for reflectance confocal microscopy (Nikon, 2002).

Single strands of substrate were transferred from the starvation media or AgNP incubation to a 35 mm dish equipped with a glass coverslip (MatTek), and covered in either fresh Pratt's or NP solution. The use of the 35 mm culture dishes was adopted in preference to sealed glass slides as they did not restrict the cells oxygen supply allowing the imaging live Choanoflagellate cells for longer. All confocal microscopy images were taken using Zeiss LSM 710 ConfoCor 3 in reflectance mode using a 488 nm laser line. In order to obtain images of both the specimen and AgNPs the bright field transmitted light images and reflected light confocal images were collected simultaneously. A combination of z stacks, time series and single image micrographs were obtained. Images from the two lines were then digitally merged into a single image, z stack or time series using the software package ImageJ. This allows both the transmitted light image and reflected light images to be viewed simultaneously.

2.5 Nanoparticle Toxicity Testing

Strands of substrate with Choanoflagellates attached were placed into 15 ml of fresh Pratt's medium 16 hrs prior to the toxicity test in order to mimic the experimental conditions used to image NP uptake. The strands of substrate were then transferred into 7 ml glass bottles and the Choanoflagellates incubated with 5 concentrations of unwashed AgNPs (5.5 mg/L, 1 mg/L, 500 μg/L, 100 μg/L, 11 μg/L and 2 μg/L). The Choanoflagellate were incubated with the NP suspensions for 4 hrs, prior to examination using phase-contrast microscopy. Additionally, two control Choanoflagellate cultures were maintained; a handling control in which the Choanoflagellate containing substrate was transferred into fresh Pratt's medium without NP exposure and a Null control in which the Choanoflagellates were left in the starvation culture. For this initial experiment a minimum of 50 Choanoflagellates along a strand of substrate for each concentration were assessed and categorised using the following criteria;

- Alive – Both microvilli and flagellum are extended, cell may or may not be actively feeding.
- Dead – Microvilli and flagellum are fully retracted, cell bodies contains condensed organelles.
- Underdetermined – Microvilli and flagellum are retracted, however no obvious changes within the cell body.
- Note: Unoccupied theca were not counted amongst the deceased cells, as death of the host cell will likely have occurred outside the timeframe of the toxicity study.

The Choanoflagellate cultures were then incubated in their respective solution for a further 20 hrs and reassessed using the toxicological criteria.

In order to establish the toxicological affect caused by AgNPs, the NPs were washed using ultrafiltration to remove excess dissolved Ag^+ from the NP suspension. Using an acid washed 10 ml Millipore Inc. ultrafiltration cell 10 ml aliquots of AgNP suspension were filtered through a 25 mm 1 kDa regenerated cellulose membrane (Millipore Inc.) under a pressure of 1bar. Before use the ultrafiltration membranes were washed for 24 hrs in 2% nitric acid to remove any metal ions which would otherwise contaminate the sample. The membrane was then neutralised for 24 hrs in ultrapure water, additionally prior to use of the membranes 5 ml of ultrapure water were filtered through them to ensure no excess acid remained. The AgNP aliquots were washed at least three times and the volume maintained at 10 ml using 0.31 mM sodium citrate solution.

This process was then repeated for the NPs washed by ultrafiltration, replicating the same handling and null controls as for the unwashed NP toxicity tests. However, for the washed NPs a positive control using the 5.5 mg/L AgNPs suspension was added. The Choanoflagellates were incubated with four concentrations of washed AgNPs (500 μg/L, 200 μg/L, 100 μg/L and 11 μg/L) for 24 hrs and accessed following the before stated criteria.

3. Results

Nanoparticle Characterisation

3.1 Nanoparticles as Synthesised

To establish any transformations which occur to the AgNPs under environmental exposure conditions it was deemed necessary to first fully characterise the physiochemical properties of the NPs as synthesised. In order to achieve this, a multi-method approach was adopted to quantify the NP properties (Domingo et al., 2009).

3.1.1 Dynamic Light Scattering

Measurements by DLS were used to identify the hydrodynamic diameter obtained from each method of AgNP synthesis, along with a measure of the polydispersity of each sample. It was found that the AgNPs prepared by method NPa had the greatest hydrodynamic diameter. A summary of which can be found in Table 3.1.

Table 3.1 Z-average diameters of silver nanoparticle prepared by 4 methods as measured by DLS. Diameters are a mean of 5 measurements ± standard deviation.

	Z-average Hydrodynamic Diameter / nm	**Polydispersity Index**
NPa	36.68 ± 0.16	0.186
NPb	22.80 ± 0.36	0.223
NPc	27.10 ± 0.26	0.173
NPd	17.56 ± 0.40	0.209

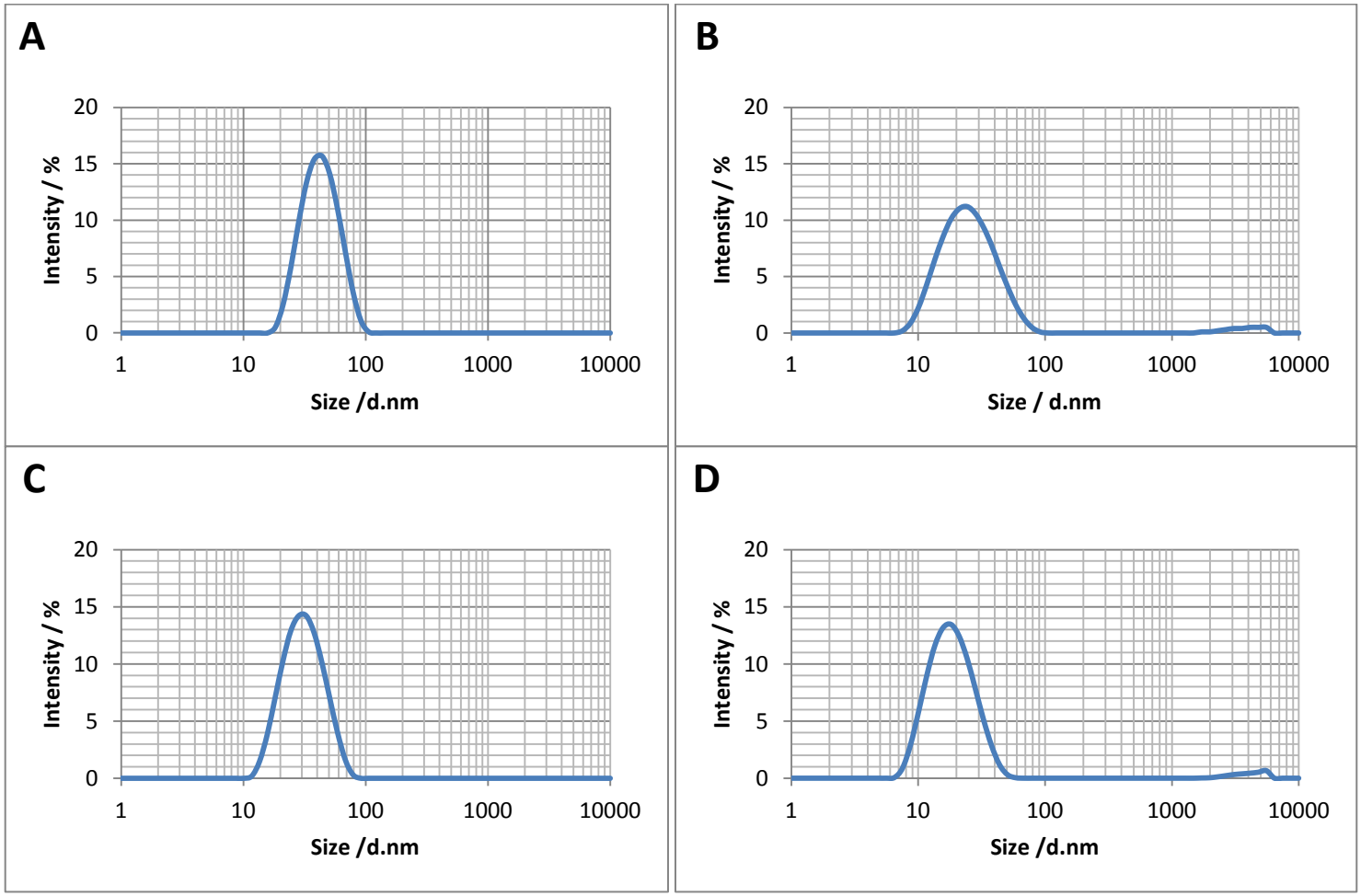

Figure 3.1 Size distributions by intensity as measured using DLS. **A**. NPa, **B**. NPb, **C**. NPc and **D**. NPd.

Additionally size distribution graphs were produced for each AgNP method of synthesis (Figure 3.1) by plotting scattering intensity versus particle size. Based upon the analysis of the DLS results it was decided that NPa, which had the greatest hydrodynamic diameter and would be most likely to be visualised by confocal reflectance microscopy and should be continued for further physicochemical analysis. Therefore the remainder of the NP characterisation consists of AgNPs synthesised via method NPa.

3.1.2 Nanoparticle Tracking Analysis

NTA which also measures hydrodynamic diameter was used to complement the results which were obtained by DLS. It was found by NTA that the AgNPs produced by method NPa possessed a hydrodynamic diameter of 46 ± 14 nm for NPa, compared to a diameter of 36.68 ± 0.16 nm as measured by DLS. A histogram containing the intensity distribution is shown (Figure 3.2).

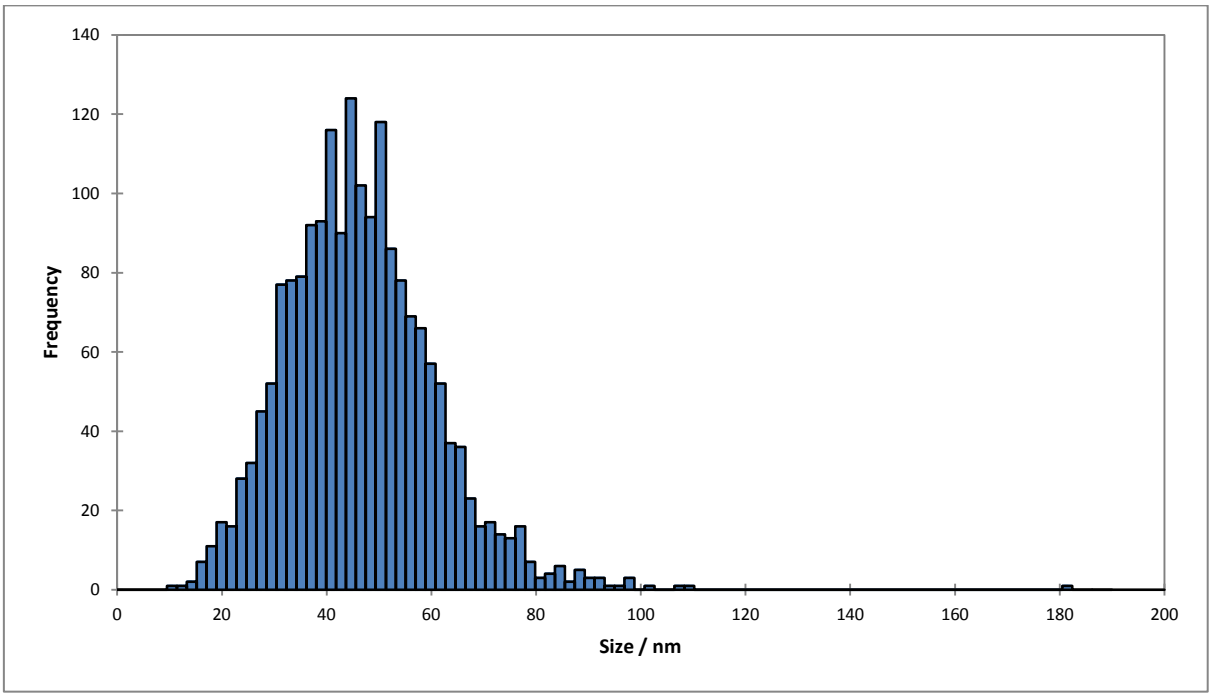

Figure 3.2 Size distribution by intensity as measured by NTA for NPa.

3.1.3 Atomic Force Microscopy

Micrographs were taken of randomly selected areas on the mica substrate examples of which are shown in figure 3.3. It was found that the mean size for NPa was 19.3 ± 6.6 nm. To attain a size distribution (figure 3.4) for the core size of the AgNP AFM was used to measure the height of a minimum of 100 NPs.

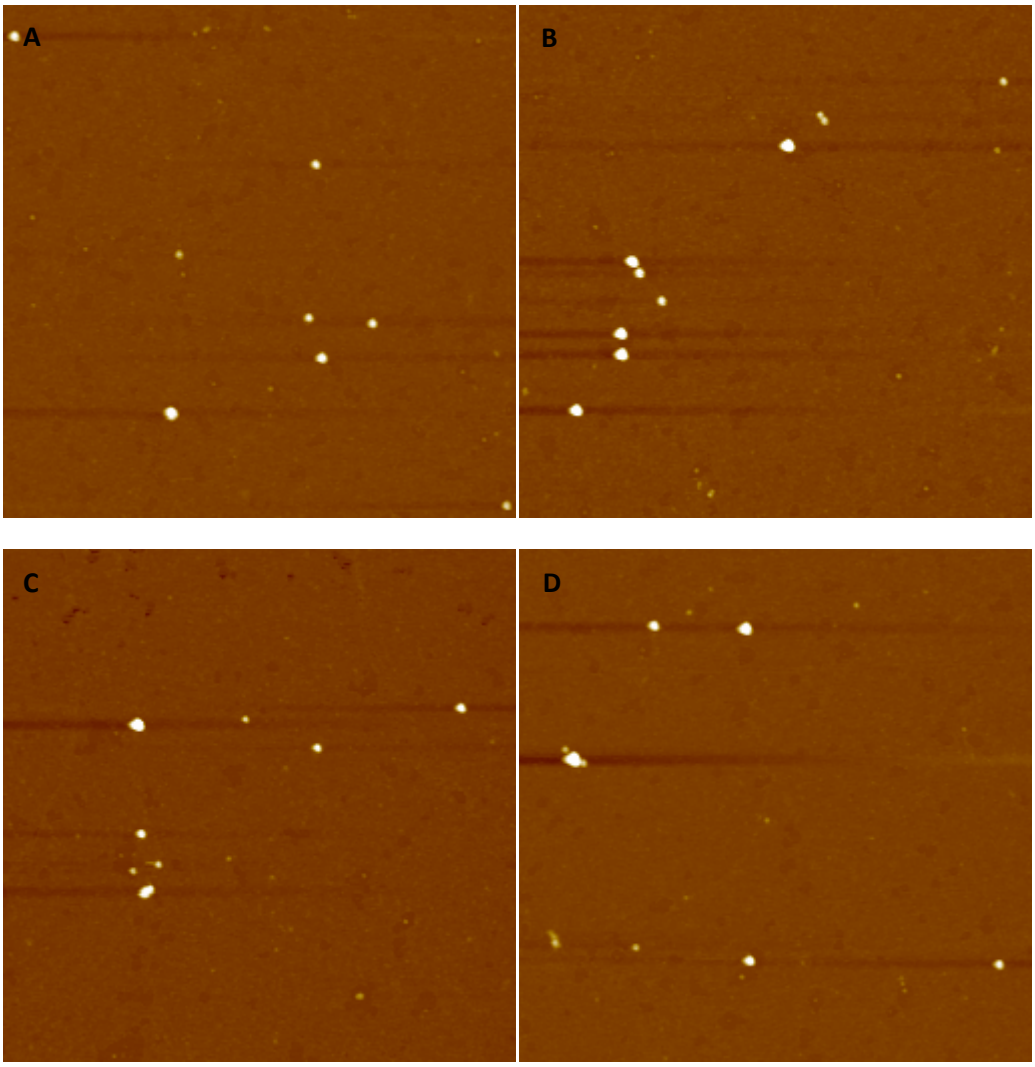

Figure 3.3 **A-D –** Typical AFM images showing silver nanoparticles NPa on a mica surface as prepared by an ultracentrifugation method. Scale 5 x 5 μm

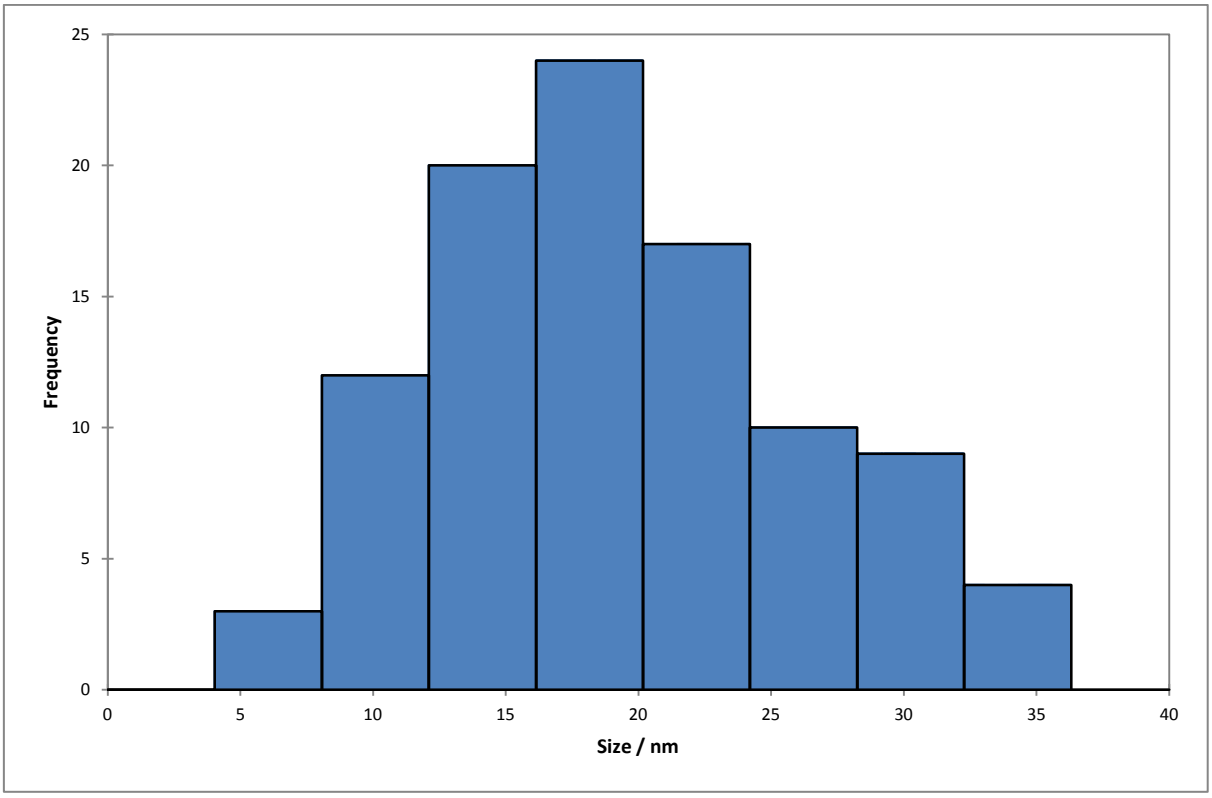

Figure 3.4 A size distribution for NPa as obtained by AFM.

3.1.4 Transmission Electron Microscopy

Electron micrographs (Figure 3.5) of NPa as synthesised were taken in order to ascertain the morphology of the NPs, as well as providing a core size distribution which may be compared to the distribution obtained by AFM. From the micrographs it was found that the NPs were roughly spherical in shape, with a mean core diameter of 17.6 ± 5.0 nm.

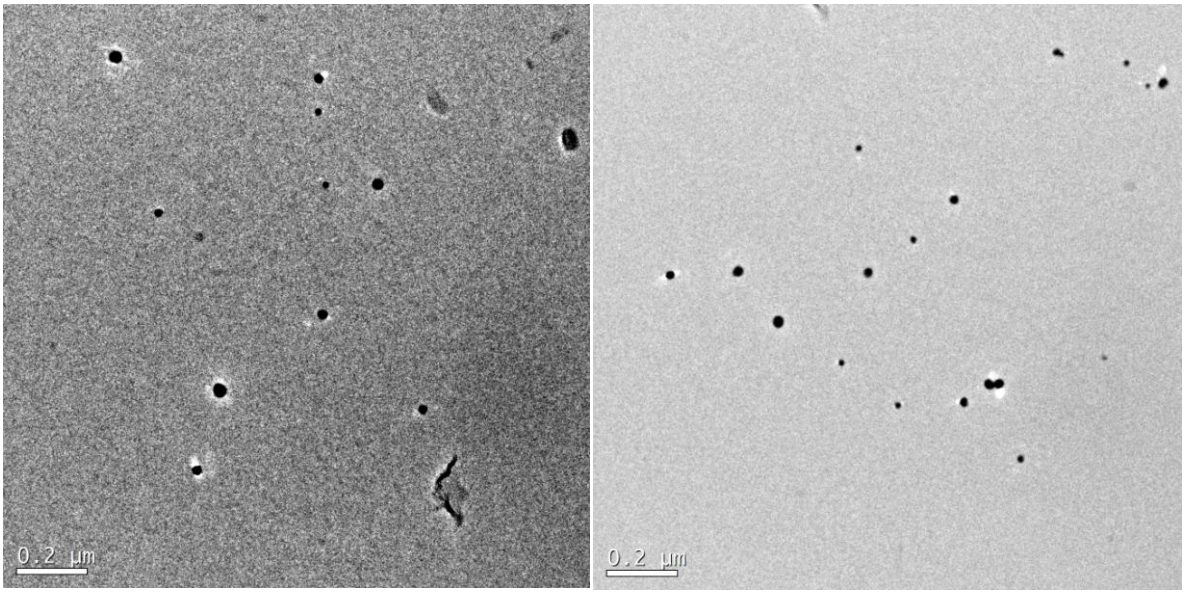

Figure 3.5 Typical TEM micrographs of silver nanoparticle NPa, taken at 10,000 times magnification.

To produce a size distribution (figure 3.6) of NPa from the electron micrographs they were analysed using the imaging software ImageJ. The Adjust Threshold function was used to select only the AgNPs present in the micrograph and subtract the background. The resulting images were then processing using the Analysis Particle function which generated an area for each particle present in the micrograph. With the assumption that each particle is spherical, using the following equation it is then possible to relate particle radius, r, to particle area, A:

Equation 3.1

$$r = \sqrt{\frac{A}{\pi}}$$

As the diameter, D, for a spherical particle is D = 2r a diameter may then be calculated in order to generate a size distribution for NPa (Figure 3.6).

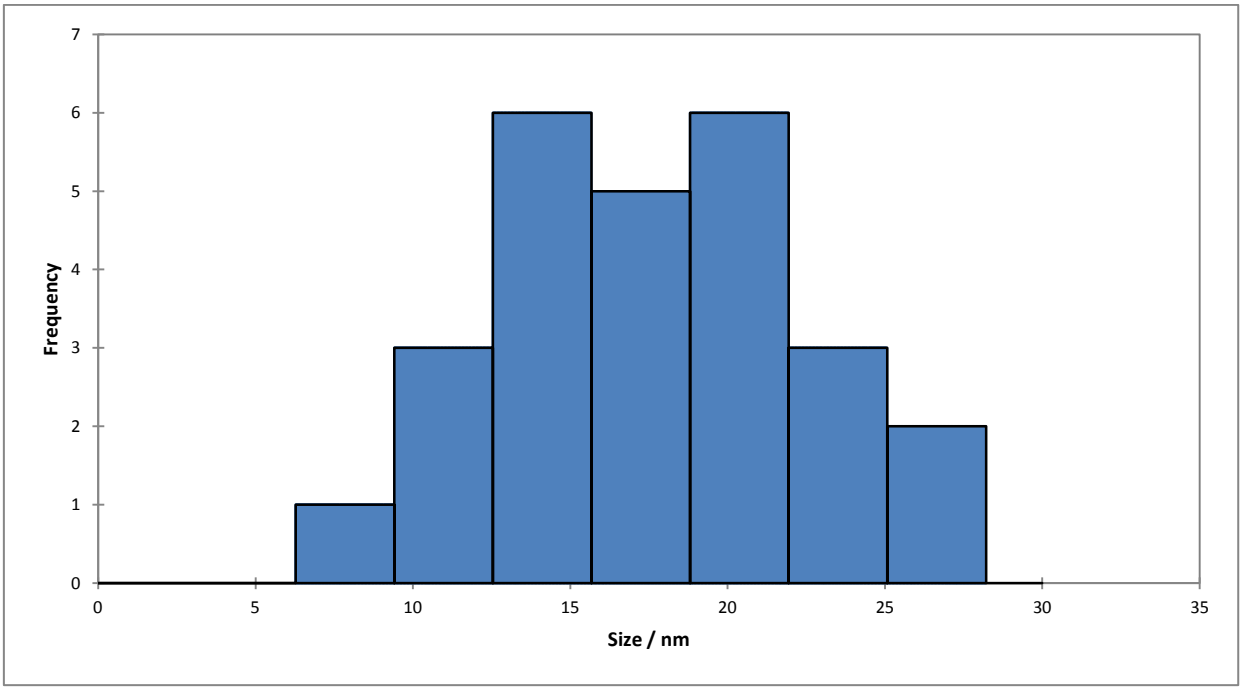

Figure 3.6 Size distribution for NPa as determined by TEM.

3.1.5 Energy Dispersive X-ray Spectroscopy

Using EDX an elemental composition of for NPa as synthesised was obtained as shown in Table 3.2 and Figure 3.7.

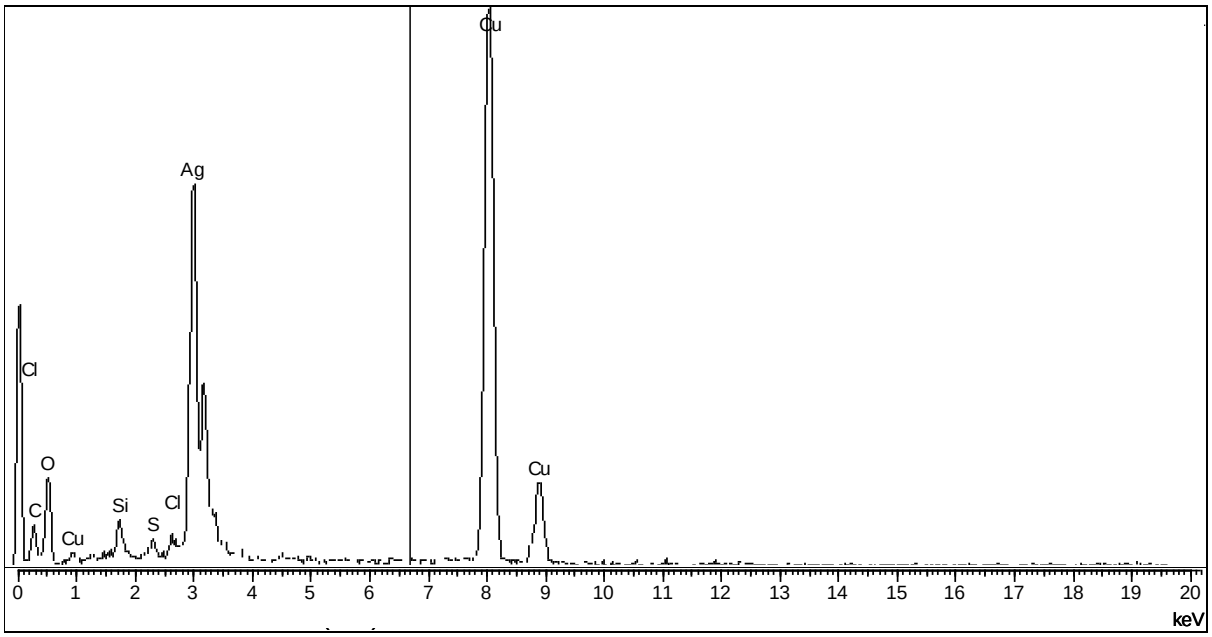

Figure 3.7 EDX spectra of NPa as synthesised.

Table 3.2 Elemental analysis for NPa as obtained by EDX

Element	Carbon	Oxygen	Silicon	Sulfur	Chlorine	Copper	Silver
Weight / %	1.50	2.87	1.04	0.64	0.07	51.34	42.55

3.1.6 UV-Vis Spectroscopy

A UV-Vis spectrum taken of NPa as synthesised showed an absorbance peak c.a. 400 nm as shown in Figure 3.8.

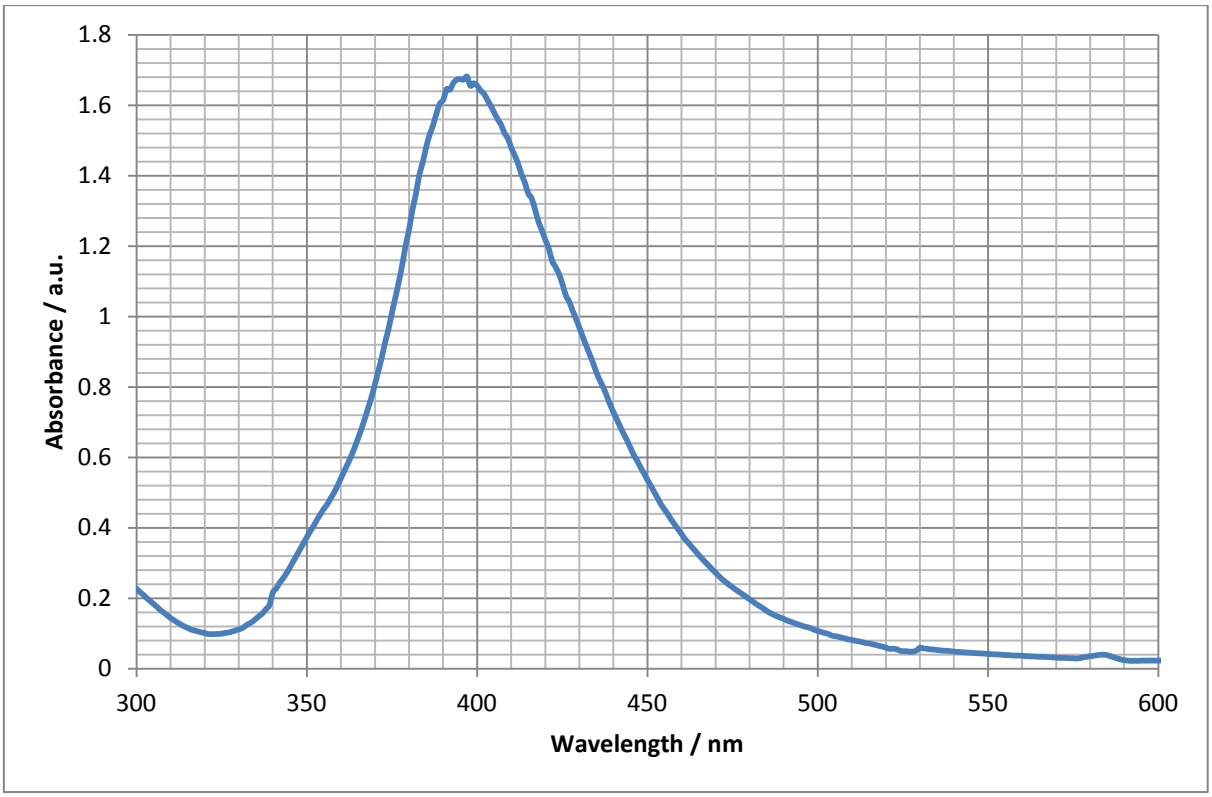

Figure 3.8 UV-Vis spectra of NPa as synthesised.

3.1.7 Excitation-Emission Matrix Fluorescence Spectroscopy

Excitation at wavelengths between 200-240 nm gave rise to emission wavelengths with a maximum intensity between 400 and 600 nm (figure 3.9). The AgNPs are capped by the sodium citrate at a concentration of 0.31 mM therefore a standard solution of the compound at the same concentration chosen as the blank solution. No significant fluorescence emission signal was detected from the blank.

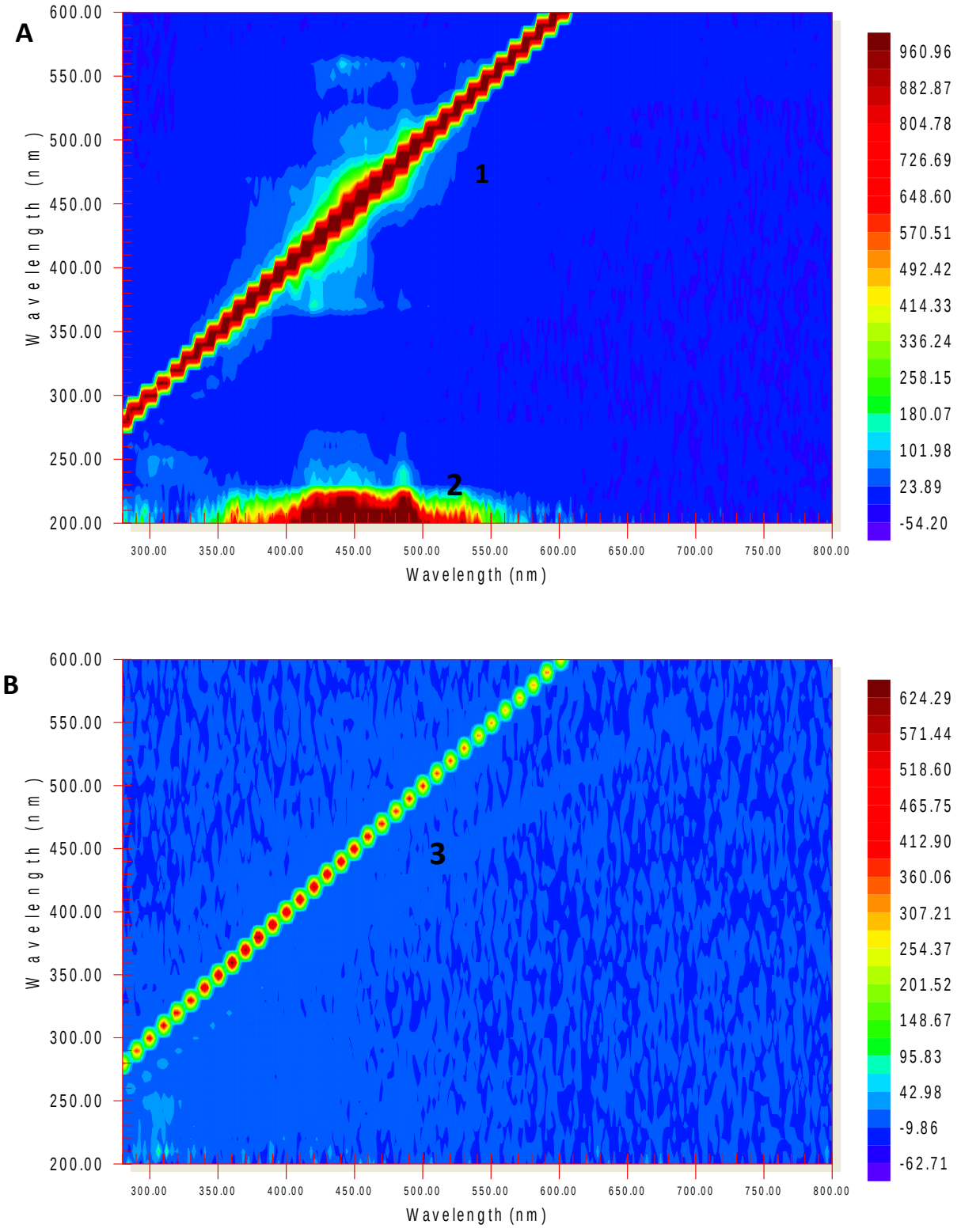

Figure 3.9 Excitation-Emission Matrices. **A** – EEM of a silver nanoparticle suspension, Area **1-** Rayleigh scattering, Area **2-** position of the emission signal. **B** - EEM of a 0.31mM standard solution of sodium citrate, Area **3-** Rayleigh scattering.

3.2 Effect of Ultracentrifugation

3.2.1 Dynamic Light Scattering

Measurements on the hydrodynamic diameter of NPa after various centrifugation times and forces to assess the affect centrifugation had on both the z-average and pdi of the NPs were made. A summary of which can be found in Table 3.3.

Table 3.3 Summary of the effect of Ultracentrifugation upon NPa.

	Z-average Hydrodynamic diameter / nm	**Polydispersity Index**
Original	33.59	0.200
15k rpm 1hr T5	25.11	0.175
10k rpm 1hr T5	28.92	0.182
10k rpm 40 mins T5	29.87	0.170
10k rpm 30 mins T5	35.68	0.237
15k rpm 1hr M5	29.41	0.254
10k rpm 1hr M5	31.84	0.247
10k rpm 40 mins M5	30.11	0.182
10k rpm 30 mins M5	32.31	0.207
15k rpm 1hr P	70.33	0.532
10k rpm 1hr P	57.50	0.510
10k rpm 40 mins P	35.39	0.397
10k rpm 30 mins P	42.52	0.471

With increasing time at 10,000 rpm the z average diameter of NPa decreased by c.a. 5 nm at 1 hr. With increasing centrifugal speed to 15,000 rpm, the z average value decreased by a further 4 nm. The z average in the pellets formed during the centrifugation increased most significantly at 15,000 rpm for 1 hr.

As shown in figure 3.10a the centrifugation process reduces the width of the intensity weighted size distribution measured for the particles suspended in the supernatant. This distribution is narrower for the samples produced at higher centrifugation speed and time. This corresponds to an increased in the size distribution width in the pellet with increasing centrifugation speed and time (Figure 3.10b).

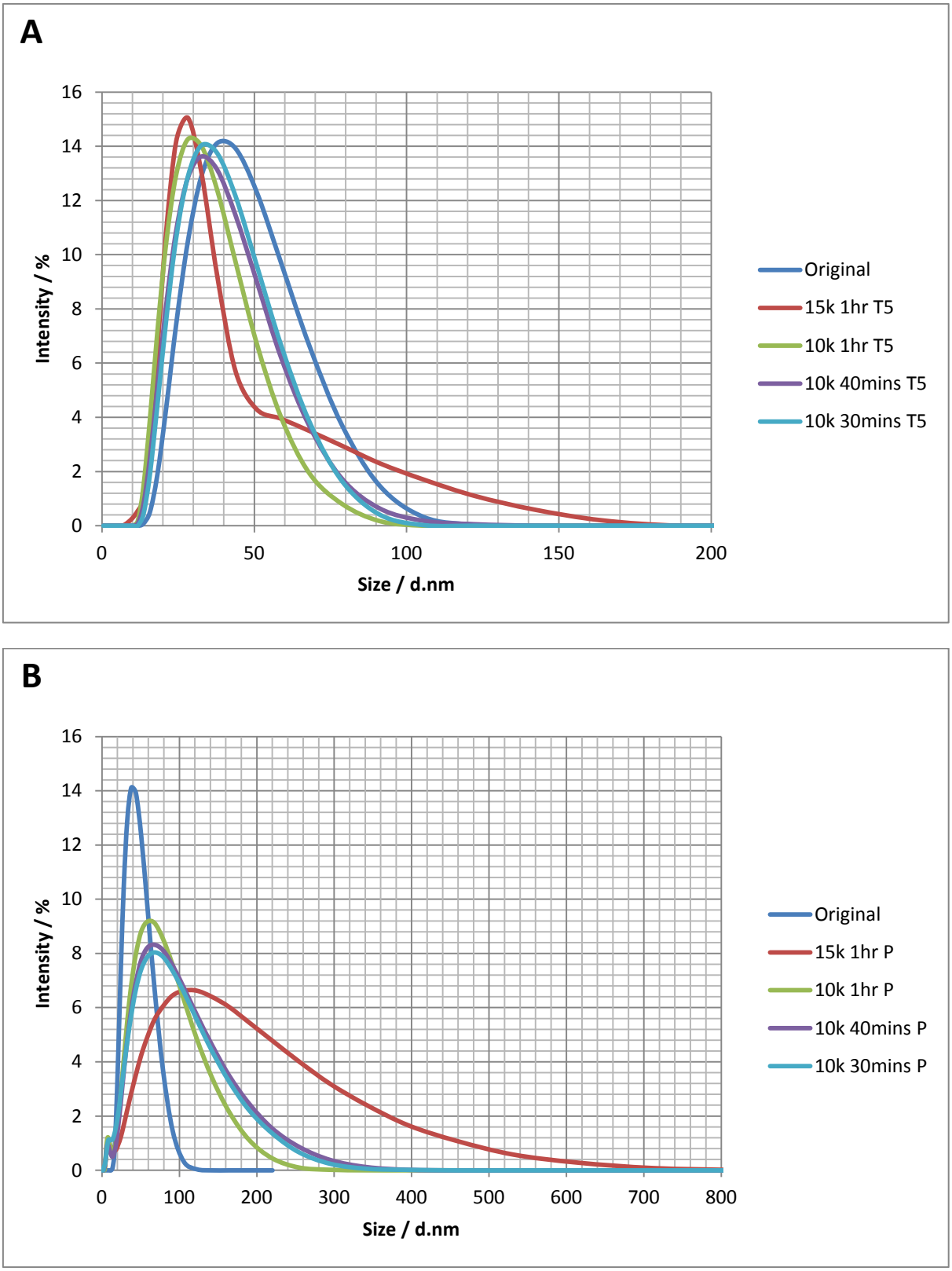

Figure 3.10 Intensity size distribution as measured by DLS showing the effect of Ultracentrifugation upon silver nanoparticles NPa. **A** – Samples taken from top 5 ml of supernatant. **B** – Samples taken from the Resuspended pellet.

3.2.2 UV-Vis Spectroscopy

Upon the ultracentrifugation of NPa a shift in the UV spectra for the AgNPs was observed. Whilst the bulk of the absorbance remained at a wavelength of 400 nm, the peak became narrower as it shifted towards lower wavelengths with increased ultracentrifugation time and force (figure 3.11).

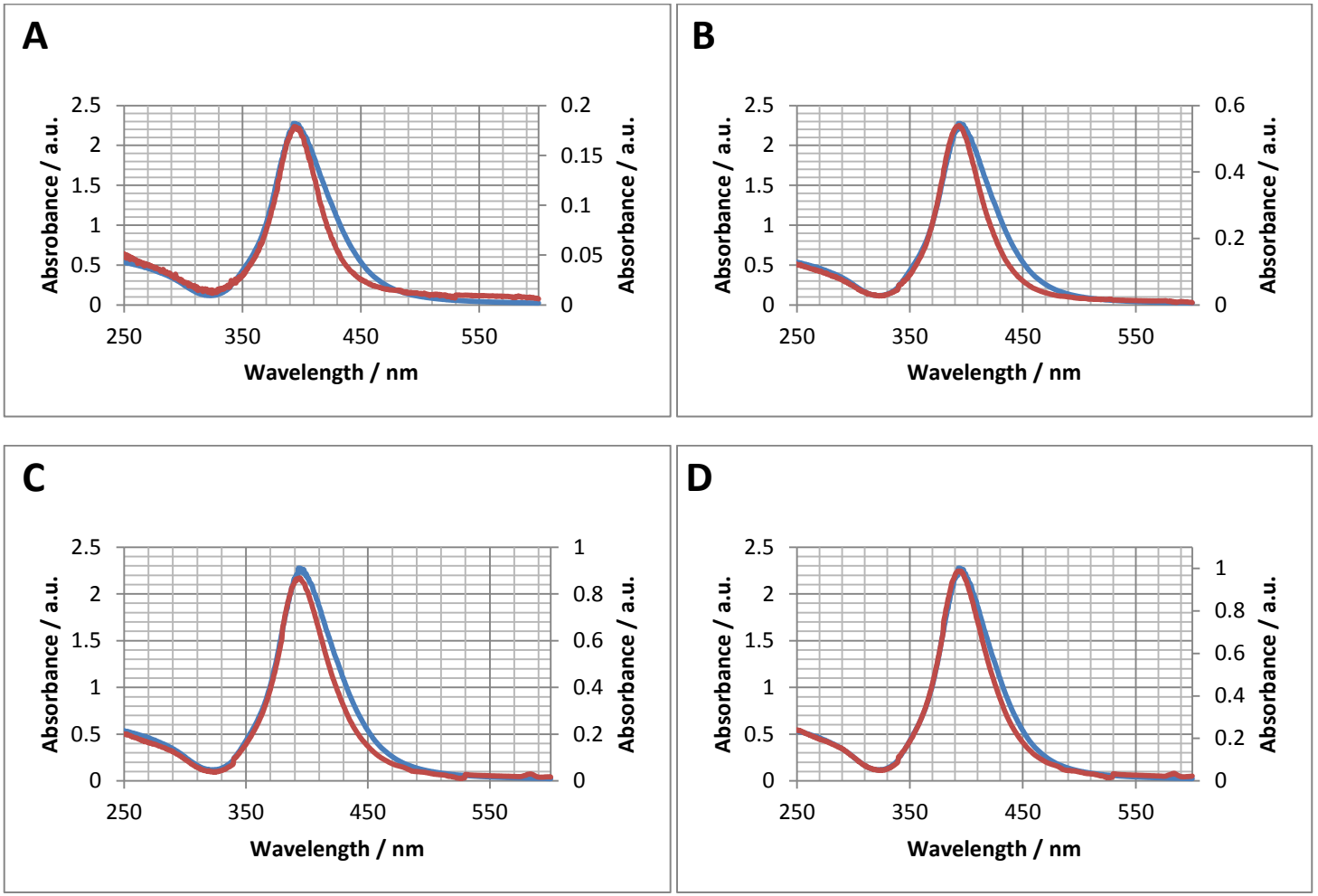

Figure 3.11 UV-Vis spectra of NPa samples at various centrifugal forces and times. A - 15k rpm 1hr, B - 10k rpm 1hr, C – 10k rpm 40 mins and D – 10k rpm 30 mins. Blue line – Original NPa, Red line – Centrifuged sample.

3.2.3 Flame Atomic Absorption Spectroscopy

Using FAAS the concentration of Ag in each of the three fractions for all centrifugation forces and times examined were measured. Using these concentration values the results were then converted into the mass of Ag per fraction. As centrifugation time was increased, the mass of Ag found in the supernatant decreased. Whilst the mass contained in the pellet was directly proportional to the centrifugation time (Figure 3.12).

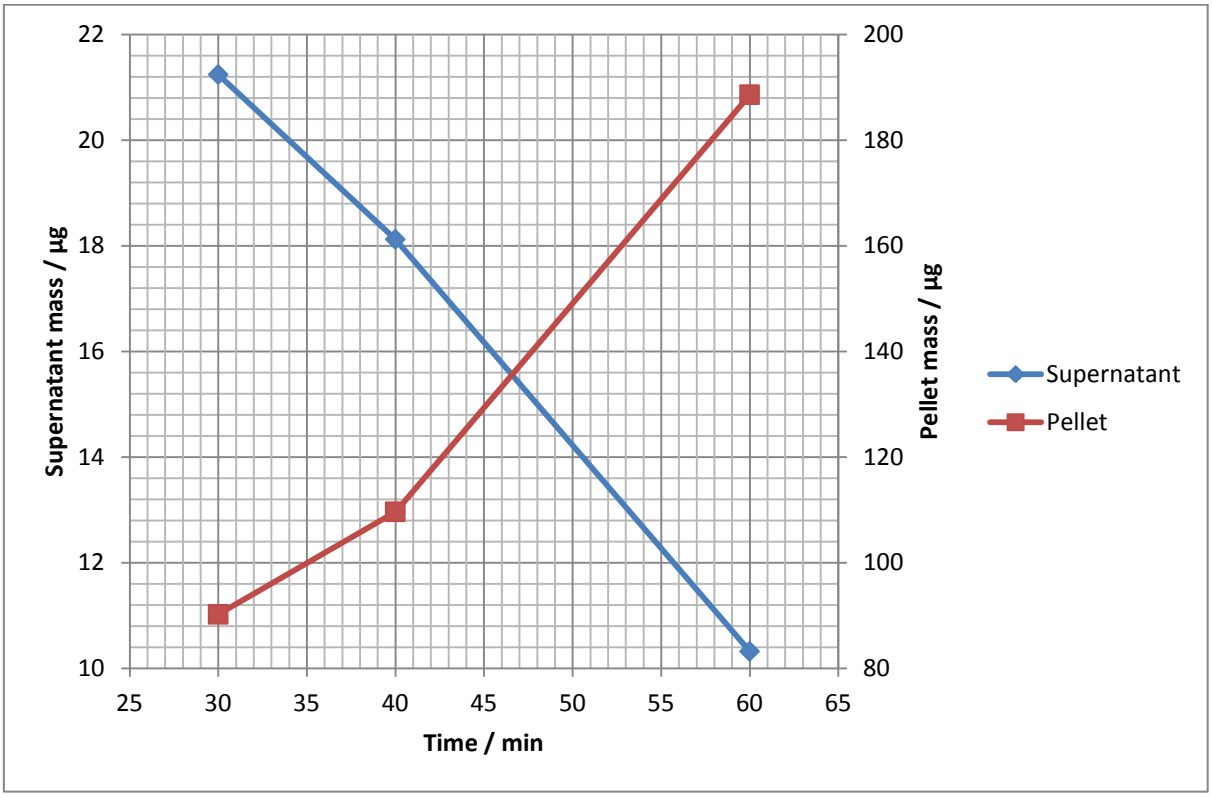

Figure 3.12 Comparison between silver mass in the pellet and supernatant at 10k rpm over time.

Similarly with increased centrifugation force more Ag mass was found in the pellet than in thesupernatant (Figure 3.13).

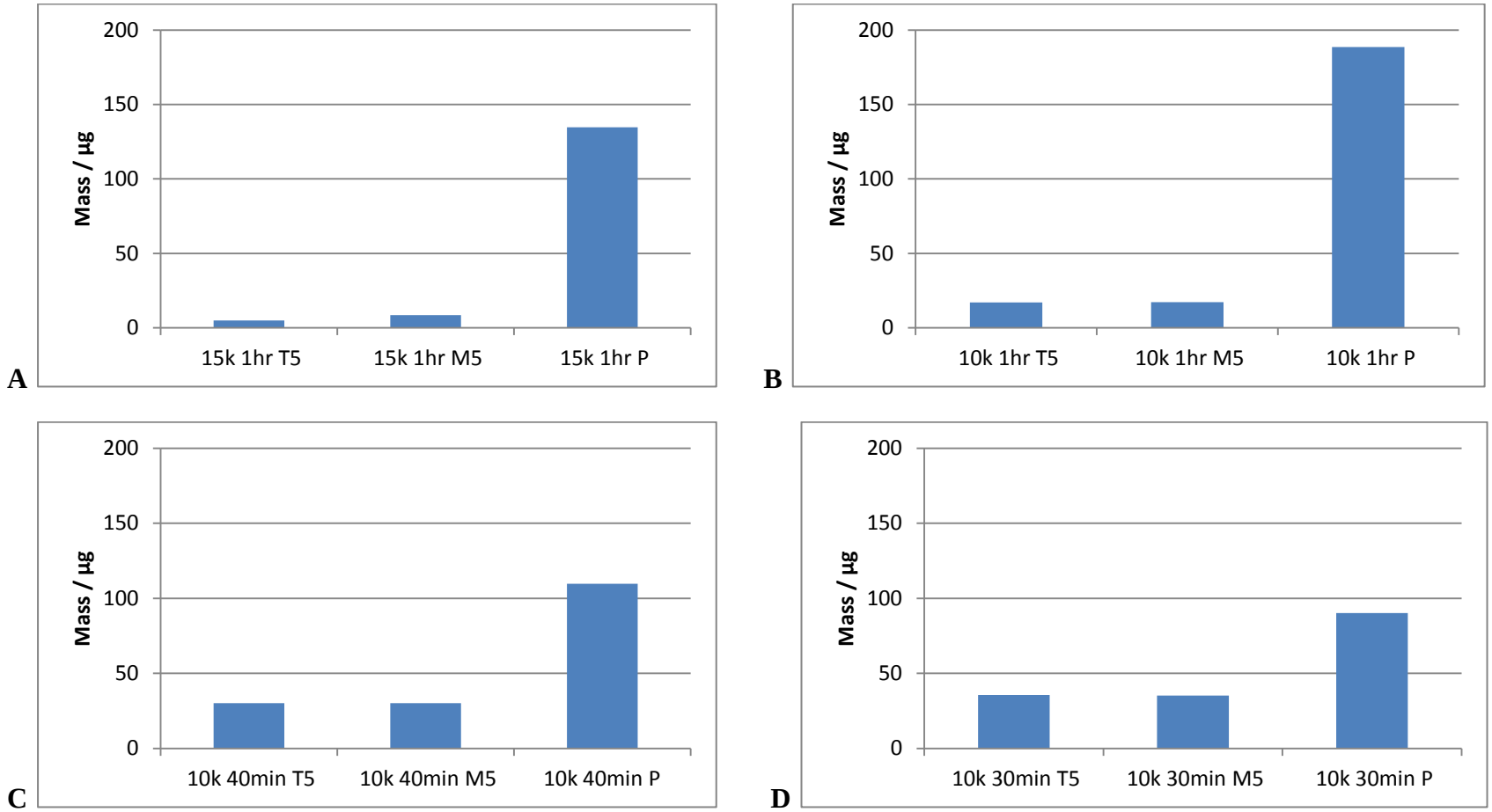

Figure 3.13 A comparison between the mass of silver found in each fraction of the centrifuge tube, under various centrifugation conditions as measured by FAAS. **A –** 15,000 rpm for 1hr, **B -** 10,000 rpm for 1hr, **C** – 10,000 rpm for 40 min and **D -** 10,000 rpm for 30 min.

3.3 Effect of Ultrafiltration

3.3.1 Dynamic Light Scattering

It was found that after ultrafiltration the hydrodynamic diameter of the AgNPs increased by approximately 5 nm to 41.32 nm as shown in table 3.4 and figure 3.14.

Table 3.4 Summary of the Z-average and Pdi of the as synthesised NPa and Ultrafiltrated nanoparticles labelled, NPu.

	Z-average Hydrodynamic Diameter / nm	**Polydispersity Index**
NPa	36.68 ± 0.16	0.186
NPu	41.32 ± 0.36	0.164

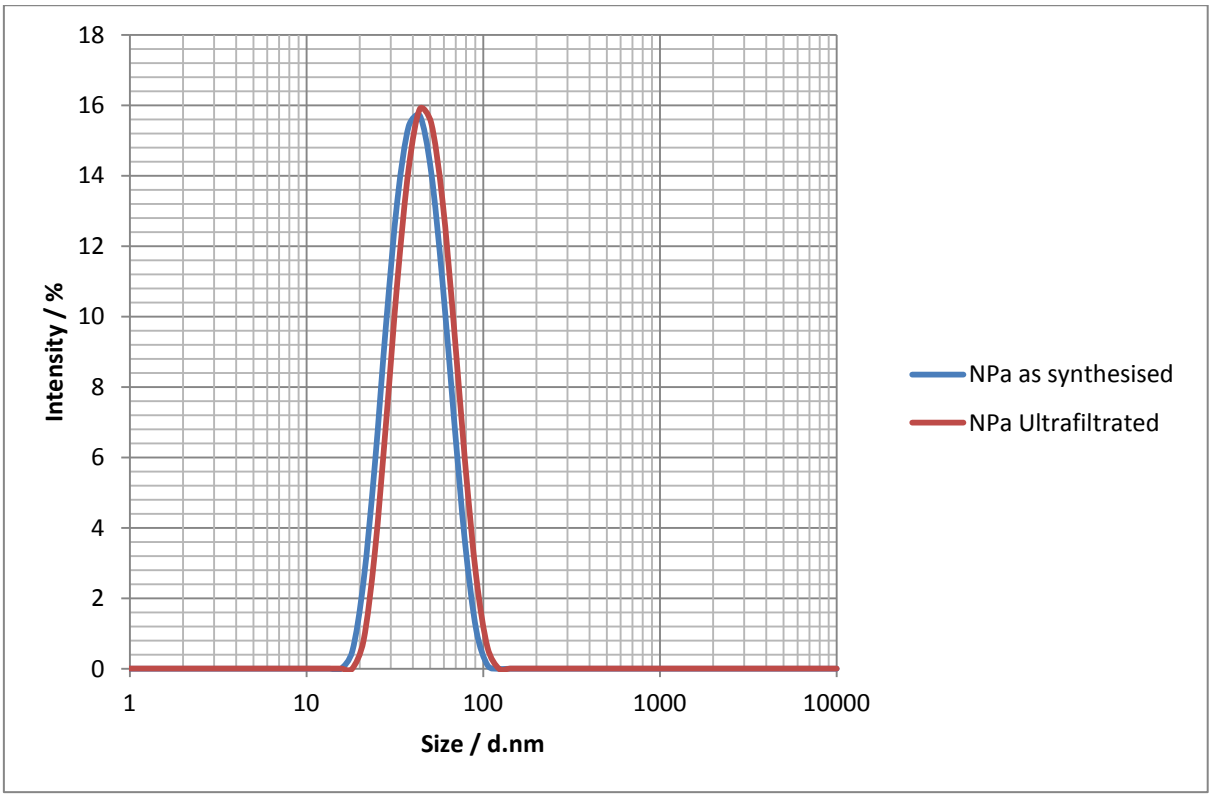

Figure 3.14: Intensity size distribution as measured by DLS showing the effect of ultrafiltration upon silver nanoparticles NPa.

3.4 Nanoparticles in Exposure Media

To better understand the interaction of the AgNPs with the Choanoflagellate cells it was necessary to characterise the NPs in Pratt's medium, as with the initial characterisation using a multi-method approach. Characterisation in the culture medium allows for any transformations which occur to the NPs to be taken into consideration when investigating their uptake into cells.

3.4.1 Dynamic Light Scattering

Six AgNP concentrations between 5.5 mg/L and 2 µg/L were prepared using an 11 mg/L NP stock suspension and undiluted Pratt's medium. These were analysed using DLS at 0 hrs, 2 hrs and 24 hrs in order to replicate the exposure times used during the Choanoflagellate uptake experiments. From the measurements the z-average hydrodynamic diameter and polydispersity index were collected and compared to that of the original NPs as synthesised. A summary of which can be found in tables 3.5, 3.6 and 3.7.

Table 3.5: Summary of Z-average hydrodynamic diameters of NPa when diluted in Pratt's medium at time 0.

	Z-average Hydrodynamic Diameter / nm	**Polydispersity Index**
Original	36.68 ± 0.16	0.186
5.5 mg/L	36.08 ± 0.20	0.185
1 mg/L	39.01 ± 1.07	0.216
500 µg/L	50.33 ± 0.64	0.379
100 µg/L	56.89 ± 2.42	0.509
11 µg/L	442.3 ± 27.92	0.331
2 µg/L	541.2 ± 17.63	0.321

Table 3.6: Summary of Z-average hydrodynamic diameters of NPa when diluted in Pratt's medium at 2 hrs.

	Z-average Hydrodynamic Diameter nm	**Polydispersity Index**
Original	36.68 ± 0.16	0.186
5.5 mg/L	36.26 ± 0.31	0.187
1 mg/L	40.47 ± 0.78	0.247
500 µg/L	46.27 ± 3.09	0.308
100 µg/L	52.80 ± 4.67	0.336
11 µg/L	457.5 ± 25.14	0.336
2 µg/L	524.5 ± 35.41	0.321

Table 3.7: Summary of Z-average hydrodynamic diameters of NPa when diluted in Pratt's medium at 24 hrs.

	Z-average Hydrodynamic Diameter / nm	**Polydispersity Index**
Original	36.68 ± 0.16	0.186
5.5 mg/L	36.57 ± 0.26	0.187
1 mg/L	38.73 ± 0.48	0.208
500 µg/L	41.73 ± 0.56	0.251
100 µg/L	49.51 ± 2.74	0.355
11 µg/L	351.2 ± 51.24	0.543
2 µg/L	425.3 ± 22.64	0.426

Immediately upon addition of the stock solution to the Pratt's medium the hydrodynamic diameter of the lowest AgNP concentrations used in the study, 11 µg/L and 2 µg/L, increased by approximately 12 and 15 times the original diameter respectively. An increase in z-average was also observed in the slightly higher concentrations, 500 µg/L and 100 µg/L, however the effect was less prominent with only a 40 to 55% increase. For all the above AgNP suspensions in Pratt's medium a minimum of a 70% increase in the polydispersity index was seen. The highest concentrations of AgNPs tested in the medium did not alter considerably when compared to the original NPa DLS data as synthesised (see figure 3.15 and figure 3.16).

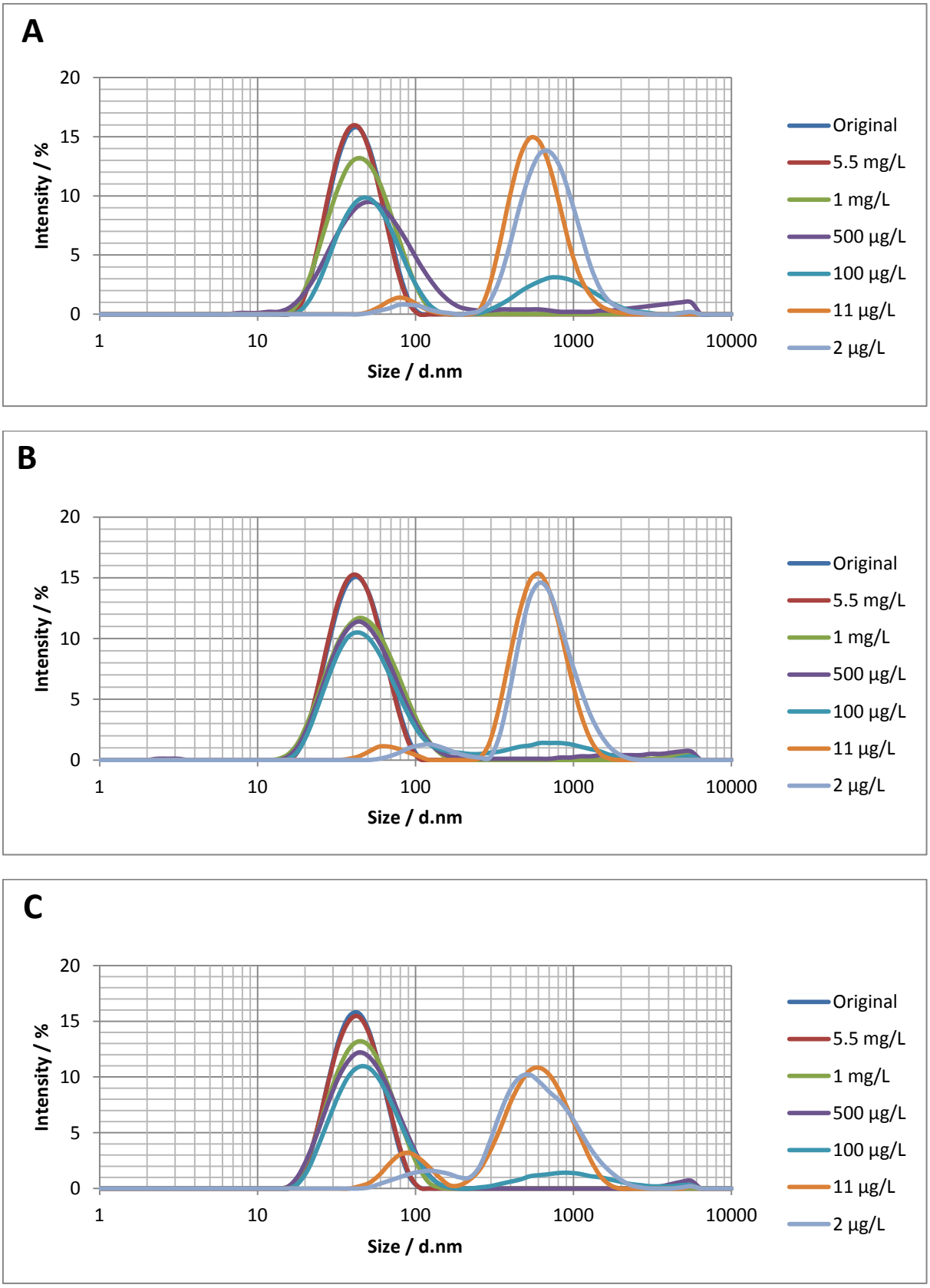

Figure 3.15 Stability of silver nanoparticles as measured by DLS. **A** – Nanoparticle stability at time 0. **B** – Nanoparticle stability at 2 hrs. **C** – Nanoparticle stability at 24 hrs.

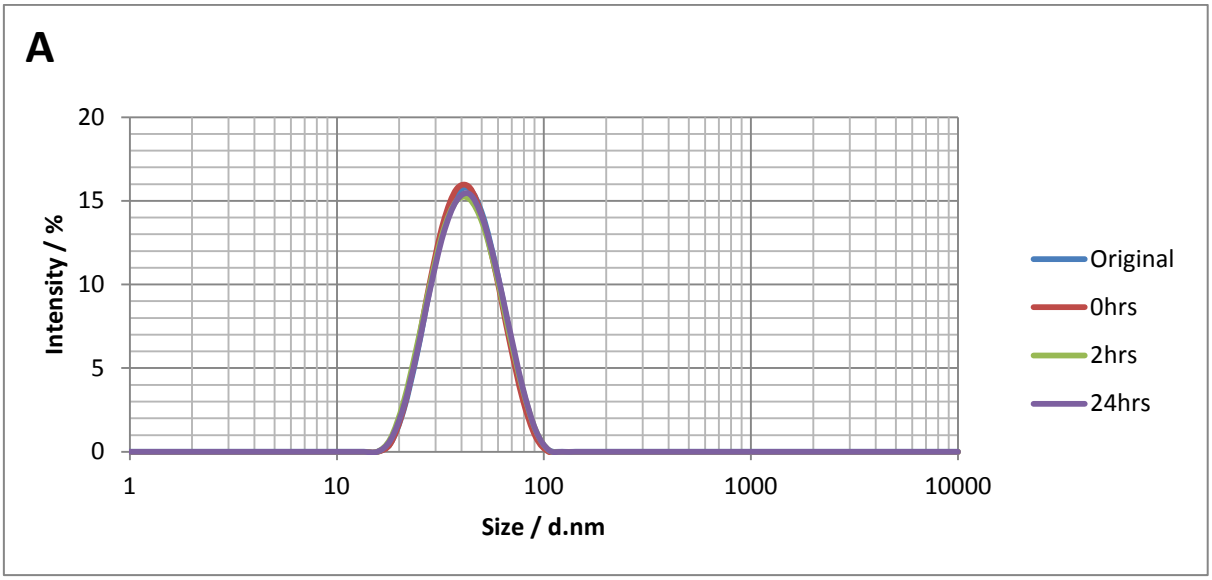
A
20
15
10
5
0
Intensity / %
1
10
100
1000
10000
Size / d.nm
Original
0hrs
2hrs
24hrs

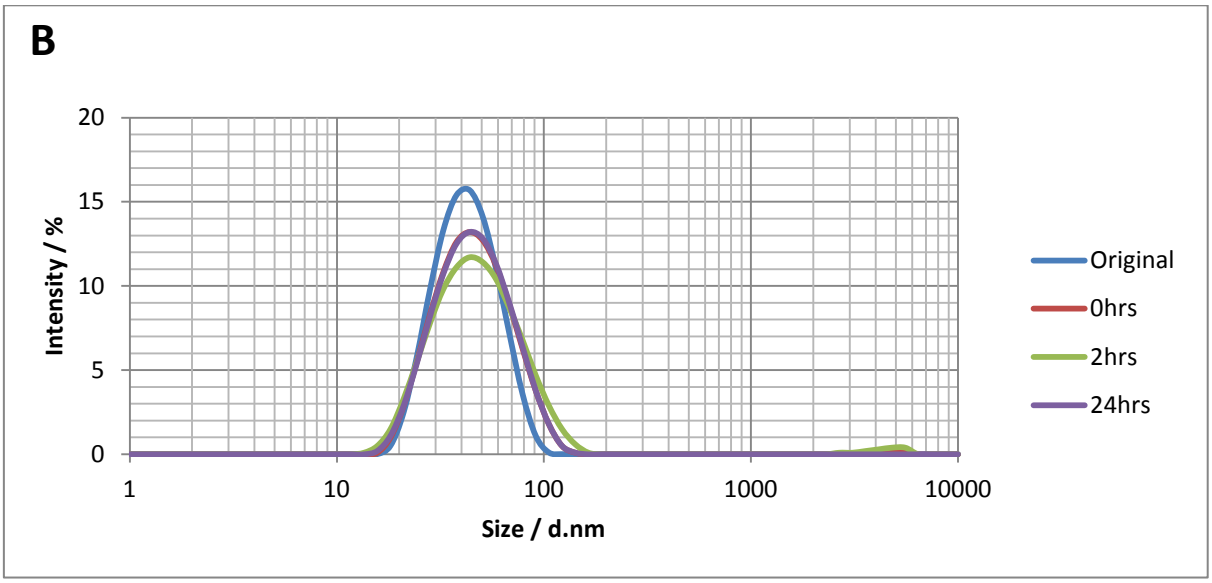
B
20
15
10
5
0
Intensity / %
1
10
100
1000
10000
Size / d.nm
Original
0hrs
2hrs
24hrs

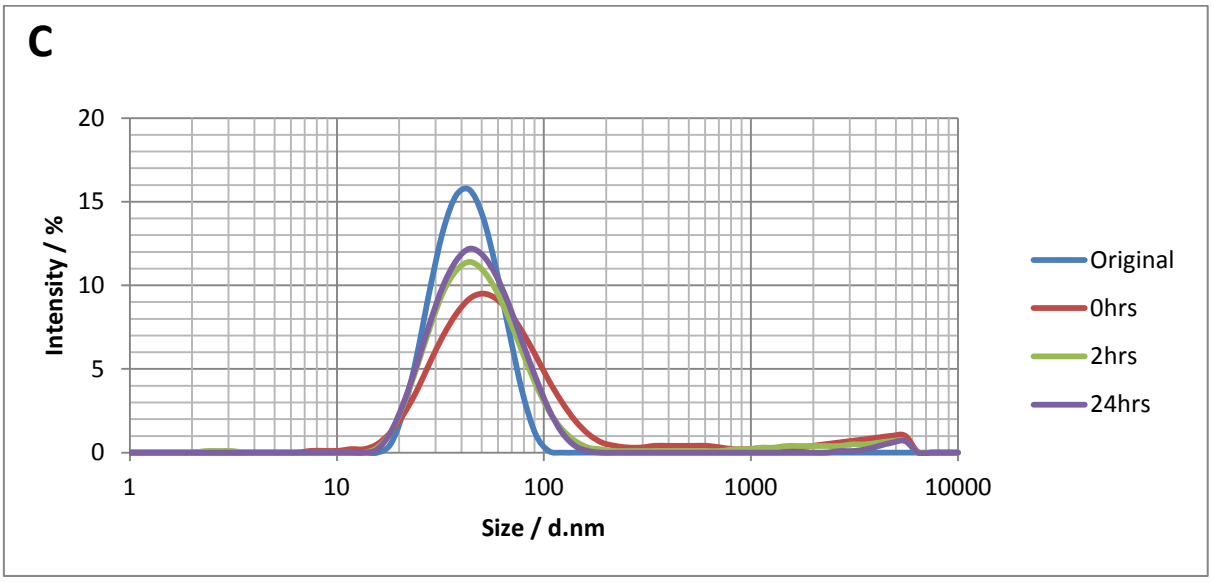
C
20
15
10
5
0
Intensity / %
1
10
100
1000
10000
Size / d.nm
Original
0hrs
2hrs
24hrs

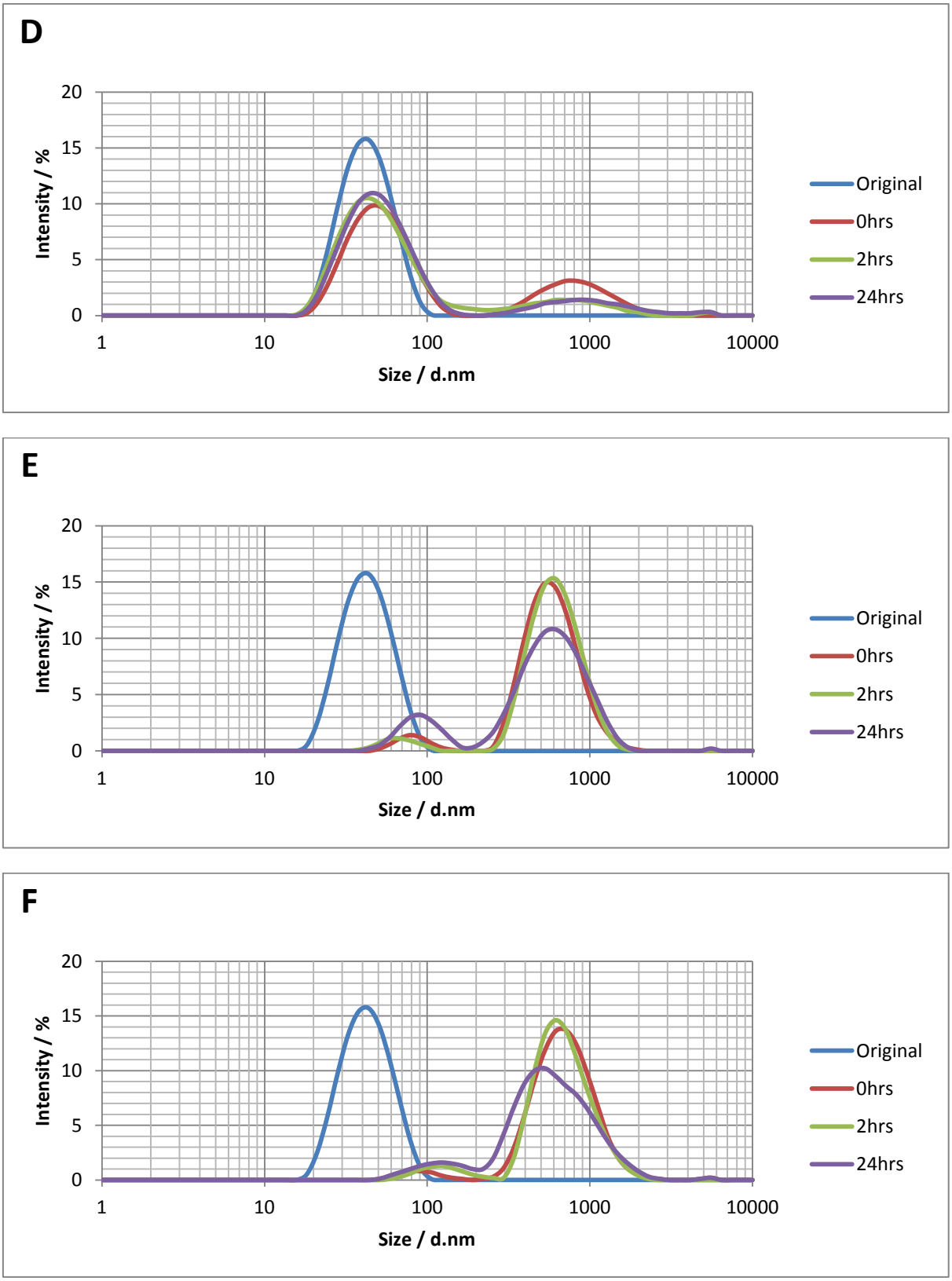

Figure 3.16 DLS sizing for NPa silver nanoparticles at different concentrations in Pratt's medium. **A** – 5.5 mg/L, **B** – 1 mg/L, **C** – 500 µg/L, **D** – 100 µg/L, **E** – 11 µg/L and **F** – 2 µg/L.

For the conclusion of the experiment neither the z average or pdi for the highest concentration, 5.5 mg/L, increased significantly or deviated from that of the original suspension as synthesised. Similarly for 1 mg/L only a slight increase in the z average and pdi was found after 24 hrs. At concentrations of 500 μg/L, 100 μg/L and 11 μg/L a significant increase in the z average of the particles was observed, with some conversion of the particles into large agglomerates. At the lowest two concentrations of 11 μg/L and 2 μg/L after 24 hrs there was almost complete conversion of the particles to agglomerates at the beginning of the experiment, by completion a drop in particle intensity was noted.

3.4.2 Atomic Force Microscopy

Using AFM it was possible to gain information on the effect Pratt's medium had upon the core size of the AgNPs. A visual comparison between the different concentrations of AgNPs in Pratt's medium indicates an increase in agglomeration state as AgNP concentration decreases.

The morphology of the particles is also seen to change as NP concentration decreases. The original NPa particles as synthesied appear spherical in shape and as individual primary particles. This is also seen in the highest concentration of AgNPs used in the medium, 5.5 mg/L, with the formation of some agglomerates. At 1 mg/L larger agglomerates are present with a reduced number of individual primary particles compared to the original NPa sample. At 500 μg/ L an increase in the size of the agglomerates in width in noticed with some smaller clusters of particles also formed. The lowest AgNP concentration exxamined by AFM, 100 μg/ L, showed fewer large agglomerates than the previous concentration. However the

particles at this lower concentration had a more irregular shape compared to those in the previous concentrations.

When investigating the effect of Pratt's medium upon the hydrodynamic diameter using DLS two lower concentrations of AgNPs were also used in addition to the ones here. However using such a low concentration of particles even with the use of ultracentrifugation would not yield enough particles on the mica surface for adequate AFM analysis.

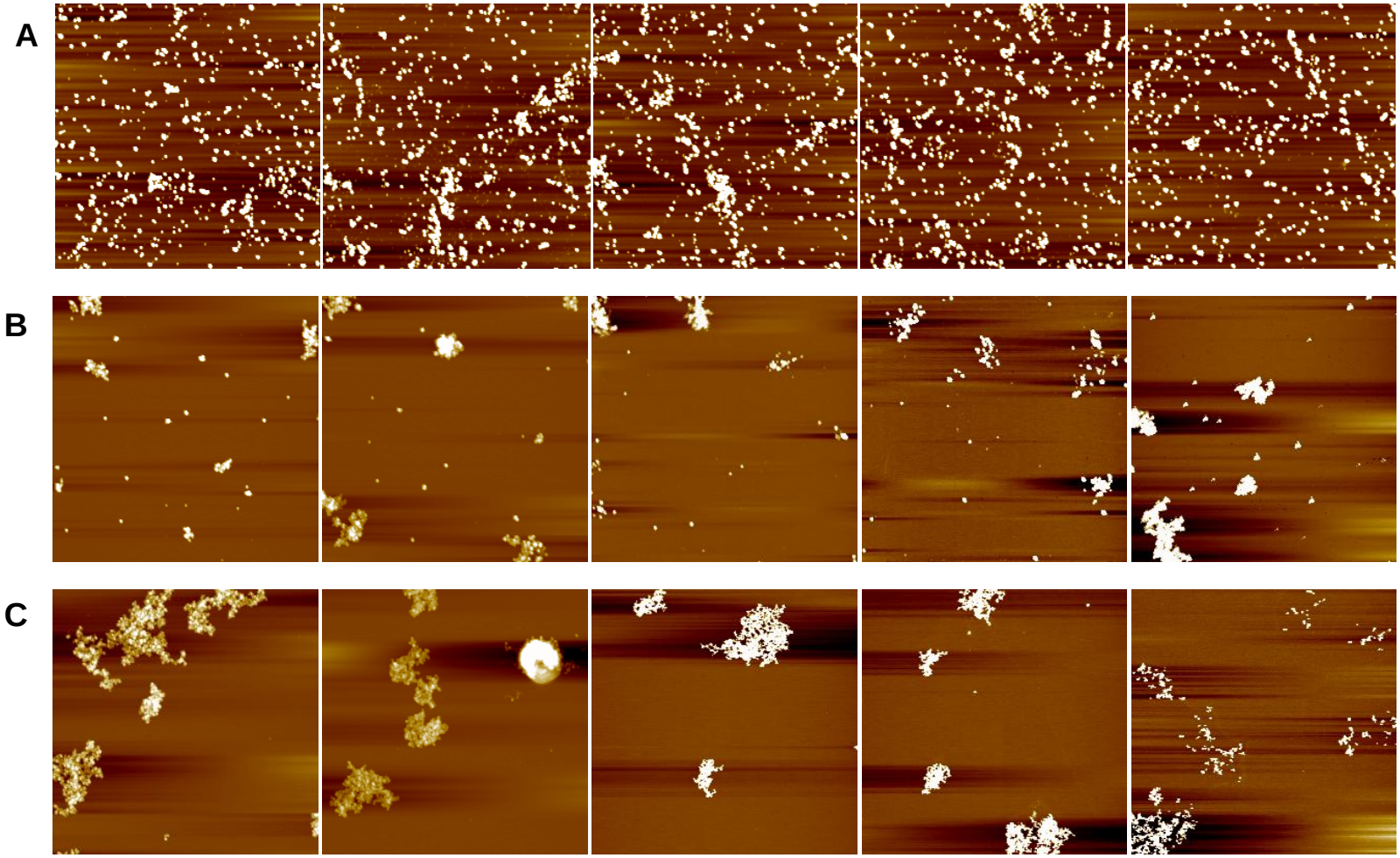
A
B
C

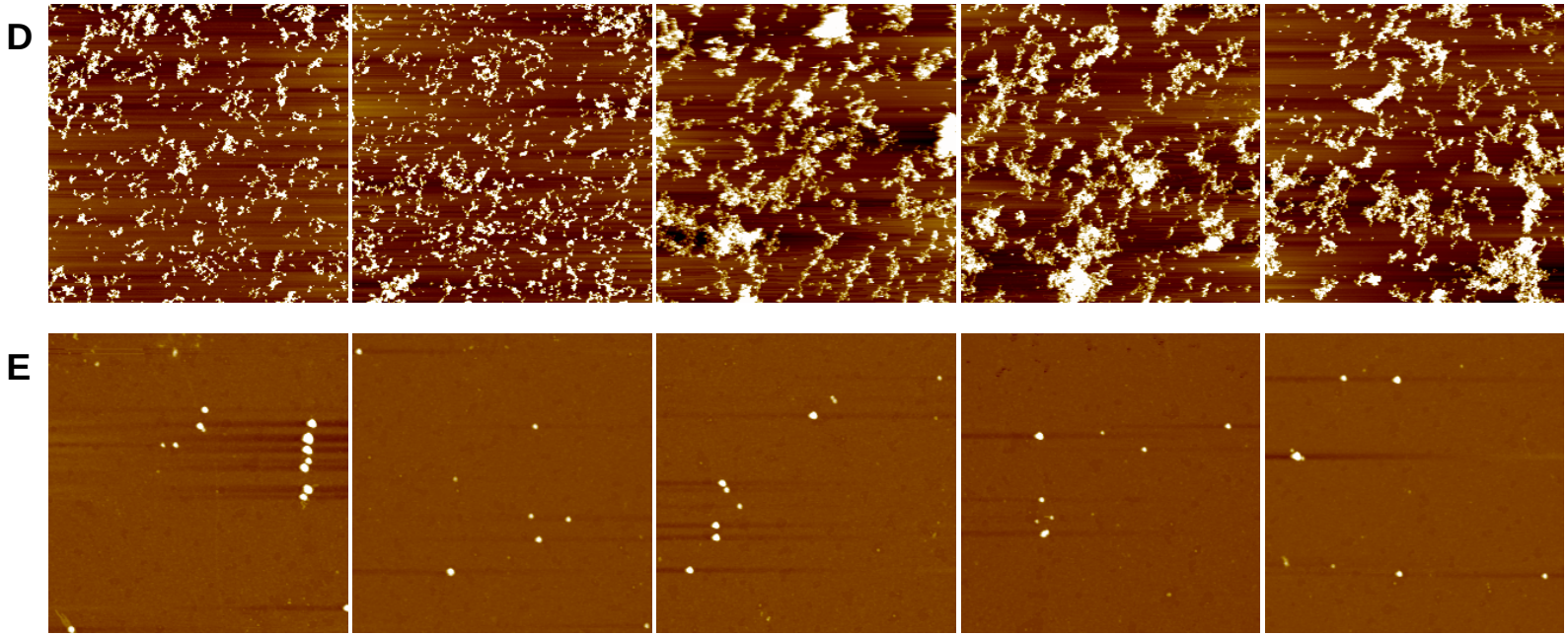

Figure 3.17: AFM Images – NPa silver nanoparticles at different concentrations in Pratt's Medium; **A** – 5.5 mg/L, **B** – 1 mg/L, **C** – 500 µg/L, **D** – 100 µg/L and **E** – Silver nanoparticles without Pratt's Medium.

Scale: Images **A-D -** 10µm x 10µm, **E -** 5µm x 5µm.

From the above micrographs core sizes for the particles in the media were found and are presented in Table 3.8. All the AgNP suspensions in Pratt's medium were shown to have increased core sizes. The largest increase in core size was found for the AgNP concentration 1 mg/L. Core size distributions for each concentration of AgNP were compared to that of the original NPa as synthesised (figure 3.18).

Table 3.8: Mean core sizes for NPa at various concentrations in Pratt's Medium.

Nanoparticle Concentration	**Core Size / nm**
Original	19.3 ± 6.6
5.5 mg/L	29.0 ± 5.9
1 mg/L	29.9 ± 15.5
500 μg/L	22.7 ± 15.7
100 μg/L	26.7 ± 9.0

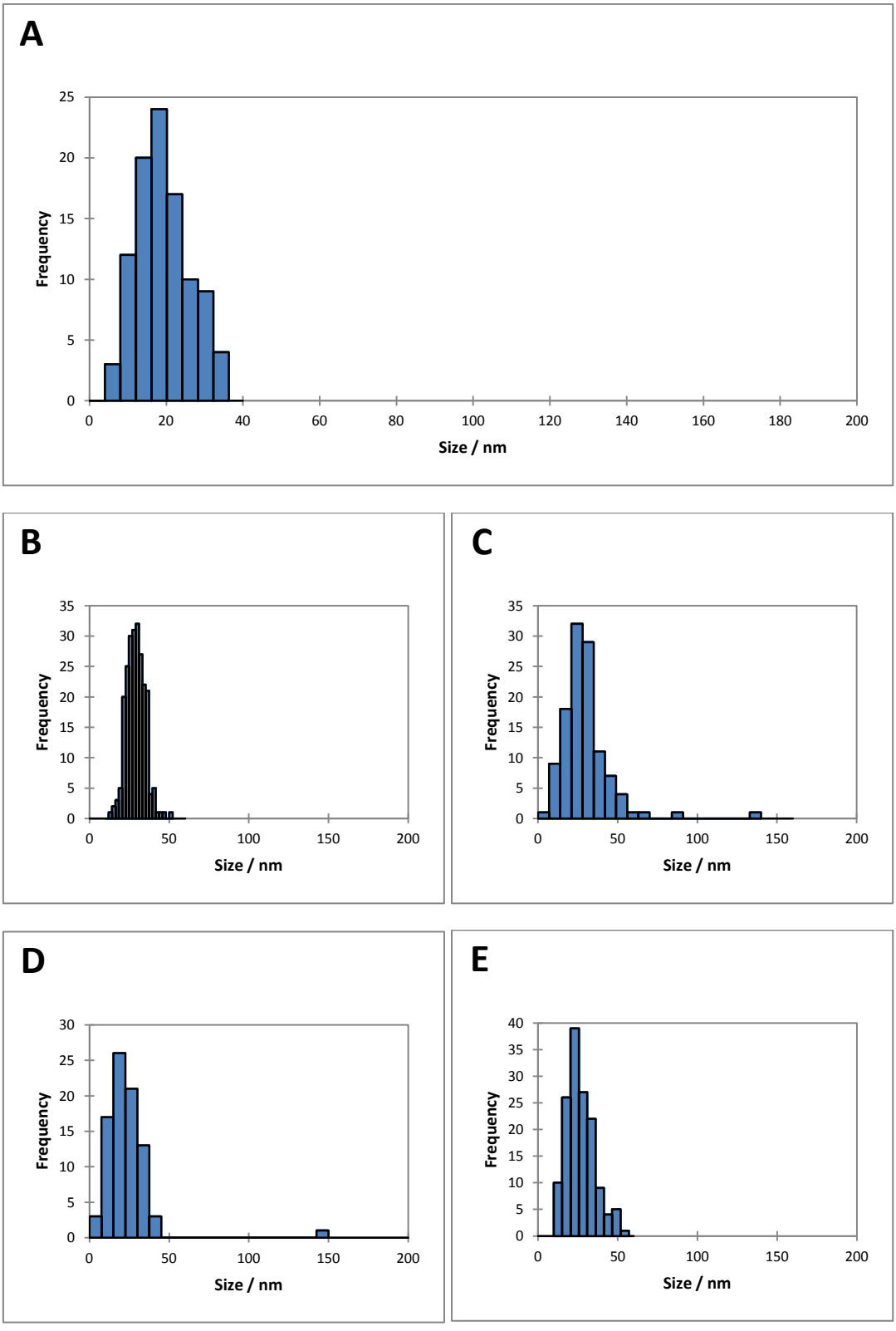

Figure 3.18 Size distributions demonstrating the effect of Pratt's medium upon nanoparticle core size as measured by AFM. **A** – Original NPa, **B** - 5.5 mg/L, **C** –1 mg/L, **D** –500 µg/L and **E** –100 µg/L.

3.4.3 UV-Vis Spectroscopy

When compared against the original NPa absorbance spectra with decreasing concentration of NP concentration there appears to be a subtle shift towards higher wavelength as seen in figure 3.19 and figure 3.20. The effect is most pronounced with the lowest concentration used in the UV-Vis experiment 100 μg/L. Due to limitations in the detection threshold of the UV-Vis spectrophotometer it was not possible to measure the absorbance from the samples below this concentration.

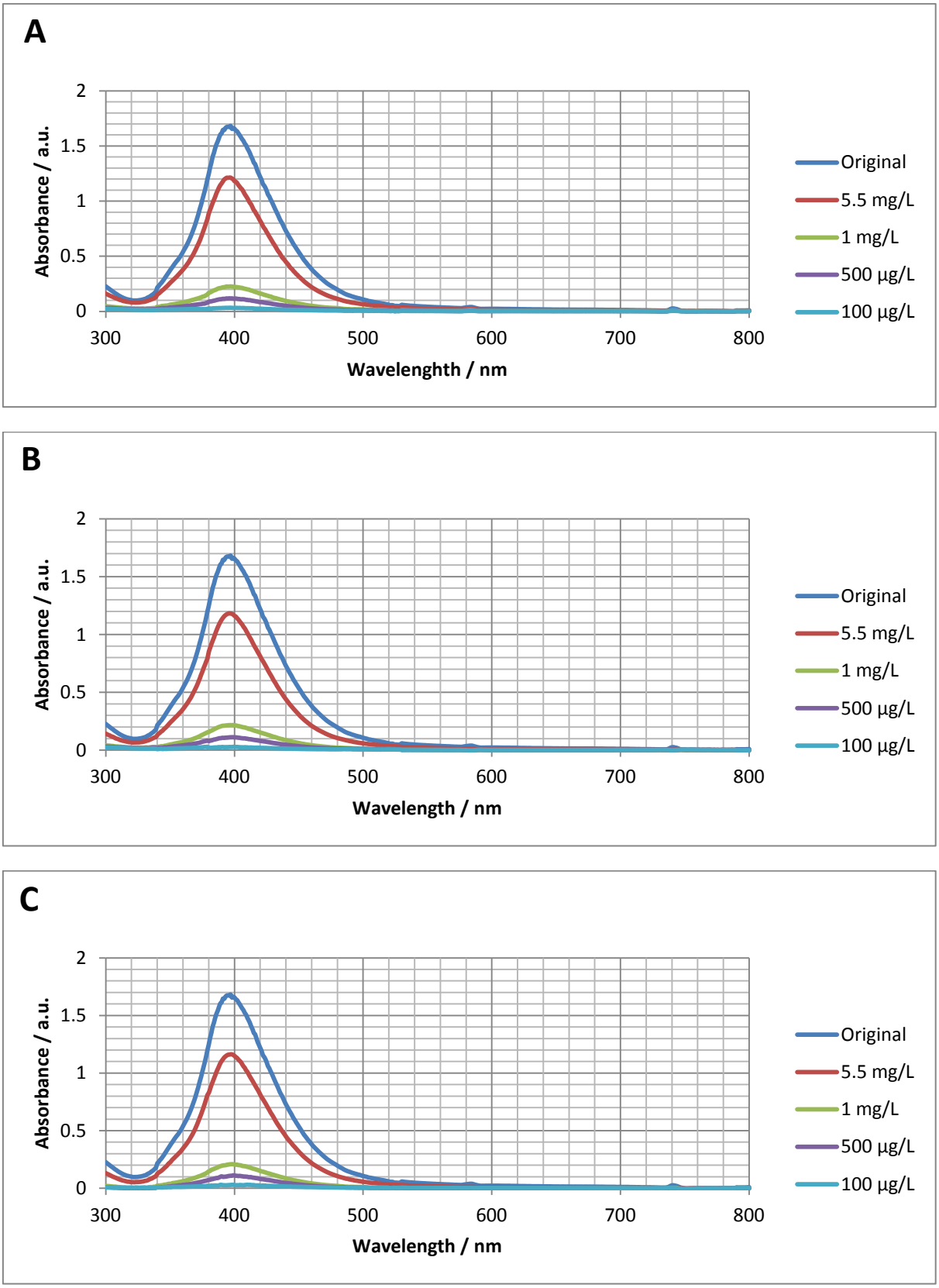

Figure 3.19 UV-Vis Spectra of NPa at different concentrations in Pratt's medium over time. **A** – 0hrs, **B** – 4hrs, **C** – 24hrs.

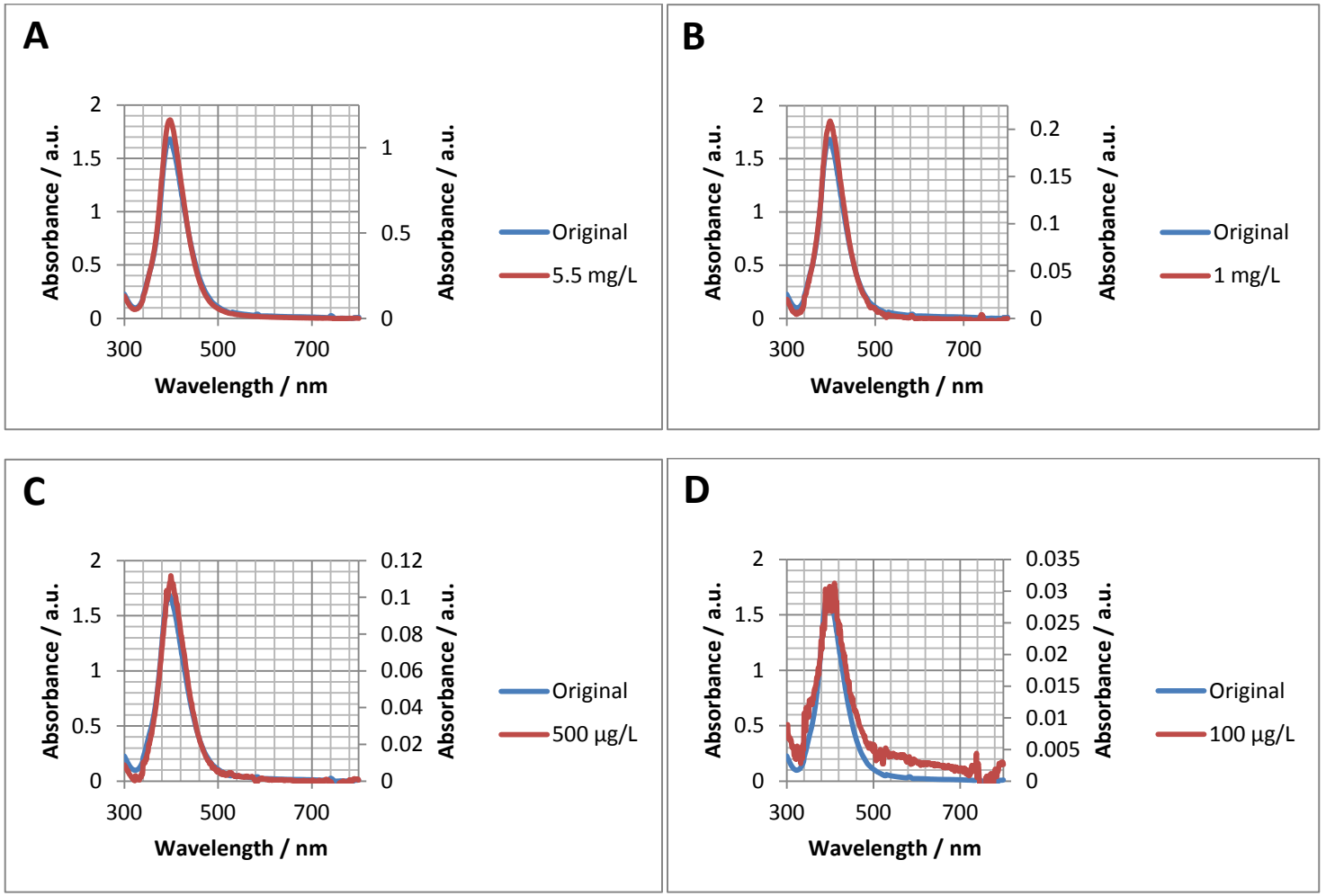

Figure 3.20 UV-Vis Spectra of NPa at different concentrations in Pratt's medium, comparison between concentrations after 24 hrs and the original NPa as synthesised. **A** – 5.5 mg/L, **B** – 1 mg/L, **C** – 500 µg/L and **D** – 100 µg/L**.**

3.5 Silver Nanoparticle Uptake in Choanoflagellates

3.5.1 Reflectance Confocal Microscopy

Light from reflective AgNPs was observed in various regions of the Choanoflagellates, in particularly large clusters of material were seen adhered to the microvilli collar and in a region below the cell nucleus (see figure 3.21).

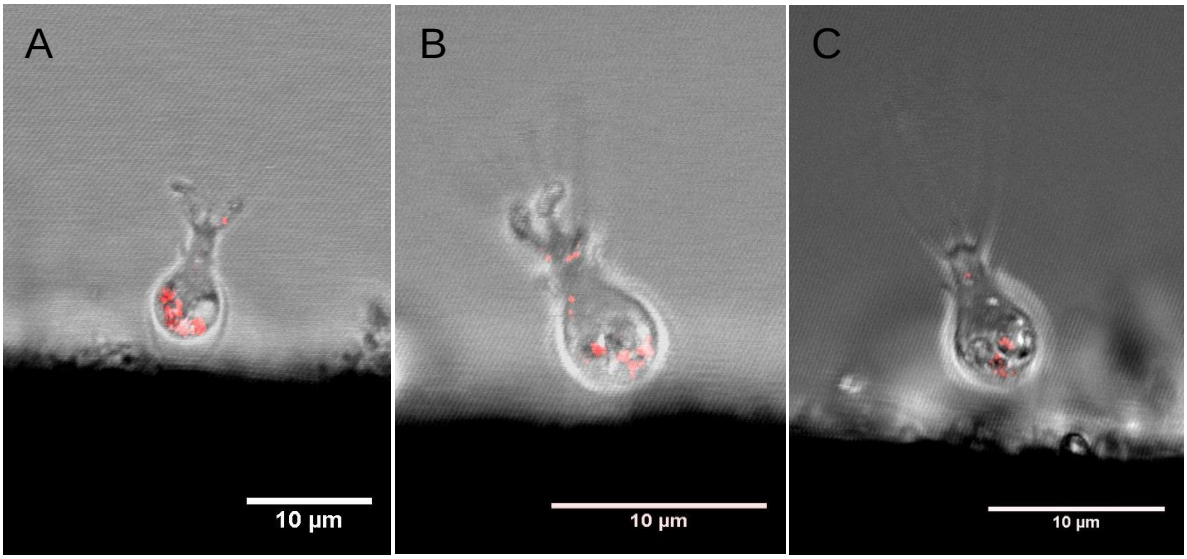

Figure 3.21: Maximum intensity projections of Choanoflagellates exposed to silver nanoparticles at various concentrations. **A –** 1 mg/L, **B –** 500 µg/L and **C –** 100 µg/L. A false red colour has been used to indicate reflected light.

At lower AgNP concentrations no uptake into the cells was observed within 2 hrs of Choanoflagellate containing substrate into the exposure medium. It was therefore decided to increase the exposure time, and incubate the Choanoflagellates in a solution of 11 µg/L for 24 hrs. This increased duration of the exposure led to AgNPs occurring within the cells as shown by figure 3.22.

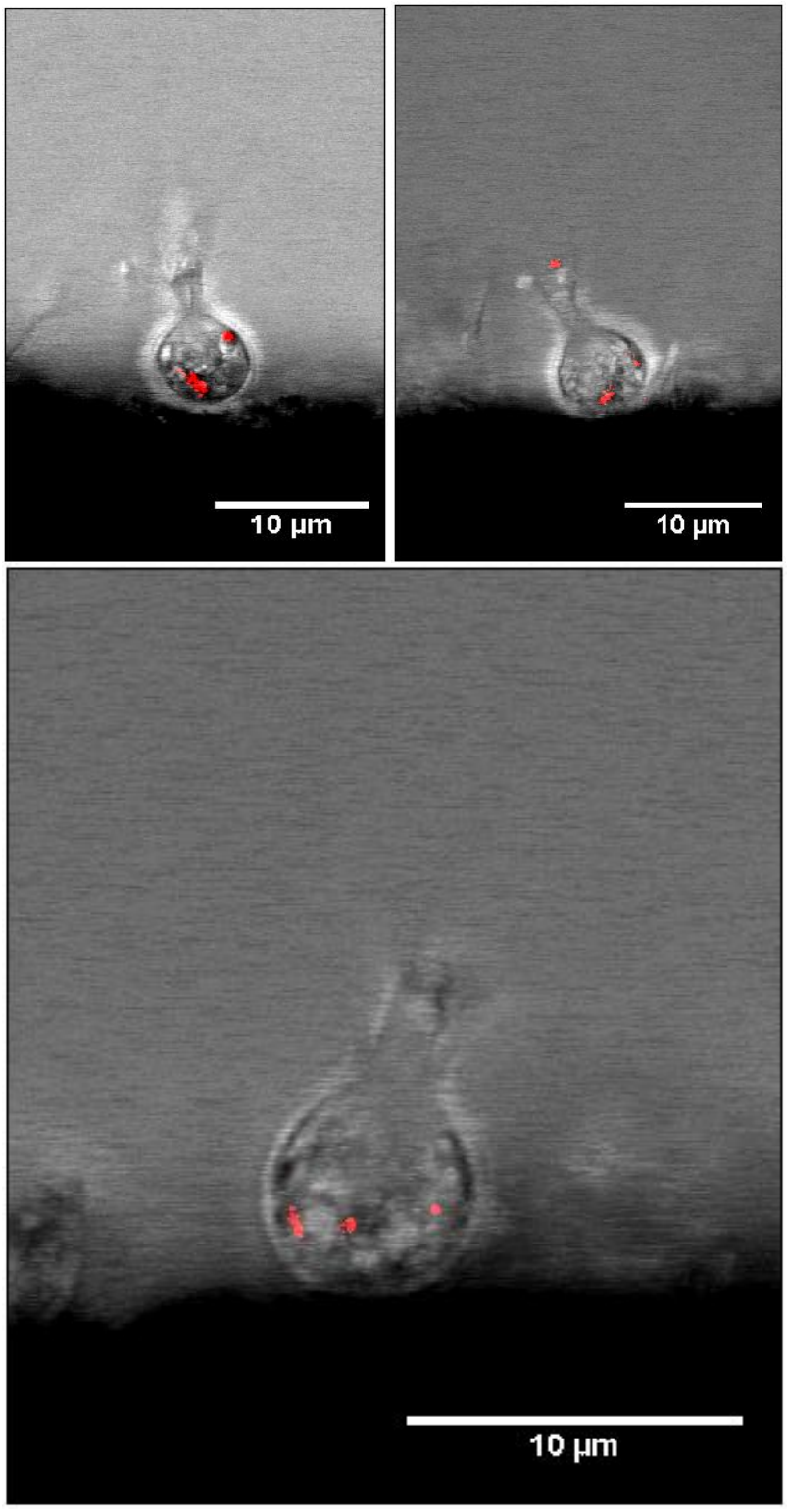

Figure 3.22: Maximum intensity projections of Choanoflagellates after incubation for 24 hrs with 11 µg/L silver nanoparticles. A false red colour has been used to indicate reflected light.

To ensure that the reflectance signal found in the exposure cultures were not as a result of other reflective material a negative control was introduced. In all the reflectance micrographs some reflectance was observed from the cell themselves, this interference was removed during the imaging process. Under the same conditions as the uptake experiments the negative control demonstrated no high intensity reflectance which was seen with the addition of the AgNPs.

To investigate the movement and handling of the AgNPs once they had been ingested by the Choanoflagellate cell a time series was taken for the highest concentration of AgNP suspension, 5.5 mg/L. The time series consists of a z stack of a Choanoflagellate cell repeatedly captured for 50 cycles. Figure 3.23 shows selected frames from the transmitted light channel of a time series at one focal plane through a Choanoflagellate cell without any false colour NP enhancement. This demonstrates movement of particles within an individual Choanoflagellate over time. In frame A of figure 3.23 the majority of the Ag material within the cell is being stored in the lowest part of the cell body, just below where the nucleus is positioned. A cluster of material is also found at the base of the flagellum, below the microvilli collar. As time progresses into frame B more material begins to accumulate at the base of the flagellum. The bulk of the Ag material can be seen to be shifted towards the left hand side of the cell. At frame C this bulk material has returned to the right hand side and shifted position higher up in the cell. By frame D the cluster of material at the base of flagellum is joined by more material moving up from the bulk storage below. By the final frame E, even more material is found at the flagellum base, with a significantly reduced amount now present in the main body of the cell. The Ag material that does remain within the Choanoflagellate cell had moved down lower towards the bottom of the cell again.

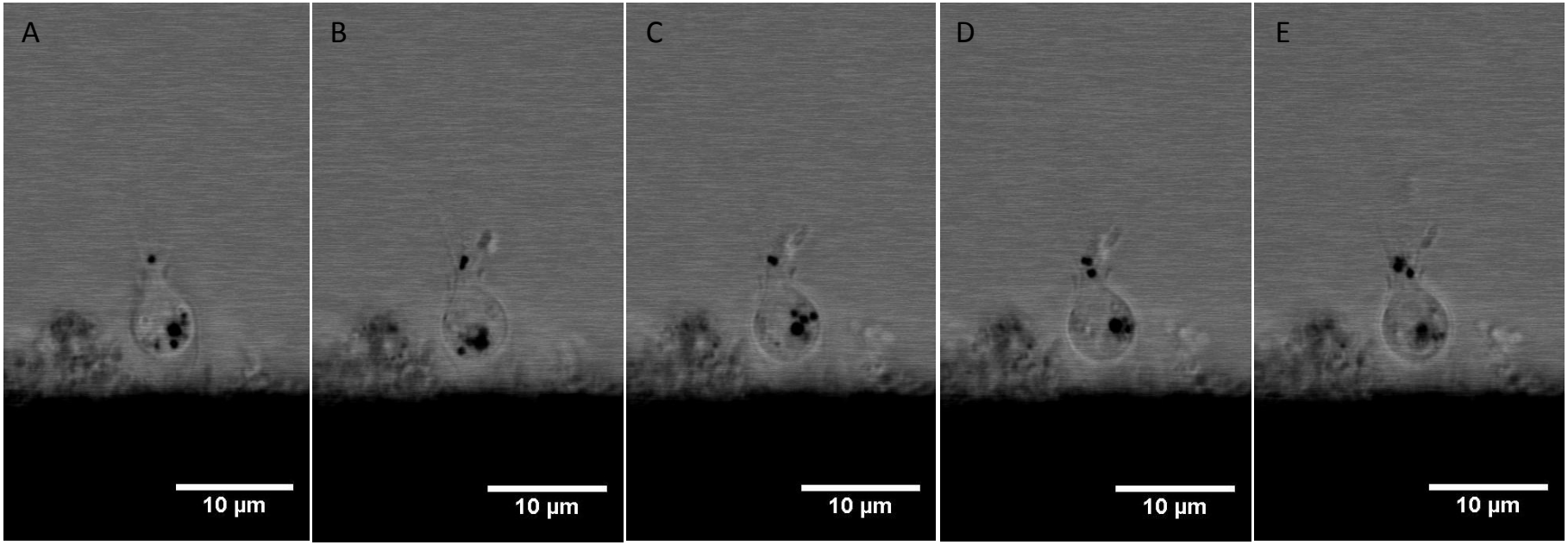

Figure 3.23. Time series of Choanoflagellates in 5.5 mg/L silver nanoparticle suspension. The opaque black dots within the cells were confirmed by the reflectance images to contain silver material.

3.6 Silver Nanoparticle Toxicity in Choanoflagellates

Ag toxicity from Ag^{+}, AgNPs or a combination of the two could potentially interfere with the ability of the Choanoflagellates to feed effectively. As a result this Ag toxicity may radically alter the uptake of AgNPs. It was therefore decided to establish the toxicity of AgNPs towards Choanoflagellate species *Salpingoeca amphoridium* over the range of concentrations used during the uptake experiments. A handling control was included in the experimental design in order to adequately account for any potential cell death which occurred as a result of the Choanoflagellates starvation process.

It was shown that during the time frame for the uptake studies of around 4 hrs, only the highest concentration of 5.5 mg/L resulted in a significant amount of cell death (figure 3.24). With all other concentrations used resulting in less than 40% mortality in the Choanoflagellate populations. For the lowest concentration observed in the uptake experiment 11μg/L the cells were exposed over a 24 hr time period. It was demonstrated during the toxicity study that at this low concentration there was little increase in the toxicity of the AgNPs at 24 hrs than at 4 hrs.

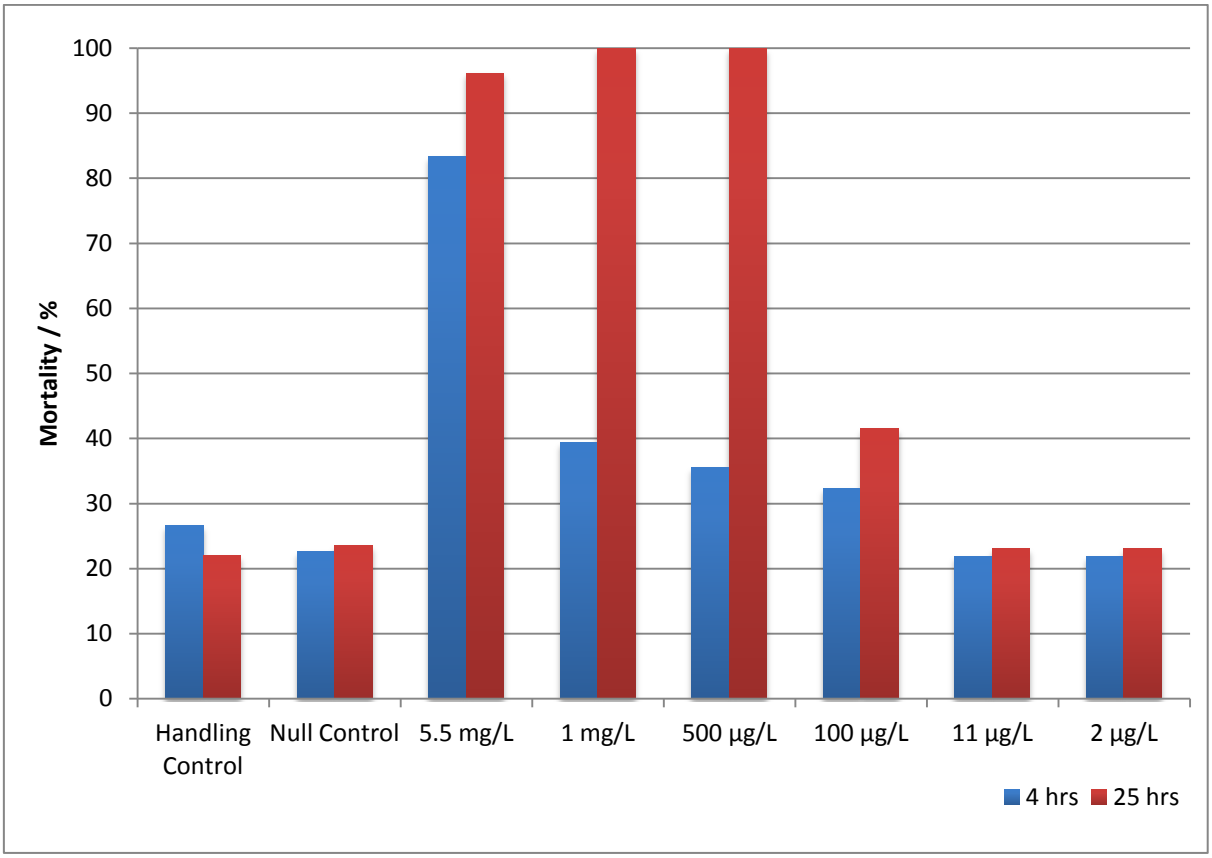

Figure 3.24 Comparison of the toxic effect of unwashed silver nanoparticles after at 4 hrs and 25 hrs. These are initial results with no replicates performed.

It was decided it was necessary to access whether the toxicity seen in the Choanoflagellates after exposure to AgNPs was as a result of the NPs themselves or as a result of the Ag^{+} associated with the NPs. To achieve this, the stock AgNP suspension was ultrafiltrated three times in order to remove Ag^{+} remaining from the NP synthesis, and from AgNPs which had dissolved. It was found that the washed AgNPs were less toxic when compared to the unwashed particles used in the uptake experiment (figure 3.25).

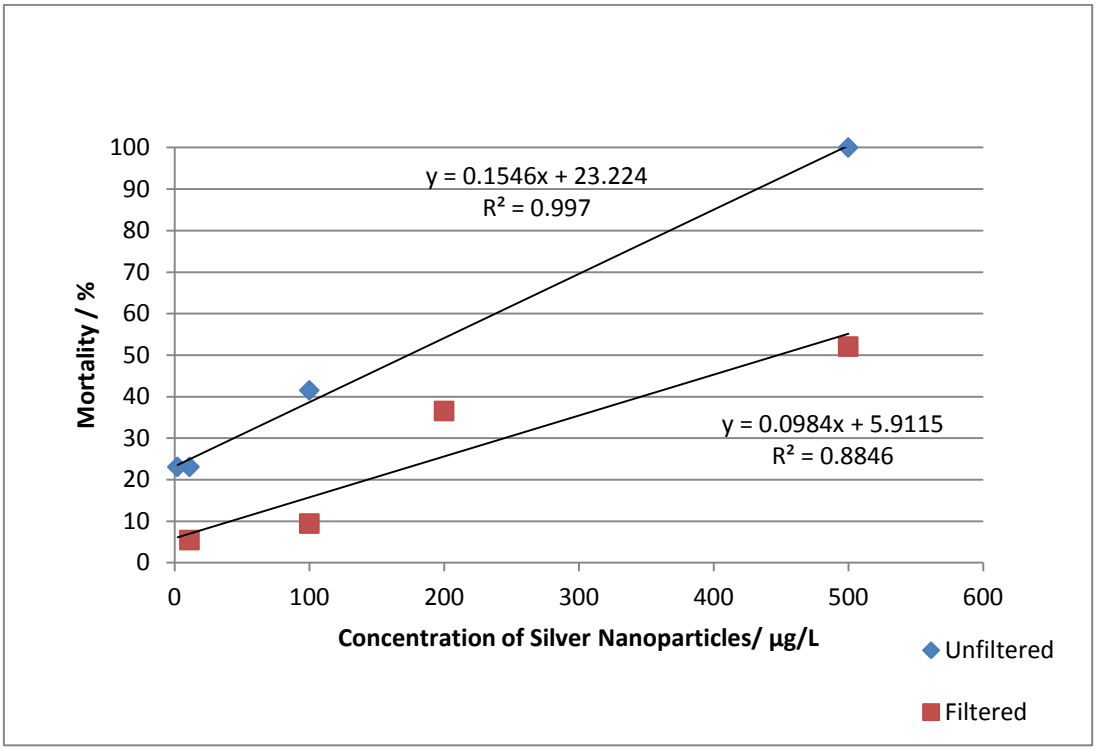

Figure 3.25 Comparison between the toxicity of washed and unwashed silver nanoparticles upon Choanoflagellates over 4 hrs. These are initial results with no replicates performed.

4. Discussion

4.1 Characterisation as Synthesised

4.1.1 Size Distributions

The hydrodynamic diameter obtained by DLS (Figure 3.1) was found to be smaller than the diameter measured by NTA (Figure 3.2). It is possible that the higher hydrodynamic diameter found by NTA is as a result of the high dilution required to perform the technique. In order for the NTA tracking software to reliably track individual particles a relativity low concentration of particles is required to prevent saturation of the video (Nanosight Ltd, 2009b). The citrate capping agent which coats the surface of the AgNP exists in equilibrium with citrate in solution. Upon dilution of the stock NPa NP suspension in ultrapure water, it is likely that some of the relatively labile citrate coating is removed when equilibrium is re-established (Cumberland and Lead, 2009). The removal of some of the citrate capping agent reduces the stability of the NP leading to an increase in particle size. Such an increase in z average diameter has been previously reported for citrate capped AgNPs, with the particles increasing in diameter from their original size of 35 nm to 42 nm in pure water (Romer et al., 2011). This agrees reasonably well with the increase found using NTA. DLS however is capable of measuring hydrodynamic diameter at far higher nanoparticle concentrations. It is therefore possible to measure the stock nanoparticle suspension without further modification.

To establish a core size of NPa AFM (figure 3.3) and TEM (figure 3.5) were used, the sizes found by the contrasting techniques were found to be consistent. A difference in diameter of approximately 15 nm is seen between the hydrodynamic diameter measured by DLS and the core diameter measured by AFM. This difference is a consequence of the different diameters measured by the two techniques. With the hydrated particle measured by light scattering

giving a hydrodynamic diameter, and the dehydrated particle measured by AFM giving just the core of the NP.

4.1.2 Chemical Properties

In order to provide a quantitative analysis of the composition of NPa EDX was used during the electron microscopy imaging of the NPs (Figure 3.7). Using the data obtained it is possible to quantify contamination from other metals, which may have impacted significantly upon subsequent toxicity testing. Not surprisingly a large proportion of the TEM grid analysed (Table 3.2) contained Ag from the particles present, along with a large quantity of copper which is a major constituent of the TEM grid used to support the AgNPs. Carbon found in the spectrum is likely to be as a result of both the citrate capping agent on the surface of the NPs and the carbon film deposited on the copper grid as a surface for NP adsorption. It is possible that the relatively small weight percentage of oxygen and sulfur found in the analysis are as a result of silver oxide and silver sulfide on the surface of the AgNPs. Oxygen atoms are also present in the capping agent, and maybe a constituent of the carbon film or as adsorbed molecular oxygen. A likely source of the silicon found in sample is low level contamination from the glassware used in the synthesis of the NPs.

UV-Vis spectroscopy (Figure 3.8) was used to measure the surface plasmon resonance to give an indication of the nanoparticle composition, with NPa absorbing strongly at 400 nm, which is the typical absorbance range for AgNPs in suspension.

It has been observed that some AgNPs may support smaller groups of atoms termed nanoclusters on their surface. These adsorbed nanoclusters whether supported by NPs or scaffolded by other means, have under some circumstances been shown to produce

fluorescence at certain excitation wavelengths. An autofluorescence emission signal from AgNPs could be used for tracking their uptake into living cells when using laser scanning confocal microscopy or similar fluorescence microscopy techniques, without the potential drawbacks associated with fluorescence labelling.

When the nanoparticle suspension NPa was investigated using excitation-emission matrix fluorescence spectroscopy (Figure 3.9) it was found that the emission wavelength would be optimal for viewing using an optical microscope, however the excitation needed to produce the emission is very low. Such a low wavelength of light is not able to penetrate the glass optics used in optical microscopy and additionally would likely be extremely harmful to living cells.

4.2 Nanoparticle Agglomeration in Media

From the DLS, AFM and UV-Vis measurements upon NPa in different dilutions of Pratt's medium it was found that higher ionic strength induced greater particle agglomeration due to removal of the citrate capping agent. The results from DLS indicate at low particle concentrations such as 2 and 11 μg/L in Pratt's medium, the AgNPs no longer exist as individual particles. However, these concentrations fall below the minimum operational range for DLS of 0.1 mg/L (Malvern Instruments, 2012), and so may not accurately reflect the agglomeration state of the particles.

During analysis of the micrographs it was found that whilst the mean core size did increase compared to that of the original NPa sample, height of the particles including the

agglomerates were lower than expected (Table 3.8). It is possible that any agglomerates formed may have been lying flat on the mica surface, giving a lower AFM size. However, there were generally a greater number of large particles found in the Pratt's medium dilutions with greater ionic strength. This is consistent with the intensity weighted size distributed attained from DLS, in which the NP concentrations greater than 11 µg/L did not initially form a large proportion of agglomerates (Figure 3.15). Instead the distribution increased in width, with pdi increasing for all particle concentrations below 5.5 mg/L.

The lowest concentration of AgNPs capable of being detected using the UV-Vis was 100 µg/L. From the higher concentrations a shift in the UV-Vis absorption peak from NPa was detected after treatment with Pratt's medium. The absorption peak moved towards higher wavelength in the spectrum, with the shift being smallest at the higher AgNPs concentration. It is well known that the optical properties of metal NPs are strongly dependent upon their size (Kelly et al., 2003). With larger particles and agglomerates absorbing higher wavelengths of light compared to the smaller particles.

The ionic strength of the Pratt's medium was calculated using the following equation:

Equation 4.1

$$I = {}^{1}/_{2}\,\Sigma(C_i Z_i^2)$$

The undiluted Pratt's Medium has an ionic strength of 1.3mM. To place the results of NPa characterisation in Pratt's medium into context they were compared to results found for another commonly used media for NP toxicity studies. The OECD recommended media for the freshwater organism *Daphnia magna* was found to have an ionic strength approximately 7 times greater than Pratt's medium. During studies in which citrate capped AgNPs were

dispersed into the OECD *D. magna* medium a ten-fold dilution was found optimum in both maintaining stable NPs without adversely affecting the organism's viability (Romer et al. 2011). At this dilution the ionic strength of the medium is 0.884 mM, which compares well to the ionic strength of the 5.5 mg/L NPa suspension, in which the AgNPs remained stable over a 24 hrs time period.

These results may be rationalised using DLVO theory. Briefly, as NPs move in suspension under the influence of Brownian motion they collide with other NPs in suspension (O'Melia, 1980). Such collisions combined with the attractive van der Waals forces can lead to the agglomeration and aggregation of the NPs. In this particular instance, to overcome these attractive forces a citrate capping agent is used to provide an electrostatic hindrance at the NP surface. As a result of the negative charges placed on the surface of the AgNPs by the presence of the citrate anion an electric double layer is created surrounding each individual NP. The thickness of the double layer is given by the reciprocal of the Debye-Huckel parameter, κ, which may be calculated using the following equation:

Equation 4.2

$$\kappa = \left(\frac{e^2 \sum n_i z_i^2}{\varepsilon k T}\right)^{1/2}$$

Where e, is the charge of an electron, $n_{i,}$ is the number concentration of ions in solution, $z_{i,}$ is the valency of ions in solution, ε, is the permittivity, k, is the Boltzmann constant and T, is the absolute temperature (Elimelech et al. 1995). The presence of ions in solution for this charge type mechanism of stabilisation may lead to a reduction in the amount of stabilisation provided, potentially leading to agglomeration of the NPs. It can be seen by inspecting the equation that as either the concentration of ions, $C_{i,}$ or the ionic charge, Z_i, of the medium

increases so does the Debye-Huckel parameter, κ, and so the thickness of the electric double layer 1/κ, decreases.

Using equation 4.2 the thickness of the double layer for AgNPs suspended in undiluted Pratt's medium is found to be 8.4 nm. When this is compared to the higher ionic strength of undiluted *Daphnia magna* medium the double layer, it is found to be less than half as thick for the Pratt's medium, at 3.2 nm. When the Pratt's medium is diluted to 50% of its original ionic strength the thickness of the calculated double layer increases to 11.9 nm. A similar increase in seen with a tenfold dilution of the *D. magna* medium with the double layer tripling in thickness to 10.3 nm compared to the undiluted medium. As this electric double layer decreases in thickness as a result of increased ionic strength, the NPs in suspension can come in closer proximity to one another. The attraction between the particles due to van der Waals forces then becomes more dominant, and at higher ionic strengths the particles are more likely to undergo agglomeration.

Based upon the results collected by DLS, UV-Vis spectroscopy and AFM it was confirmed that as the ionic strength of the Pratt's medium increases for all the concentration of AgNPs apart from 5.5 mg/L, the agglomeration state of the particles also increases. However as previously mentioned, the DLS data for concentrations below 100 μg/L, may not be valid due to the limitations in the DLS technique. It is on the strength this evidence that the null hypothesis, H_0, may be rejected with confidence. The alternative hypothesis H_A, which states, in dilutions of Pratt's medium with greater ionic strength nanoparticle stability will decrease and therefore agglomeration will increase, is therefore accepted.

4.3 Nanoparticle Uptake by Choanoflagellates

Upon entrainment in the current induced by the motion of the flagellum prey particles are brought through the microvilli collar of the Choanoflagellates. As would be expected if this were the case with AgNPs, clusters of reflected light were located within the collar. Once captured the prey particles would be expected to be brought towards the base of the microvilli, before the particle is engulfed by the cell via a pseudopod mediated mechanism. In the reflectance micrographs small areas of reflectance are located in the top of the cell body above the nucleus. Upon entrance in the cell body the membrane bound prey particles then move down below the nucleus to form food vacuoles. In the micrographs the area below the nucleus at the base of the cell body is where the majority of the reflectance signal is located. Therefore the locations in which the reflected light is detected are consistent with the handling expected of prey particles by the Choanoflagellates.

To ensure that the reflected light originates from within the Choanoflagellate cell itself optical slices through the cells at various focal planes were taken to compose z stacks. Little or no reflected light was found from the outermost planes that were imaged, with high amounts of reflected light found in the planes taken from the centre of the cells. This indicates that the majority of reflective material is within the cell, with very little material adsorbed onto the outer surface.

As shown in figure 1.3 members of the Choanoflagellate family Salpingoecidae possess a firm polysaccharide theca, the flask shaped theca of *Salpingoeca amphoridium* is a means for the cell to attach to substrate and resist the propeller motion generated by the flagellum. The theca surrounds the cell body and acts as an impenetrable barrier to particles. This ensures that no particles could have passively penetrated into the cell body. Therefore any particles

which have entered into the Choanoflagellate cell body must have done so through the site where active transportation of prey particles occurs.

Based on the data from DLS and AFM it was found that the higher concentrations of AgNPs are likely to interact with the Choanoflagellate cells as dispersed particles, in the absence of any biological effects. In contrast for the lowest concentration, 11 μg/L, the Ag material is most likely to be available to the Choanoflagellates as large agglomerates rather than individual particles. The NPs themselves cannot be resolved with an optical microscope so it was not possible to ascertain the diameter of the particles within the Choanoflagellates. However it would be reasonable to speculate that upon entry into the cell the particles would be brought in close proximately to one another within food vacuoles. This could facilitate further particle agglomeration. The environment within the food vacuoles is likely to be acidic and this would lead to protonation and loss of charge on the citrate capping, promoting dissolution of the AgNPs.

Using the filtration rate obtained from previously measured Choanoflagellates of 6.4 nl h^{-1} (Boenigk and Arndk, 2000) it is possible to estimate the mass of AgNPs encountered by each individual flagellate (Table 4.1). This calculation was performed with the assumption that the NP concentration remained constant throughout experiment. This assumption is likely to be more valid for the experiments performed at higher concentrations of NPs as a lower proportion of the NPs would be lost via sedimentation and uptake by other individuals. For the lower concentrations a larger proportion of the AgNPs are likely to have aggregated and sedimented or undergone dissolution over the 24 hr incubation period.

Table 4.1 Estimated mass of silver nanoparticles encountered by an individual Choanoflagellate cell at different incubation times.

Concentration of Silver Nanoparticles	Mass of Silver nanoparticles at 1 hr / ng	Mass of Silver nanoparticles at 24 hrs / ng
5.5 mg/L	0.03520	0.84480
1 mg/L	0.00640	0.15360
500 μg/L	0.00320	0.07680
100 μg/L	0.00064	0.01536
11 μg/L	7.04×10^{-5}	0.00170

Additionally not all of the AgNPs nanoparticles encountered by the Choanoflagellates may necessarily be assimilated by the cell. No evidence of AgNP assimilation was found when Choanoflagellate cells were exposed to concentrations below 100 μg/L over a duration of 1hr. However after 24 hrs reflectance was detected from within the cells at concentrations as low as 11 μg/L. Bearing in mind the previously discussed limitations, a threshold for detection using reflectance microscopy between 0.00064 and 0.0017 ng may be predicted.

In addition to whether Choanoflagellates were capable of taking up AgNPs, how they handle the particles afterwards is also of interest. To investigate this a time series was taken of an individual Choanoflagellate cell which had ingested a large amount of the reflective Ag material. The experiment was conducted at a relatively high AgNP concentration in order to give the greatest chance of visualising the particle movements. These high concentrations however have been shown to be significantly harmful towards the cells (Figure 3.24). The images taken during the time series depicted the Ag material inside the Choanoflagellate being redistributed around the cell. Several large boluses of material were transported away

from the main bulk of Ag material positioned at the base of the cell, towards another cluster at the base of the flagellum. A likely explanation of this redistribution of this material, is that it was being prepared for ejection from the cell.

Using the data obtained by reflectance confocal microscopy in addition to the current knowledge of Choanoflagellate physiology and feeding strategy it is possible to confirm with confidence that AgNPs can be ingested by Choanoflagellate cells. With increased exposure time NP ingestion can even be viewed at levels as low as 11 μg/L. This concentration of AgNPs is approaching the current predicted environmental concentration of 0.03 μg/L, as estimated during a realistic exposure scenario by Muller and Nowack (2008).

Based upon the evidence provided by reflectance confocal micoscopy the null hypothesis, H_1, can be rejected with confidence. The alternative hypothesis, H_B, which states, AgNPs will be assimilated by the Choanoflagellate *Salpingoeca amphoridium*, is therefore accepted.

4.4 Nanoparticle Toxicity in Choanoflagellates

Within a AgNP suspension Ag^+ is present and capable of adsorbing on the surface of Ag NPs, creating a complex environment of Ag^0 solids, free Ag^+ or its complexes, and surface-adsorbed Ag^+ (Liu and Hurt, 2010). From the results it can be seen that the particles washed via ultrafiltration were less toxic that those which were unwashed (Figure 3.25). Although less toxic the NP alone were still capable of inducing cell mortality at concentrations as low as 100 μg/L over 24 hrs. Possible mechanisms for this particle dependent toxicity may include the production of ROS, through the NP surface chemistry or disruption of organelles within

the Choanoflagellates (Nel et al., 2006). Dissolution of the AgNPs within the cells to release Ag^+ may also contribute to the toxicity of the washed particles (Park et al., 2010).

The toxicity induced in the Choanoflagellates by the AgNPs may complicate the handling of the particles once taken up by the cells, particularly at higher particle concentrations. As particles with are highly toxic towards the Choanoflagellates are more likely to be ejected from the cells. At higher AgNP concentrations it is also possible that the ability of the cells to ingest particles will be decreased. However no evidence to support this was found during this study.

The AgNPs used during the toxicity studies were found to be toxic towards Choanoflagellates at levels as low as 500 μg/L. Therefore it was decided to reject the null hypothesis H_2, which states silver nanoparticles will not be toxic towards Choanoflagellates. Instead the alternative hypothesis, silver nanoparticles will be toxic to Choanoflagellates, will be accepted.

The toxicity finding are consistent with those from a study introducing washed and unwashed silver nanoparticle to human skin keratinocytes, in which the washed particles were found to be non toxic. The unwashed particles however after a 24 hr exposure induced a dose-dependent decrease in cell viability at a concentration of 0.34 μg/ml (Samberg et al., 2010). However, in the case of the toxicity towards Choanoflagellates even the washed particles demonstrated some increase in mortality. Navarro et al. (2008) when using cysteine ligands to bind free Ag^+ found a cessation of the toxic effect from the AgNPs also, however the algal cells used presented with morphological changes such as; displaying cellular shrinkage and acquisition of an irregular shape. Although, the toxicity of the AgNPs was greater than for the equivalent dose of Ag^+, therefore not all of the toxicity from the AgNPs could be attributed to the production of Ag^+.

Based on the result from the toxicity study performed with the Choanoflagellate *Salpingoeca amphoridium* to compare the effect of washed and unwashed particles, unwashed AgNPs were found to be more toxic. Therefore it was decided to reject the null hypothesis, H_3, in favour of the alternative hypothesis, H_D which states that, the toxicity of AgNPs towards Choanoflagellates will be greater for particles which are unwashed compared to those washed by ultrafiltration.

4.5 Post-synthesis modification

4.5.1 Ultracentrifugation

As anticipated the effect of increased duration and increased force of centrifugation leads to a decrease in z average as measured by DLS (Figure 3.3). The reduction in z-average is through the sedimentation of larger particles in the NPa size distribution leading to a narrower distribution comprised of smaller particles in the supernatant (Figure 3.10a). The pellets which formed as a result of the centrifugation process contain particles with significantly increased z-averages (Figure 3.10b). This is directly proportional to the increase in centrifuge duration and increased centrifuge force. A likely contributing factor to the large increase in z average size in the pellet is the agglomeration which may occur as a result of the high density of nanoparticles reduced to the centrifuge tube.

Whether through particles from the pellet becoming resuspended into the supernatant or from contamination from the rotor bucket, small quantities of larger particles were found to be present in the DLS data for the centrifuged samples. These particles were too large to have remained in suspension during the centrifugation processing. They did however have an impact upon the calculated pdi for each of the centrifugation treatments on NPa. Whilst it can

be seen that the particles in the pellet are far more polydisperse than those in the suspension. An accurate assessment of whether the centrifugation process has reduced the polydispersity of the samples is difficult. At the greatest centrifugal force at 15, 000 rpm (Figure 3.10a) the intensity weighted distribution appears significantly narrower than the original sample. A 'long tail' is also present in the distribution, and is likely an artefact from these larger particles.

As a result of their surface plasmon resonance NPs are capable of interacting with light leading to absorbance in the UV-Vis region, with larger particles interacting with longer wavelengths of light than their smaller counterparts. A comparison between the UV-Vis spectrum performed on NPa as synthesised and the samples which had been centrifuged revealed a shift in the absorbance peak associated with AgNPs (Figure 3.1). With increased sedimentation of the larger particles through an increase force and time the UV-Vis absorbance shifts towards a lower wavelength, with the absorbance peak becoming narrower.

Through the use of FAAS as would be expected the mass of Ag in the pellet formed during centrifugation was much greater than that found in the supernatant. Only 9% of the Ag mass found in the supernatant for the samples centrifuged at 15,000 rpm for 1hr, compared with 44% of silver mass found in the supernatant of the sample centrifuged at 10,000 rpm for 30 mins.

With such low concentrations of AgNPs found the supernatant of the centrifuged samples this represents a substantial reduction in the yield for the production of these NPs. Therefore it is very unlikely such a post synthesis method would be appropriate for refining NP size in applications where large quantities of NP are required. However for environmentally realistic toxicity experiments, particularly those investigating the chronic effect of NPs only small

quantities of NPs are needed. In such testing where size dependent effects may be of interest, producing NPs with a well defined size distribution may be of greater priority than nanoparticle yield.

Unexpectedly the mass found in the pellet for 15,000 rpm for 1hr was approximately 30% lower than that found at 10,000 rpm for 1hr. With increased force the solid silver material adheres more strongly to the bottom of the centrifuge tube than for the 10,000 rpm sample. Therefore the reduced mass found in the 15,000 rpm pellet could potentially be explained by an increase in difficulty in fully re-suspending the pellet.

4.5.2 Ultrafiltration

During the removal of excess silver ions using the process of the ultrafiltration it was found that the hydrodynamic diameter of NPa increased by approximately 11% (Table 3.4). The increase in diameter after ultracentrifugation is likely a result of the addition of sodium citrate added to replace the solution lost through the process. Upon addition of excess sodium citrate a re-establishment of equilibrium between the particle surface and the solution may have resulted in an increase in citrate capping. Use of DLS also showed that ultrafiltration did not cause the formation of large agglomerates or introduce large particles into the suspension (Figure 3.14).

5. Conclusions

Using a chemical reduction method, AgNPs capped with sodium citrate were produced in four different sizes. The largest of these NPa was characterised using a range of techniques to provide hydrodynamic diameter, core size and chemical composition. Choanoflagellates were cultured in Pratt's medium upon strands of substrate with a *Klebsiella pneumonae* food source. To allow Choanoflagellate cells to be exposed to the NPs, the particles were suspended in the Pratt's medium. It was predicted that when suspended in the medium as a result of the ions present, the particles undergo agglomeration and increase in size. It was hypothesised that this increase in agglomeration and particle size would be proportional to the ionic strength of the Pratt's medium used.

In order to test this hypothesis the particles were suspended in Pratt's medium at various concentrations and their hydrodynamic diameter, core size and chemical composition characterised. When compared to the original NPa as synthesised it was found that the agglomeration state of the NPs did increase with increasing ionic strength. This corresponds well to work found in the literature (Romer et al. 2011).

Choanoflagellate cells have previously been found to ingest sub-micron polystyrene NPs. With the introduction of the potentially toxic AgNPs to the environment it was predicted these types of organism could be adversely affected. It was hypothesised that Choanoflagellate cells would be capable of assimilating AgNPs. To test this Choanoflagellate cells were incubated with AgNPs for different durations and particle concentrations. The cells were then examined using reflectance confocal microscopy, a technique in which highly reflective particles such as those comprised of Ag act as effective probes. It was discovered that Choanoflagellates cells were capable of ingesting the particles, even at concentrations as low as 11 μg/L, with a

24 hr exposure time. Through a combination of single images, z stacks and time series the position and movement of Ag material was examined within the Choanoflagellate cells. The position and handling of the material by the cells mimicked observations in the primary literature of Choanoflagellate feeding mechanisms. With the reflective particles found adhered to the cell microvilli collar, within areas associated with psuedopod formation and in the lowest part of the cell body in which food vacuoles are stored. At a particle concentrations of 5.5 mg/L some evidence was found to suggest the cells were also capable of ejecting the material they had ingested.

To quantity the effect that AgNPs had upon the Choanoflagellates toxicity tests were performed under conditions set to mimic those of the uptake experiments. It was found that the greater exposure time, particularly for the higher concentrations increased the AgNP toxicity. It also was hypothesised that AgNPs which had been washed using ultrafiltration would show reduced toxicity to those which had not. The two sets of particles were compared during 24 hr test, with the unwashed particles proving to have a much greater toxicity.

6. Further Work

From the conclusions of this work, several suggestions for future work are presented below. The suggestions are presented in order of importance, with the first suggestions being the most likely to improve current knowledge of NP uptake in protozoa.

- The use of reflectance confocal microscopy has allowed for the imaging of AgNP uptake by the Choanoflagellates *Salpingoeca amphoridium*. Although through a limitation in the resolution in optical microscopy it is unable to provide any information on transformations which occur to the NPs within the Choanoflagellates.

To better understand the interactions which occur between the NPs and the Choanoflagellates after ingestion it would also be advantageous to collect images of the NPs within the cells in relation to the organelles.

For future investigation in the uptake of AgNPs in Choanoflagellates a combination of electron microscopy (EM) and EDX should be considered for use on cyrosectioned cells. EM would allow for the sizes of any AgNP agglomerates to be accurately measured. It would also allow for information to be gained on how the particles are contained within the cell. Appropriate staining of the sections for the purpose of EM would allow for the organelles of the Choanoflagellates to be visualised. Where the particles are within the cell and how they are contained may convey some information on the mechanism of toxicity in this case. For instance NPs in food vacuoles may be exposed to an acidic environment which could enhance particle dissolution. Unbound particles however may be capable of disrupting the function of organelles such as the mitochondria, to produce harmful ROS.

In combination with EM, EDX can be used to certify the presence of Ag in the Choanoflagellates as indicated by the reflectance confocal microscopy. Additionally, chemical changes in the elemental composition of the NPs may also be detected such as oxidation or interaction with thiol containing compounds.

- In addition to being predacious towards bacteria Choanoflagellates are themselves predated upon by larger multi-cellular organisms, such as the filter feeding water flea *Daphnia magna*. Therefore the question as to whether AgNPs ingested by Choanoflagellates are capable of travelling up the food chain is raised. Future work

could include studies in which Choanoflagellates incubated with AgNPs are fed to an organism such as *Daphnia magnia*. With these significantly larger organisms extraction of the gut is possible and would allow for analysis of the contents, potentially reflectance confocal microscopy may be useful for that purpose. Another valuable piece of information which could be obtained from this type of study is whether the AgNPs show enhanced toxicity to larger organisms through bioaccumulation.

- Clearly the ionic strength in the medium used to expose living organisms to NPs has a large impact upon the agglomeration state of the NPs. In order to investigate effects which solely occur as a result of the use of NPs it is desirable to maintain the minimal amount of agglomeration possible. It has been shown in previous studies with citrate capped AgNPs in other media, that with a reduction in ionic strength to 0.884 mM it is possible to maintain NP stability (Romer et al., 2011). This was also found to be the case with the 5.5 mg/L NP suspension with an ionic strength of 0.65 mM. However for the lower concentrations of NPs used this ionic strength was much greater. Therefore to reduce the issue of NP agglomeration at lower doses it is proposed that diluted Pratt's medium should be tested. Ideally the medium should have an ionic strength at or below 0.884 mM in order to maintain particle stability. As well as ensuring the stability of the NPs however, the diluted medium must also be capable of supporting the growth of the Choanoflagellates, particularly during the longer duration experiments.

- Alternatively the use of other capping agents has been successfully demonstrated with the synthesis and stabilisation of AgNPs. In particular, PVP and thiolated-PEG have demonstrated an increased affinity to the AgNP surface compared to the relatively labile citrate molecule. These capping agents provide NP stability via steric hinderence and are not as strongly affected by increasing ionic strength as charged based capping agents. As a result of this NPs capped with these stabilising agents tend to show an increased resistance to agglomeration in various media. Future work with these particles may provide a greater understanding of the interaction between individual AgNPs and Choanoflagellates at low particle concentrations. Compared to the interaction of the Ag agglomerates seen with the citrate capped particles at low NP concentrations.

- To provide useful data upon the potential implications for NP release into the environmental it is desirable to use concentrations of AgNPs which are as close to environmentally realistic as possible. To allow characterisation of particles in media at these lower concentrations refinement of the UV-spectroscopy will be required. The use of cuvettes with increased length should be considered for future work. An increased pathlength would allow for a greatly increased detection limit.

- It is the novel size dependent effects of NPs which may potentially lead to an increased toxicity when compared to that of their bulk counterparts. To investigate these size dependent effects it is necessary to have NPs with are as monodispersed as possible. Ultracentrifugation has been shown capable of reducing the width of the size distribution of a batch of AgNPs by the sedimentation and removal of the largest

particles. It has also under some circumstances been shown capable of reducing the pdi of the particles as a consequence of this distribution narrowing effect. It was only possible to investigate a relatively small range of centrifuge forces and durations during this study. Therefore to optimise the conditions for this post synthesis modification technique, a more comprehensive investigation would need to be conducted. NPa used in this study were only moderately monodispersed when compared to the particles synthesised by other synthesis methods such as NPc. Particles from these methods could yield a much more monodispersed batch, with a pdi approaching the optimum 0.1. The technique could potentially be expanded to accommodate all the particle size range produced from NPb, NPc and NPd methods. However additional work would need to be conducted to again optimise the conditions to sediment the largest particles from the size distribution without removing all particles from the supernatant.

References

Adl, S., Simpson, A.G.B., Farmer, M.A., Andersen, R.A., Anderson, O.R., Barta, J.R., et al. (2005). The New Higher Level Classification of Eukaryotes with Emphasis on the Taxonomy of Protists. **J. Eukaryot. Microbiol.,** 52(5): 399–451

Aguilera, J.M. and Stanley, D.W. (1999). **Microstructural Principles of Food Processing and Engineering.** Springer, 2nd Edition.

Ammann, M., Burtscher, H., Siegmann, H. C. (1990). Monitoring volcanic activity by characterisation of ultrafine aerosol emissions. **J. Aerosol. Sci.,** 21(1): 275-278

Ashby, M.F., Ferreira, P.J. and Schodek, D.L. (2009). Nanomaterials, Nanotechnologies and Design. Elsevier Ltd. ISBN: 978-0-7506-8149-0. 41-43

Asharani, P., Wu, Y. L., Gong, Z. Y., and Valiyaveetil, S. **(**2008) Toxicity of silver nanoparticles in Zebrafish models. **Nanotechnology,** 19

Asharani, P., Wu, Y. L., Gong, Z. Y., and Valiyaveetil, S. (2011). Comparison of the toxicity of silver, gold and platinum nanoparticles in developing zebrafish embryos. **Nanotoxicology,** 5(1): 43–54

Auffan M, Rose J, Bottero J, Lowry G, Jolivet J and Wiesner M. (2009). Towards a definition of inorganic nanoparticles from an environmental, health and safety perspective. **Nature Nanotechnology** 4: 634-641

Baalousha, M. and Lead, J.R. (2012). Rationalizing Nanomaterial Sizes Measured by Atomic Force Microscopy, Flow Field-Flow Fractionation, and Dynamic Light Scattering: Sample Preparation, Polydispersity, and Particle Structure. **Environ. Sci. Technol.,** 46 (11): 6134–6142

Baker, A. (2002). Spectrophotometric discrimination of river dissolved organic matter. **Hydrological Processes,** 16(16): 3203-3213.

Bar-Ilan, O., Albrecht, R. M., Fako, V. E. and Furgeson, D.Y. (2009). Toxicity Assessments of Multisized Gold and Silver Nanoparticles in Zebrafish Embryos. **Small**, 5(16): 1897–1910

Benn, T.M and Westerhoff, P. (2008) Nanoparticle Silver Released into Water from Commercially available Sock Fabrics. **Environ. Sci. Technol.,** 42: 4133–4139

Bergh, O., Borsheim, K.Y., Bratbak, G. and Heldal, M. (1989). High abundances of viruses found in aquatic environments. **Nature,** 340: 467-468

Bhushan, B. (2004). **Springer Handbook of Nanotechnology.** Springer. p385-394

Blaser, S.A., Scheringer, M., MacLeod, M., et al. (2008) Estimation of cumulative aquatic exposure and risk due to silver: Contribution of nano-functionalized plastics and textiles. **Science of the Total Environment,** 390 (2-3): 396-409

Boenigk, J. and Arndt, H. (2000). Comparative studies on the feeding behavior of two heterotrophic anoflagellates: the filterfeeding choanoflagellate *Monosiga ovata* and the raptorial-feeding kinetoplastid *Rhynchomonas nasuta*. **Aquat. Microb. Ecol.,** 22: 243–249

Boenigk, J. and Arndt, H. (2002). Bacterivory by heterotrophic flagellates: community structure and feeding strategies. **Antonie van Leeuwenhoek,** 81: 465–480

Borkovec, M. (2002). "Dynamic Light Scattering". In Krister, H. (eds) (2002). **Handbook of Applied Surface and Colloid Chemistry,** Vol. 1-2. John Wiley & Sons. p365-367

Bury, N. R., Walker, P. A. and Glover, C. N. (2003). Nutritive metal uptake in teleost fish. **The Journal of Experimental Biology,** 206: 11-23

Cao, G. (2004). **Nanostructures and Nanomaterials – Synthesis, Properties and Applications. World Scientific.** ISBN: 9814322504

Carr, M., Leadbeater, B. S. C., Hassan, R., Nelson, M., and Baldauf, S. L. (2008). Molecular phylogeny of choanoflagellates, the sister group to Metazoa. **PNAS,** 105(43): 16641-16646

Cavalier-Smith, T. (1993). Kingdom protozoa and its 18 phyla. **Microb. Rev.,** 57: 953-994

Chinnapongse, S. L., MacCuspie, R.I. and Hackley, V.A. (2011). Persistence of singly dispersed silver nanoparticles in natural freshwaters, synthetic seawater, and simulated estuarine waters. **Science of the Total Environment.** 409: 2443–2450

Choanoflagellate Lifedesk. Available by: www.choanoflagellates.lifedesks.org/. Accessed on: 03/08/12.

Claxton, N.S., Fellers, T.J. and Davidson, M.W. (2008). Laser Scanning Confocal Microscopy. Available from: http://www.olympusconfocal.com/theory/LSCMIntro.pdf. Accessed 31/06/12.

CPS Instruments, (2007), Available from: http://www.cpsinstruments.eu/pdf/Introduction %20Differential%20Sedimentation.pdf. Accessed on: 17/06/12

Cranfield University (2010). Available from: http://www.cranfield.ac.uk/cds/cfi/eds.html. Accessed on 08/06/12

Croteau, M., Misra, S. K., Luoma, S. N. and Valsami-Jones, E. (2011). Silver Bioaccumulation Dynamics in a Freshwater Invertebrate after Aqueous and Dietary Exposures to Nanosized and Ionic Ag. **Environ. Sci. Technol.**, 45: 6600–6607

Cumberland S. A. and Lead J. R. (2009) Particle size distributions of silver nanoparticles at environmentally relevant conditions. **Journal of Chromatography A**, 1216 (52): 9099-9105.

Das, R., Nath, S.S., Chakdar, D., Gope G. and Bhattacharjee, R. (2009). Preparation of Silver Nanoparticles and Their Characterization. **Azojono - Journal of Nanotechnology online.** 5: 1-6

Davies, A., Lewis, D. J., Watson, S. P., Thomas, S. G., and Pikramenou, Z. (2011). pH-controlled delivery of luminescent europium coated nanoparticles into platelets. **PNAS,** 109(6): 1862–1867

Diez, I. and Ras, R.H.A. (2011). Fluorescent silver nanoclusters, **Nanoscale,** 3: 1963-70

Domingos, R.F., Baalousha, M.A., Ju-Nam, Y., Reid, M.M., Tufenkji, N., Lead, J.R., et al. (2009). Characterizing manufactured nanoparticles in the environment: multimethod determination of particle sizes. **Environ Sci Technol.,** 43: 7277‑7284

Doty, R. C., Tshikhudo, T. R., Brust, M., and. Fernig, D.G. (2005). Extremely Stable Water-Soluble Ag Nanoparticles. Chem. Mater. 17: 4630-4635

Ebnesajjad, S. and Khaladkar, P.R. (2005). **Fluoropolymers applications in chemical processing industries – the definitive user's guide and databook.** William Andrew Inc.

Elimelech, M., Gregory, J., Jia, X. and Williams, R.A. (1995). **Particle Deposition and Aggregation - Measurement, Modelling and Simulation.** Elsevier.

European Commission (2011). Commission Recommendation on the definition of nanomaterial.

European Environment Agency. Urban waste water treatment (CSI 024) – Assessment. Available from: www.eea.europa.eu/data-and-maps/indicators/urban-waste-water-treatment/urban-waste-water-treatment-assessment-3. Accessed 28/06/12.

Feng, Q. L., Wu, J., Chen, G. Q., Cui, F. Z., Kim, T. N. and Kim, J. O. (2000). A mechanistic study of the antibacterial effect of silver ion on Escherichia coli and Staphylococcus aureus**. J. Biomed. Mater. Res.,** 52: 662-668.

Fenchel, T. (1982). Ecology of heterotropic microflagellates IV. Quantative occurrence and importance as bacterial consumers. **Marine ecology progress series,** 9: 35-42

Fenchel, T. (1986). Protozoan filter feeding. **Prog. Protistol.,** 1: 65-113

Foldbjerg, R., Olesen, P., Hougaard, M., Dang, D. A., Hoffmann, H. J. and Autrup H. (2009). PVP-coated silver nanoparticles and silver ions induce reactive oxygen species, apoptosis and necrosis in THP-1 monocytes. **Toxicology Letters,** 190: 156–162

Fukuda, H. And Koike, I. (2000). Feeding currents of particle-attached nanoflagellates—a novel mechanism for aggregation of submicron particles. **Mar. Ecol. Prog. Ser.,** 202: 101–112

Hackley, V.A. and Clogsten, J.D. (2007). Measuring the Size of Nanoparticles in Aqueous Media Using Batch-Mode Dynamic Light Scattering. NIST - NCL Joint Assay Protocol, PCC-1, Version 1.1

Handy, R.D., Shaw, B.J. (2007). Toxic effects of nanoparticles and nanomaterials: implications for public health, risk assessment and the public perception of nanotechnology. **Health Risk Soc.,** 9: 125–144

Handy, R.D., von der Kammer, F., Lead, J. R., Hassellov, M., Owen, R. and Crane, M. (2008). The ecotoxicology and chemistry of manufactured nanoparticles. **Ecotoxicology,** 17: 287–314

Hasegawa, S., Wakamatsu, S., Ohara, T., Itano, Y., Saitoh, K., Hayasaki, M., Kobayashi, S. (2007) Vertical profiles of ultrafine to supermicron particles measured by aircraft over Osaka metropolitan area in Japan. **Atmos. Environ.,** 41: 717–729

Henglein, A. and Giersig, M. (1999). Formation of Colloidal Silver Nanoparticles: Capping Action of Citrate. **J. Phys. Chem. B.,** 10: 9533-9539

Higson, S. (2004). **Analytical Chemistry**. Oxford University Press, p 185

Hou H, Takamatsu T, Koshikawa MK, Hosomi M (2005) Migration of silver, indium, tin, antimony and bismuth and variations in their chemical fractions on addition to uncontaminated soils. **Soil Sci**. 170: 624-39

Jenway (2009). Model 6800 UV-Vis spectrophotometer User Manual.

Ju-Nam Y and Lead JR (2008), Manufactured nanoparticles: An overview of their chemistry, intereactions and potential environmental implications. **Science of the Total Environment,** 400: 396-414

Kaegi, R., Voegelin, A., Sinnet, B., Zuleeg, S., Hagendorfer, H., Burkhardt, M. and Siegrist, H. (2011). Behavior of Metallic Silver Nanoparticles in a Pilot Wastewater Treatment Plant. **Environ. Sci. Technol.,** 45 (9): 3902–3908

Karpov, S.A. and Leadbeater, B.S.C. (1997). Cell and Nuclear Division in a Freshwater Choanoflagellate, *Monosiga ovata* Kent. **European Journal of Protistology,** 33: 323-334

Kelly, K.L., Coronado, E., Zhao, L.L. and Schatz, G.C. (2003). The Optical Properties of Metal Nanoparticles: The Influence of Size, Shape, and Dielectric Environment. J**. Phys. Chem. B.,** 107: 668-677

Kelsall, R., Hamley, I. and Geoghegan, M. (2005) **Nanoscale science and technology.** John Wiley & Sons. ISBN-10: 0-470-85086-8

Koike, I., Shigemitsu, H., Kazuki, T. and Kazuhiro, K. (1990). Role of sub-micrometre particle in the ocean. **Nature,** 345: 242-244

Lansdown, A. B. G. (2006) Silver in Health Care: Antimicrobial Effects and Safety in Use, **Curr. Probl. Dermatol.,** 33: 17–34

Larese, F. F., D'Agostin, F., Crosera, M., Adami, G., Renzi, N., Bovenzi, M. and Maina, G. (2009). Human skin penetration of silver nanoparticles through intact and damaged skin. **Toxicology,** 255: 33–37

Lead, J. R., and Wilkinson, K. J. (2006). Aquatic Colloids and Nanoparticles: Current Knowledge and Future Trends. **Environmental Chemistry.** 3(3): 159-171

Leadbeater, B.S.C. and Morton, C. (1974). A microscopical study of a marine species of *Codosiga* James-Clark (Choanoflagellata) with special reference to the ingestion of bacteria. **Biological Journal of the Linnean Society.** 6(4): 337–347

Leadbeater, B.S.C., Yu, Q., Kent, J. and Stekel, D.J. (2009). Three-dimensional images of choanoflagellate loricae. **Proc. R. Soc. B.,** 276: 3-11

Lee, K. J., Nallathamby, P. D., Browning, L. M., Osgood, C. J. and Xu, X. N. (2007), In vivo imaging of transport and biocompatibility of single silver nanoparticles in early development of Zebrafish embryos. **ACS Nano** 1 (2): 133-143

Levard, C., Reinsch, B.C., Michel, F.M., Oumahi, C., Lowry, G.V. and

Brown, G.E. (2011). Sulfidation Processes of PVP-Coated Silver Nanoparticles in Aqueous Solution: Impact on Dissolution Rate. **Environ. Sci. Technol.** 45: 5260–5266

Li, N., Xia, T. and Nel, A. E. (2008). The role of oxidative stress in ambient particulate matter-induced lung diseases and its implications in the toxicity of engineered nanoparticles. **Free Radical Biology & Medicine,** 44: 1689-1699

Liu, J. And Hurt, R. H. (2010). Ion Release Kinetics and Particle Persistence in Aqueous Nano-Silver Colloids. **Environ. Sci. Technol.,** 44: 2169–2175

Lowry, G.V., Gregory, K.B., Apte, S.C. and Lead, J.R. (2012a). Transformations of Nanomaterials in the Environment. **Environ. Sci. Technol.,** 46: 6893−6899

Lowry, G.V., Reinsch, B.C., Espinasse, B.P., Badireddy, A.R., Richardson, C. J., Bryant, L.D., et al. (2012b). Long-Term Transformation and Fate of Manufactured Ag Nanoparticles in a Simulated Large Scale Freshwater Emergent Wetland. **Environ. Sci. Technol.,** 46: 7027−7036

Lovestam G, Rauscher H, Roebben G, Kluttgen B, Gibson N, Putaud J and Stamm H (2010). Considerations on a definition of nanomaterial for regulatory purposes. Joint Research Centre reference report.

Luca, S. (2004). Atomic Absorption Spectrophotometry (AAS). Petrik Lajos Vocational School for Chemistry.

Luoma, S.N. and Rainbow, P. (2005). Why Is Metal Bioaccumulation So Variable?

Biodynamics as a Unifying Concept. **Environ. Sci. Technol.**, 39(7): 1921-1931

Luoma, S.N. (2008). Silver nanotechnologies and the environment: old problems or new challenges? Woodrow Wilson International Institute for Scholars and PEW Charitable Trusts

Malvern Instruments Ltd. (2011). Dynamic Light Scattering common terms defined. Inform white paper.

Malvern Instruments Ltd. (2012). Available from: www.malvern.com/labeng/technology /dynamic_light_scattering.htm Accessed on 06/08/12.

Marchant, H.J. and Scott, F.J. (1993). Uptake of sub-micrometre particles and dissolved organic material by Antarctic choanoflagellates. **Mar. Ecol. Prog. Ser.,** 92: 59-64

Mueller, N.C. and Nowack, B. (2008), Exposure Modelling of Engineered Nanoparticles in the Environment. **Environ. Sci. Technol.,** 42: 4447-4453

Nanosight Ltd. (2009a). Review - Applications of Nanoparticle Tracking Analysis (NTA) in Nanoparticle Research. M110B.

Nanosight Ltd. (2009b). Technical Note How to make Concentration Measurements using NanoSight LM Series Instruments. M500B.

Navarro, E., Piccapietra, F., Wagner, B., Marconi, F., Kaegi, R., Odzak, N., et al. (2008). Toxicity of Silver Nanoparticles to Chlamydomonas reinhardtii. **Environ. Sci. Technol.,** 42 8959–8964

Nel, A., Xia, T., Madler, L. and Li, N. (2006). Toxic Potential of Materials at the Nanolevel. **Science**, 311: 622-627

Nikon (2002). Available from: http://www.microscopyu.com/print/articles/confocal/reflectedconfocalintro-print.html. Accessed on: 04/07/12

Nowack, B. and Bucheli, T.D. (2007). Occurrence, behavior and effects of nanoparticles in the environment. **Environmental Pollution,** 150(1): 5–22

O'Melia, C. R., (1980). Aquasols: The behaviour of small particles in aquatic systems. **Environmental Science and Technology.** 14(9): 1052-1060

Orme, B.A.A., Blake, J.R. and Otto, S.R. (2003). Modelling the motion of particles around choanoflagellates. **J. Fluid Mech.,** 475: 333-355

Paddock, S. (2002). Confocal Reflection Microscopy: The "Other" Confocal Mode. **BioTechniques,** 32(2): 274-278

Park, E., Bae, E., Yi, J., Kim, Y., Choi, K., Lee S., et al. (2010). Repeated-dose toxicity and inflammatory responses in mice by oral administration of silver nanoparticles. **Environmental Toxicology and Pharmacology,** 30: 162–168

PerkinElmer (2006). An Introduction to fluorescence spectroscopy.

Pettitt, M.E. (2001). Prey capture and ingestion in choanoflagellates. Ph.D. thesis, University of Birmingham.

Pettitt, M.E., Orme, B.A.A., Blake, J.R. and Leadbeater, B.S.C. (2002). The hydrodynamics of filter feeding in choanoflagellates. **European Journal of Protistology.** 30: 313-332

Pishkenari, H.N., Jalili, N. and Meghdari, A. (2006). Acquisition of high-precision images for non-contact atomic force microscopy. **Mechatronics,** 16: 655–664

Pronk, M., Goldscheider, N. and Zopfi, J. (2009): Microbial communities in karst groundwater andtheir potential use for biomonitoring. **Hydrogeology Journal,** 17(1): 37-48

Römer, I., White, T. A., Baalousha, M., Chipman K., Viant, M. R. and Lead, J. R. (2011). Aggregation and dispersion of silver nanoparticles in exposure media for aquatic toxicity tests. **Journal of Chromatography A,** 1218(27): 4226–4233

Samberg, M. E., Oldenburg, S. J. and Monteiro-Riviere, N.A. (2010). Evaluation of Silver Nanoparticle Toxicity in Skin in Vivo and Keratinocytes in Vitro. **Environmental Health Perspectives,** 118(3): 407-413

Scalf, J and West, P. (2006). Part I- Introduction to Nanoparticle Characterisation with AFM. Pacific Nanotechnology.

SCENIHR (2010). Scientific basis for the definition of the term "Nanomaterial".

Shaw, B. J. and Handy, R. D. (2011). Physiological effects of nanoparticles on fish: A comparison of nanometals versus metal ions. **Environment International**, 37: 1083–1097

Sherr, E.B. (1988). Direct use of high molecular weight polysaccharide by heterotrophic flagellates. **Nature,** 335: 348-351

Sherr, E.B. and Sherr B. (1988). Role of Microbes in Pelagic Food Webs: A Revised Concept. **Limnology and Oceanography,** 33(5): 1225-1227

Shimeta, J. (1993). Diffusional encounter of submicrometer particles and small cells by suspension feeder. **Limnol. Oceanogr.,** 38(2): 456-465

Thakkar, K.N., Mhatre, S.S. and Parikh, R.Y. (2010). Biological synthesis of metallic nanoparticles. **Nanomedicine: Nanotechnology, Biology, and Medicine.** 6: 257–262.

University College Davis (2012). Available from http://chemwiki.ucdavis.edu/ PhysicalChemistry/Spectroscopy/Electronic_Spectroscopy/Electronic_Spectroscopy. Accessed on 07/08/12.

Wang, C., Wang, L., Wang, Y., Liang, Y. and Zhang, J. (2012). Toxicity effects of four typical nanomaterials on the growth of Escherichia coli, Bacillus subtilis and Agrobacterium tumefaciens. **Environ Earth Sci.,** 65: 1643–1649

Webb, R.H. (1996). Confocal optical microscopy. **Rep. Prog. Phys.,** 59: 427–471

Wells, M.L. and Goldberg, E.D. (1991). Occurence of small colloids in seawater. **Nature.** 352: 342-344

Wilkinson, K. J.; Balnois, E.; Leppard, G. G.; Buffle, J. (1999). Characteristic Features of the Major Components of Freshwater Colloidal Organic Matter Revealed by Transmission Electron and Atomic Force Microscopy. **Colloids Surf. A.,** 155: 287−310

Wood, C. M., Playle R. C. and Hogstrand, C. (1999). Physiology and modelling of mechanisms of silver uptake and toxicity in fish. **Environmental Toxicology and Chemistry,** 18(1): 71–83

Woodrow Wilson International Institute for Scholars and PEW Charitable Trusts, Nanotechproject, Available from: www.nanotechproject.org [accessed 28/06/12].

Yguerabide, J. and Yguerabide, E.E. (1998). Light-scattering submicroscopic particles as highly fluorescent analogs and their use as tracer labels in clinical and biological applications— Theory. **Anal. Biochem.,** 262: 137–156.

Zhao, C. and Wang, W. (2010). Biokinetic Uptake and Efflux of Silver Nanoparticles in Daphnia magna. **Environ. Sci. Technol.,** 44: 7699–7704

Zoloterev, V.A. (2010). Nanosafety as a new direction of transboundary biomonitoring. International Conference "Transboundary Aquifers: Challenges and New Directions".